



<sup>10</sup>  
**I29A**  
**206**  
**CIVIL ENGINEERING STUDIES**

STRUCTURAL RESEARCH SERIES NO. 386

**FINITE ELEMENT APPROACH FOR THE PREDICTION  
OF INELASTIC BEHAVIOR  
OF SHEAR WALL-FRAME SYSTEMS**

Metz Reference Room  
Civil Engineering Department  
B106 C. E. Building  
University of Illinois  
Urbana, Illinois 61801

by  
**O. YUZUGULLU**  
and  
**W. C. SCHNOBRICH**

ISSUED AS A TECHNICAL  
REPORT OF A RESEARCH  
PROGRAM SPONSORED

by  
The National Science Foundation  
Grant No. GK 11190

UNIVERSITY OF ILLINOIS  
URBANA, ILLINOIS  
MAY 1972

FINITE ELEMENT APPROACH FOR THE PREDICTION  
OF INELASTIC BEHAVIOR OF SHEAR WALL-FRAME SYSTEMS

BY

O. YUZUGULLU

and

W. C. SCHNOBRICH

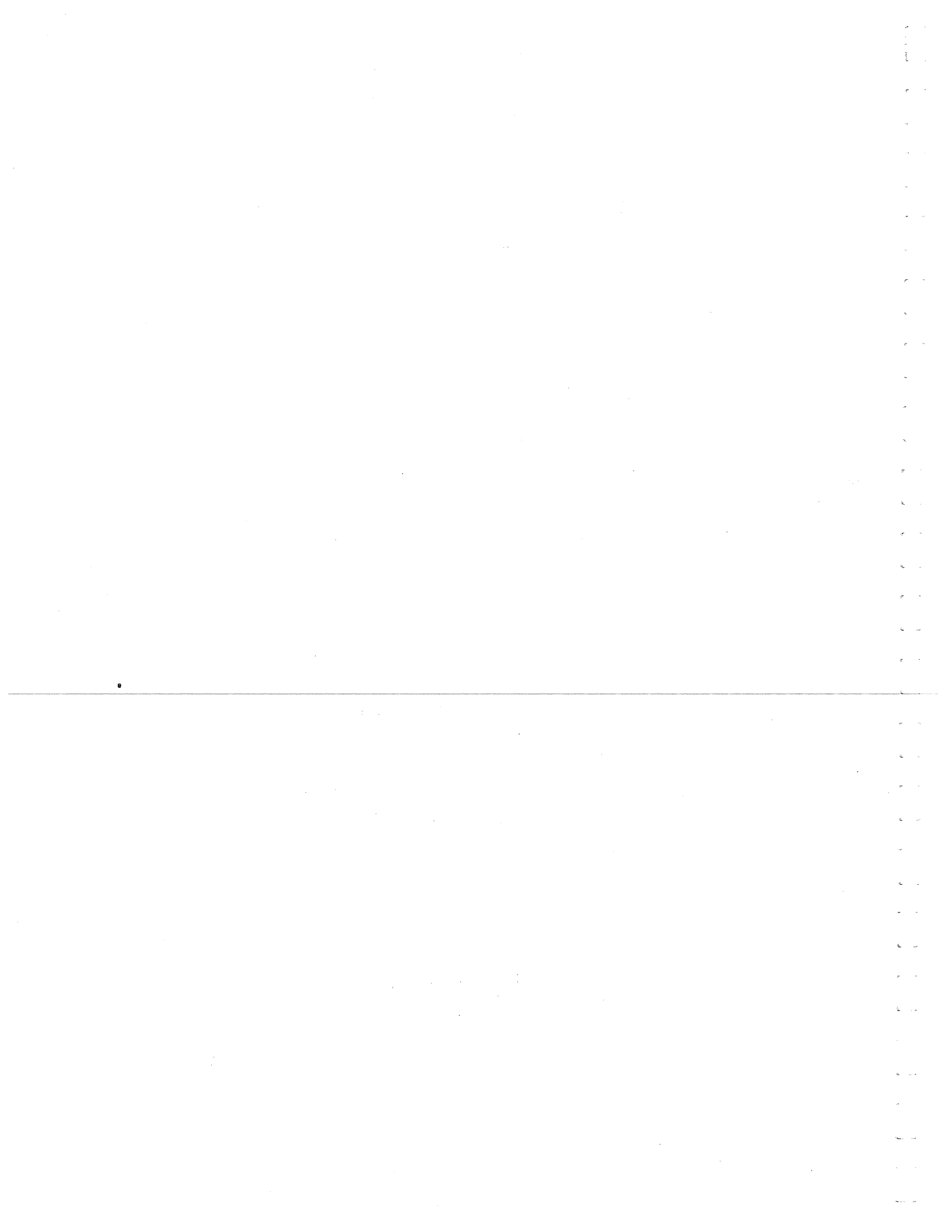
Metz Reference Room  
Civil Engineering Department  
B106 C. E. Building  
University of Illinois  
Urbana, Illinois 61801

Issued as a Technical  
Report of a Research  
Program Sponsored

by

The National Science Foundation  
Grant No. GK 11190

UNIVERSITY OF ILLINOIS  
URBANA, ILLINOIS  
MAY 1972



Acknowledgments

The results reported herein were developed in a research study supported by the National Science Foundation under Grant NSF GK 11190.

The contributions of Professors Bijan Mohraz, D.A.W. Pecknold and S. L. Paul are gratefully acknowledged. Also the discussions with M. A. Salem Research Assistant in Civil Engineering were quite helpful.

The computational work was carried out on the IBM System 360/75 of the Computing Services Office of the University of Illinois.



## TABLE OF CONTENTS

| CHAPTER |  | Page |
|---------|--|------|
| 1       | INTRODUCTION .....   | 1    |
|         | 1.1 General .....  | 1    |
|         | 1.2 Previous Work .....  | 2    |
|         | 1.3 Object and Scope .....   | 4    |
|         | 1.4 Notation .....   | 5    |
| 2       | DESCRIPTION OF THE MODEL .....   | 7    |
|         | 2.1 Description of the Finite Elements Used .....                      | 7    |
|         | 2.1.1 Reinforced Concrete Wall Elements .....                          | 7    |
|         | 2.1.2 Flexural Elements for the Frame .....                            | 8    |
|         | 2.1.3 Link Elements .....  | 9    |
|         | 2.2 Material Properties .....  | 9    |
|         | 2.3 Behavior of the Wall Elements .....                                | 10   |
|         | 2.3.1 Elastic Behavior up to Cracking .....                            | 10   |
|         | 2.3.2 Elastic Behavior After Cracking .....                            | 13   |
|         | 2.3.3 Crack Modes .....  | 15   |
|         | 2.3.4 Definition of a "Crack Width" .....                              | 15   |
|         | 2.3.5 Plastic Behavior After Cracking .....                            | 16   |
|         | 2.3.6 Plastic Behavior of Uncracked Concrete .....                     | 16   |
|         | 2.3.7 Termination of Plastic Behavior of Concrete .....                | 17   |
|         | 2.4 Behavior of the Frame Elements .....                               | 18   |
|         | 2.5 Behavior of the Link Elements .....                                | 19   |
| 3       | METHOD OF SOLUTION .....   | 21   |
|         | 3.1 Elastic Analysis .....   | 21   |
|         | 3.2 Incremental Analysis .....   | 22   |
|         | 3.2.1 General .....  | 22   |
|         | 3.2.2 Cracking .....   | 23   |
|         | 3.2.3 Plasticity .....   | 25   |
|         | 3.2.4 Mathematical Correspondence of Method 1 and<br>Method 2 .....    | 28   |
|         | 3.3 Computation of Pseudo Stresses and Pseudo Loads .....              | 28   |
|         | 3.3.1 Pseudo Stresses Due to Cracking .....                            | 28   |
|         | 3.3.2 Pseudo Stresses Due to Uniaxial Plasticity .....                 | 29   |
|         | 3.3.3 Pseudo Stresses Due to Plasticity of Uncracked<br>Concrete ..... | 29   |
|         | 3.3.4 Computation of the Pseudo Loads .....                            | 29   |
| 4       | NUMERICAL RESULTS .....  | 31   |
|         | 4.1 General .....  | 31   |
|         | 4.2 Deep Beam .....  | 31   |
|         | 4.2.1 Experimental Behavior .....                                      | 32   |
|         | 4.2.2 Behavior Predicted from the Analysis .....                       | 32   |
|         | 4.2.3 Variation of Stresses .....                                      | 34   |

|  | Page |
|--|------|
| 4.3 Shear Panel .....  | 34   |
| 4.4 Reinforced Concrete Shear Wall-Frame System .....  | 37   |
| 4.4.1 General .....  | 37   |
| 4.4.2 Behavior of the Specimen During the Text .....   | 38   |
| 4.4.3 Solution 1 .....   | 38   |
| 4.4.4 Solution 2 .....   | 41   |
| 5 SUMMARY AND CONCLUSIONS .....  | 44   |
| FIGURES .....  | 49   |
| APPENDIX   |      |
| A DEVELOPMENT OF THE ELEMENT STIFFNESS MATRICES AND COMPUTA-<br>TION OF STRESSES AND STRAINS ..... | 101  |
| B .....  | 109  |
| REFERENCES .....   | 123  |
| VITA .....   | 126  |

#### LIST OF TABLES

##### TABLE

|  |     |
|--|-----|
| B.1 Behavior of the Deep Beam (G24S-11) .....  | 109 |
| B.2 Moment, Shear and Axial Forces Acting at the Reference<br>Axis ( P = 100 tons, Solution 2) ..... | 110 |

#### LIST OF FIGURES

##### FIGURE

|   |    |
|---|----|
| 1. Constant Strain Triangle .....   | 49 |
| 2. Quadrilateral Element Composed of Four Constant Strain<br>Triangles .....            | 49 |
| 3. Comparison of Mesh Details .....   | 50 |
| 4. Stiffness Comparison of the Built-up Quadrilateral and<br>Rectangular Elements ..... | 51 |
| 5. Frame Elements .....   | 52 |
| 6. Link Elements .....  | 53 |
| 7. Biaxial Strength of Concrete .....   | 54 |
| 8. Stress-Strain Diagrams .....   | 55 |

|    | Page  |
|----|---|
| 9  | Distribution of the Reinforcement ..... 56  |
| 10 | Principal Stresses and Cracking ..... 56  |
| 11 | Crack Modes for Wall Elements ..... 57  |
| 12 | Assumed Strain Distributions for the Flexural Elements..... 58  |
| 13 | Assumed Crack Modes for the Flexural Elements ..... 59  |
| 14 | Schematic Diagram to Illustrate Crack Propagation<br>(Method 1: Initial Stress Method Using Variable Stiff-<br>ness Within an Increment) ..... 60   |
| 15 | Schematic Diagram to Illustrate Crack Propagation<br>(Method 2: Initial Stress Method Using Constant Stiff-<br>ness Within an Increment) ..... 61   |
| 16 | Comparison of Paths of Deformation ..... 62   |
| 17 | Schematic Illustration of the Distribution of Pseudo<br>Stresses Due to Biaxial Plasticity of Concrete ..... 63                                     |
| 18 | Pseudo Stresses Released Due to Cracking ..... 64   |
| 19 | Schematic Illustration of the Pseudo Stresses Released Due to<br>Plasticity of a Component Material (Cracked Concrete or<br>Reinforcement) ..... 65 |
| 20 | Deep Beam G24S-11 [20] ..... 66   |
| 21 | Discretized Model (Specimen G24S-11) ..... 67   |
| 22 | Crack Propagation (Specimen G24S-11) ..... 68   |
| 23 | Crack Propagation (Specimen G24S-11) ..... 69   |
| 24 | Experimental Crack Pattern (Specimen G24S-11) [20] ..... 60   |
| 25 | Comparison of Analytical and Experimental Load-Displacement<br>Diagrams (Specimen G24S-11) ..... 71   |
| 26 | Comparison of Load Versus Tension Steel Strains (Specimen<br>G24S-11) ..... 72  |
| 27 | Geometry and the Cross-Sectional Properties of Specimen W2<br>[17] ..... 73   |
| 28 | Comparison of the Load-Displacement Curves (Specimen W2) ... 74   |
| 29 | Layout of Mesh 1 (Specimen W2) ..... 75   |
| 30 | Layout of Mesh 2 (Specimen W2) ..... 76   |
| 31 | Region of Cracking for Two Different Values of Shear Factor<br>(Specimen W2, Mesh 1) ..... 77   |
| 32 | Comparison of the Experimental and Analytical Crack<br>Patterns (Specimen W2, Mesh 1) ..... 78  |
| 33 | Details of Specimen A-1 [21] ..... 79   |
| 34 | Physical Properties of the Materials Used in Specimen A-1[21] 80  |
| 35 | Load Versus Relative Vertical Displacement of the Supports<br>[21] ..... 81   |
| 36 | Load Versus Horizontal Displacement of the Supports [21] ... 82   |
| 37 | Comparison of the Load-Displacement Curves (Specimen A-1,<br>Solution 1) ..... 83   |
| 38 | Experimental Crack Pattern (Specimen A-1) [21] ..... 84   |
| 39 | Discretized Model (Specimen A-1) ..... 85   |
| 40 | Link Elements (Specimen A-1) ..... 86   |
| 41 | Comparison of Load-Displacement Curves (Specimen A-1,<br>Solution 1) ..... 87   |
| 42 | Effect of Shear Transfer on Cracking (Specimen A-1,<br>Solution 1) ..... 88   |
| 43 | Crack Pattern at 100 tons of Load (Specimen A-1, Solution 1) 89   |



|      |  |     |
|------|--|-----|
| 44   | Crack Pattern at 140 tons of Load (Specimen A-1,<br>Solution 1) .....          | 90  |
| 45   | Crack Pattern at 180 tons of Load (Specimen A-1,<br>Solution 1) .....          | 91  |
| 46   | Comparison of the Load Displacement Curves (Specimen A-1,<br>Solution 1) ..... | 92  |
| 47   | Flexural Deformations .....  | 93  |
| 48   | Grading Mesh Suggested .....   | 94  |
| 49   | Crack Pattern at 140 tons of Load (Specimen A-1,<br>Solution 2) .....          | 95  |
| 50   | Comparison of the Load-Displacement Curves (Specimen A-1,<br>Solution 2) ..... | 96  |
| 51   | Comparison of the Load-Displacement Curves (Specimen A-1,<br>Solution 2) ..... | 97  |
| 52   | Suggested Layering of a Flexural Element [18] .....                            | 98  |
| 53   | Frame Moments at P = 100 Tons (Before Cracking) .....                          | 99  |
| 54   | Frame Moments at P = 100 Tons (Before Cracking) .....                          | 100 |
| B.1  | Stress Distribution at Section A-A (Specimen G24S-11).....                     | 111 |
| B.2  | Stress Distribution at Section A-A (Specimen G24S-11).....                     | 112 |
| B.3  | Stress Distribution at Section A-A (Specimen G24S-11) .....                    | 113 |
| B.4  | Stress Distribution at Section A-A (Specimen G24S-11).....                     | 114 |
| B.5  | Stress Distribution at Section A-A (Specimen A-1,<br>Solution 1) .....         | 115 |
| B.6  | Stress Distribution at Section A-A (Specimen A-1,<br>Solution 1).....          | 116 |
| B.7  | Stress Distribution at Section A-A (Specimen A-1,<br>Solution 1) .....         | 117 |
| B.8  | Stress Distribution at Section A-A (Specimen A-1,<br>Solution 1) .....         | 118 |
| B.9  | Stress Distribution at Section A-A (Specimen A-1,<br>Solution 1) .....         | 119 |
| B.10 | Stress Distribution at Section A-A (Specimen A-1,<br>Solution 2) .....         | 120 |
| B.11 | Stress Distribution at Section A-A (Specimen A-1,<br>Solution 2) .....         | 121 |
| B.12 | Link Forces at P = 100 tons (Before Cracking) .....                            | 122 |

## CHAPTER 1

## INTRODUCTION

## 1.1 General

In the active earthquake areas of the world destructive earthquakes can always be expected. In the past they have caused enormous property damage and loss of life. The primary objective of the structural engineer should therefore be to design the structure in such a way that it will resist moderate earthquakes without damage and should not collapse or cause loss of life even under severe earthquakes. To achieve this, a better understanding of the behavior of the structure as a whole and the behavior of each structural element is necessary.

In the seismic design of framed structures it is generally accepted that the inclusion of shear walls to the structure produces an economical design. Shear walls are commonly used as the main elements in resisting the lateral loads especially in modern glass walled multistory buildings. They normally stiffen the structure against mild earthquakes and wind but at the same time they may invite larger shear forces to be generated from earthquake motions.

Knowledge of the interactive forces between the frames and the shear walls is important to the structural engineer since this knowledge of their magnitude is necessary in proportioning the lateral load carried by the shear walls and the framed portions of the structure. Determination of these interactive forces presents a major difficulty in the analysis.

## 1.2 Previous Work

Most of the previous analytical work on shear walls treated those walls as deep beams. Shear walls are weakened by vertical bands of openings such as for doors and windows. These arrangements of walls are called "coupled shear walls." They have been investigated in several recent publications.

Rosman [1] gave a continuous solution in which the discrete system of connecting beams is replaced by an equivalent continuous medium. Based on Rosman's theory, Coull and Choudhury [2] [3] and later Coull and Irwin [4] presented a graphical method for determining the stresses and deflections in coupled shear walls. Rosenblueth and Holtz [5], Cardan [6] and Gould [7] have analytically modelled the shear walls in the framed structures as a cantilever beam supported by elastic reactions.

Khan and Sbarounis [8] suggested a method of analysis which attempts to satisfy the compatibility of displacement between the wall and the frame by an iteration process.

A summary of the experimental research performed on frames with filler walls is given in Ref. [9]. Although there has been considerable research on frames with filler walls, tests on frames with reinforced or plain concrete walls are very limited [10] [11].

The prediction of load-deflection characteristics of shear wall-frame systems is of interest and importance in the design of structures to resist lateral loads such as those resulting from earthquake shocks.

Most of the above-mentioned investigations are limited by various simplifying assumptions as to loading, boundary conditions and material properties. In all of these studies only elastic behavior was taken into consideration. Recent research has clearly demonstrated, however, that

inelastic behavior must be considered in order to approach the earthquake problem in a realistic manner. On the other hand recent earthquakes [12] have pointed out that although the behavior of a shear wall may be favorable under static loading conditions, the behavior of that wall may also be quite different under dynamic conditions. No rigorous analytical or accurate experimental study is available which deals with the behavior of shear wall-frame systems under statically repeated, alternating or actual dynamic conditions. Little is known about the stiffness degradation of shear wall-frame systems as the loading cycles.

Recent development of the finite element method of continuum mechanics offers a convenient and versatile tool to be used in understanding the behavior of shear walls and their effect on the behavior of the structural frame. The finite element method has been applied to various static problems [13]. It has proved to be as effective and powerful in dynamic analysis as it has been in the static analysis [14].

Application of the finite element method to the idealization of reinforced concrete was started by Ngo and Scordelis [15] and expanded later by Nilson [16]. Recently, using constant strain triangular elements, Cervenka and Gerstle [17] investigated the behavior of reinforced concrete panels under monotonic and under cyclic in-plane loads. The loads were carried well into the inelastic range. An experimental investigation was also carried out for the above mentioned panels. The panels were like deep beams and did not have a frame around them. An analytical study of infilled frames was made by Franklin [18]. Three special types of finite elements were used for the discretization. The infill did not include any reinforcement. An approach was followed whereby it was possible to use the actual stress-strain relationship of the materials in a multilinear form.

In this study the loads were applied in one direction up to the disintegration of the structure due to excessive cracking and no plasticity was considered.

A lumped parameter model has also been successively used by Fedrokiw [19] to study the behavior of masonry infilled frames. Here it is concluded that there is a general need for analytical and experimental work directed toward predicting the stiffness characteristics and the inelastic behavior of shear wall-frame structures.

### 1.3 Object and Scope

A shear wall basically occupies a two dimensional region and receives forces from the enclosing frame. These forces are in the plane of the wall thus the force system creates a plane stress problem.

The object of this study is to approach the solution of reinforced concrete shear wall-frame systems analytically using the finite element technique as the tool. Tensile crack propagation in concrete and inelastic behavior of steel and concrete in compression are incorporated in the analysis. The behavior of the reinforced concrete shear wall-frame system is predicted under monotonically increasing loading conditions.

In order to test the validity of the assumptions made with regard to the material behavior and characteristics of the finite element method used, the analytical results are compared with the experimental results [20] [21] [17].

## 1.4 Notation

All symbols have been defined in the text where they appear first. Following is a summary of the symbols used. A letter with a single underline means a vector, with double underlines means a matrix.  $\Delta$  is used to denote finite increments.

|  |  |
|--|--|
| $\underline{\underline{B}}$                | Transformation matrix relating strains to the nodal displacements.       |
| $\underline{\underline{D}}$                | Composite material property matrix in XY coordinate system.              |
| $\underline{\underline{D}}^c$              | Uncracked material property matrix of concrete.                          |
| $\underline{\underline{D}}_{ep}$           | Elasto-plastic material property matrix.                                 |
| $\underline{\underline{D}}_{\alpha}^s$     | Material property matrix of the reinforcement in XY coordinate system.   |
| $\underline{\underline{D}}_{\alpha}^{i s}$ | Material property matrix of the reinforcement in X'Y' coordinate system. |
| $E^c$                                      | Modulus of elasticity of concrete.                                       |
| $E^s$                                      | Modulus of elasticity of the reinforcement.                              |
| $F_t, F_s$                                 | Strength of a link element in tension and shear.                         |
| $F(\sigma)$                                | Function defining the yield surface.                                     |
| $k_h, k_v$                                 | Stiffness of a link element tangent and normal to the contact area.      |
| $\underline{k}$                            | Uncracked element stiffness matrix.                                      |
| $\underline{K}$                            | Stiffness matrix of the structure.                                       |
| $\underline{k}_{cr}$                       | Cracked element stiffness matrix.  |
| $n$  | Ratio of $E^s$ to $E^c$ .  |
| $p$  | Percentage of reinforcement.   |
| $\underline{P}$                            | Vector of nodal forces of the structure.                                 |
| $\underline{\bar{P}}$                      | Vector of pseudo nodal loads.  |
| $\underline{T}_{\epsilon}$                 | Strain transformation matrix.  |

|                             |   |
|-----------------------------|---|
| $\underline{T}$             | Stress transformation matrix.                               |
| $\underline{u}$             | Vector of nodal displacements of an element.                |
| $\underline{U}$             | Vector of nodal displacements of the structure              |
| $\sigma_1, \sigma_2$        | Principal stresses.   |
| $\sigma_t$                  | Tensile strength of concrete.                               |
| $\sigma_0^c$                | Yield stress of concrete under uniaxial compression.        |
| $\sigma_0^s$                | Yield stress of the reinforcement.                          |
| $\sigma_{x'}^s$             | Steel stresses referred to concrete area in $X'$ direction. |
| $\underline{\sigma}$        | Vector of total stresses.                                   |
| $\underline{\sigma}^c$      | Vector of concrete stresses in XY coordinate system.        |
| $\underline{\sigma}^-$      | Vector of pseudo stresses.                                  |
| $\underline{\sigma}^{1s}$   | Vector of steel stresses in $X'Y'$ coordinate system.       |
| $\underline{\epsilon}$      | Vector of total strains.                                    |
| $\underline{\epsilon}^c$    | Vector of concrete strains in XY coordinate system.         |
| $\underline{\epsilon}^{1c}$ | Vector of concrete strains in $X'Y'$ coordinate system.     |
| $\nu$                       | Poisson's ratio.  |

## CHAPTER 2

## DESCRIPTION OF THE MODEL

## 2.1 Description of the Finite Elements Used

In this research the reinforced concrete shear wall-frame system is modeled by a finite element array. This array is built up of three types of elements:

- 1) Quadrilateral elements for the wall or frame,
- 2) special flexure elements for the frame, and
- 3) link elements to connect the wall elements to the frame elements.

## 2.1.1 Reinforced Concrete Wall Elements

Constant strain triangular elements (Fig.1) have been widely used for the analysis of plane stress problems. These elements work especially well for the idealization of bodies with irregular boundaries. Since the element is constant strain and hence constant stress, the results obtained from it frequently require interpretation. The calculated stresses can be assumed to represent the stress state at the centroid of an element. However, a more uniform stress field normally results from averaging the stresses of the various elements connected at each node. Depending upon the arrangement of the elements, a triangular element may show directionality; that is, the structure may behave in a certain way for one arrangement and in another way for a different arrangement. This averaging procedure helps in an effort to suppress any directionality present in the element layout.

A quadrilateral element composed of four constant strain triangles



was chosen to represent the wall elements (Fig. 2). If a structure is discretized by the use of both constant strain triangular elements and also by the quadrilateral elements assembled from the CST elements as shown in Fig. 3, it is obvious that in the case of quadrilateral elements used, the band width of the system stiffness matrix is decreased, mesh details are simplified and the stress values are improved by averaging the stresses about the common interior meeting point of the four triangles. The derivation of the element stiffness matrix which is obtained by a simple condensation of the center node is given in Appendix A.

If rectangular plane stress elements are used instead of the built-up quadrilateral elements to discretize the wall there is some loss of accuracy. This can be anticipated from a comparison of the traces of the element stiffness matrices (given in Fig. 4). A lower value is obtained for the quadrilateral element which indicates that the quadrilateral element is a more flexible element. Since these are both conforming elements and therefore too stiff, the more flexible element is the more desirable.

The steel bar reinforcement for the wall is assumed to be smeared out and uniformly distributed over each quadrilateral element.

### 2.1.2 Flexural Elements for the Frame

The quadrilateral elements transmit in-plane forces to the frame at the connecting nodes. One of these forces is normal to the frame member axis while the other is parallel to it. Bending moments and shear forces in the frame members are produced by the normal forces. On the other hand, parallel components not only produce axial forces but they also produce additional bending moments by virtue of the eccentricity of the line of action from the axis of the frame member. If frame members are considered as line elements in the

usual manner, then the effect of the depth is apt to be neglected in the assembly phase of the structural stiffness matrix. Fig. 5 shows a flexural element [18] in which the above effect is taken into consideration by transforming the six generalized displacements acting at the member reference axis as eight generalized displacements acting at the corners of the element. Development of the element stiffness matrix is summarized in Appendix A.

### 2.1.3 Link Elements

A special type like element made out of two orthogonal fictitious springs is used to connect the wall to the frame as shown in Fig. 6.a. The idea was adapted by Franklin [18] from the bond-link concept introduced by Ngo and Scordelis [15]. With this type of element it is possible to lock or to release the two connected nodes depending upon the magnitude of the interacting forces between the wall and the frame. The derivation of the element stiffness matrix is given in Appendix A.

## 2.2 Material Properties

Concrete and reinforcing steel constitute the materials for both the wall and the frame elements.

Test results concerning the material under biaxial states of stress are very limited. Those tests that have been reported were primarily directed towards defining failure or yield rather than the determination of a stress-strain law. The most recent investigation for the failure envelope of concrete under biaxial states of stress is the experimental study carried out by Kupfer, Hilsdorf and Rusch [22]. Fig. 7 shows the experimental failure envelope obtained. Mikkola and Schnobrich [23] presented a

yield criterion to approximate the experimental envelope given by Kupfer, Hilsdorf and Rusch. In this study the Von Mises yield criterion as shown in Fig. 7 is adapted for the biaxial compression of concrete. In case of uniaxial state of stress (reinforcement and the cracked concrete) the Von Mises yield criterion corresponds to an elastic-perfectly plastic stress-strain relationship (Fig. 8).

Maximum normal stress theory is assumed for tension cracking of the concrete (Fig. 7). Cracked concrete is assumed to carry normal stresses in the direction of the crack. Also, due to the irregular surface of the cracks, some shear can be transferred across a crack. This phenomena is termed aggregate interlock.

Deformation is assumed to be uniform, that is, concrete and the reinforcement have the same strains, which implies that full bond is maintained. This full bond is assumed to remain even in the crack regions.

## 2.3 Behavior of the Wall Elements

During the loading process the material can behave in various ways.

### 2.3.1 Elastic Behavior up to Cracking

Referring to Fig. 9, consider a concrete wall with unit dimensions. Up to cracking or yielding the concrete is assumed to be isotropic and linearly elastic. Therefore the material property matrix which relates the stresses and the strains can be written from Hooke's Law for plane stress:

$$\underline{\sigma}^C = \underline{D}^C \underline{\epsilon}^C \quad (2.1)$$

where

$$\underline{\sigma}^c = \begin{Bmatrix} \sigma_x \\ \sigma_y \\ \tau_{xy} \end{Bmatrix} \text{concrete} \quad \underline{\epsilon}^c = \begin{Bmatrix} \epsilon_x \\ \epsilon_y \\ \gamma_{xy} \end{Bmatrix} \text{concrete}$$

and

$$\underline{D}^c = \frac{E^c}{1-\nu^2} \begin{bmatrix} 1 & \nu & 0 \\ \nu & 1 & 0 \\ 0 & 0 & \frac{1-\nu}{2} \end{bmatrix} \quad (2.1a)$$

$E^c$ : modulus of elasticity of concrete

$\nu$ : Poisson's ratio of concrete

$\underline{D}^c$ : uncracked material property matrix of concrete.

This wall element contains reinforcement parallel to the  $X'$  axis, which makes an angle  $\alpha$  with the  $X$  axis.

Defining the percentage of reinforcement as

$$p = \frac{\text{area of reinforcement}}{\text{concrete area}}$$

the stress-strain relation of the reinforcement in the  $X'Y'$  coordinate system can be written as:

$$\underline{\sigma}^{1s} = \underline{D}_{\alpha}^{1s} \underline{\epsilon}^{1c} \quad (2.2)$$

where

$$\underline{\sigma}^{1s} = \begin{Bmatrix} \sigma_{x'} \\ 0 \\ 0 \end{Bmatrix}$$

and

$$\underline{\epsilon}^{1c} = \begin{Bmatrix} \epsilon_{x'} \\ \epsilon_{y'} \\ \gamma_{xy'} \end{Bmatrix} \text{concrete}$$

$$\underline{D}_{\alpha}^{1s} = \begin{bmatrix} pE^s & 0 & 0 \\ 0 & 0 & 0 \\ 0 & 0 & 0 \end{bmatrix}$$

and

$E^S$ : modulus of elasticity of the reinforcement

$\sigma_{x'}^S$ : steel stress referred to concrete area.

The following transformation rules [13] are valid to rotate the stresses and the strains from the global coordinate system to any other cartesian system  $x'y'$  positioned at an angle  $\alpha$  relative to the original global system:

$$\underline{\sigma}' = \underline{T}_{\sigma} \underline{\sigma} \quad (2.3)$$

$$\underline{\epsilon}' = \underline{T}_{\epsilon} \underline{\epsilon} \quad (2.4)$$

where

$$\underline{T}_{\sigma} = \begin{bmatrix} c^2 & s^2 & 2cs \\ s^2 & c^2 & -2cs \\ -cs & cs & c^2 - s^2 \end{bmatrix}$$

and

$$\underline{T}_{\epsilon} = \begin{bmatrix} c^2 & s^2 & cs \\ s^2 & c^2 & -cs \\ -2cs & 2cs & c^2 - s^2 \end{bmatrix}$$

$$c = \cos \alpha$$

$$s = \sin \alpha$$

Applying the above transformation rules to the material property matrix of the reinforcement  $\underline{D}_{\alpha}^S$ , the following global material property matrix  $\underline{D}_{\sigma}^S$  is obtained:

$$\underline{D}_{\sigma}^S = \underline{T}_{\sigma}^{-1} \underline{D}_{\alpha}^S \underline{T}_{\epsilon} \quad (2.5)$$

It can be shown by the principle of contragradience that

$$\underline{T}_{\sigma}^{-1} = \underline{T}_{\epsilon}^T$$

Composite material property matrix for the reinforced concrete model is obtained as the sum of the material property matrices of concrete and reinforcement:

$$\underline{\underline{D}} = \underline{\underline{D}}^C + \underline{\underline{D}}_{\alpha}^S \quad (2.6)$$

If additional reinforcement is present at an angle  $\alpha_1$  from the X-axis then the material property matrix takes the following form:

$$\underline{\underline{D}} = \underline{\underline{D}}^C + \underline{\underline{D}}_{\alpha}^S + \underline{\underline{D}}_{\alpha_1}^S \quad (2.7)$$

With this procedure any number of reinforcement directions can be accommodated. Due to the presence of reinforcement, the reinforced concrete model is no longer isotropic. The directions of the principal stresses and the principal strains may be different [24]. The magnitude of the deviation depends on the reinforcement ratio and the applied total stresses. For the range of stresses which are likely to occur in practice this deviation is relatively small [25] [24] [17].

### 2.3.2 Elastic Behavior After Cracking

Concrete is assumed to crack when a principal stress  $\sigma_1$  or  $\sigma_2$  reaches the tensile strength  $\sigma_t$  of concrete, Fig. 10. It is assumed that the cracked concrete can no longer carry any tensile forces perpendicular to the crack but maintains some amount of shear stiffness because of the irregular surface of the crack. Therefore for an open crack, the material property matrix of the cracked concrete, Fig. 10, can be written in the U, V-coordinate system as follows:

$$\underline{\underline{D}}_{cr}^C = \begin{bmatrix} d_{11} & 0 & 0 \\ 0 & 0 & 0 \\ 0 & 0 & d_{33} \end{bmatrix} \quad (2.8)$$

where

$$d_{11} = E^c$$

$$d_{33} = \frac{E^c}{2(1+\nu)} \quad (\text{for full shear transferability across the crack})$$

The cracked material property matrix  $\underline{D}_{=cr}^c$  can be transformed into the global system through the use of  $\underline{T}_{=e}$  and  $\underline{T}_{=\sigma}$  matrices which were defined in Eqs. 2.3 and 2.4, respectively. Hence the material property matrix of the cracked concrete takes the following form in the global coordinate system:

$$\underline{D}_{=cr}^c = \underline{T}_{=e}^T \underline{D}_{=cr}^c \underline{T}_{=e} \quad (2.9)$$

the explicit form of which is:

$$\underline{D}_{=cr}^c = \begin{bmatrix} c^4 d_{11} + 4c^2 s^2 d_{11} & c^2 s^2 d_{11} - 4c^2 s^2 d_{33} & c^3 s d_{11} - 2cs(c^2 - s^2) d_{33} \\ s^2 c^2 d_{11} - 4c^2 s^2 d_{33} & s^4 d_{11} + 4c^2 s^2 d_{33} & cs^3 d_{11} + 2cs(c^2 - s^2) d_{33} \\ c^3 s d_{11} - 2cs(c^2 - s^2) d_{33} & cs^3 d_{11} + 2cs(c^2 - s^2) d_{33} & c^2 s^2 d_{11} + (c^2 - s^2)^2 d_{33} \end{bmatrix}$$

where

$$c = \cos \beta$$

$$s = \sin \beta$$

If the material contains reinforcement in two orthogonal directions parallel to the global coordinate system, then the composite material property matrix takes the following form:

$$\underline{D} = \underline{D}_{=cr}^c + E^c \begin{bmatrix} nP_x & 0 & 0 \\ 0 & nP_y & 0 \\ 0 & 0 & 0 \end{bmatrix}$$

where

$$n = E^s / E^c$$

$P_x$ : percentage of reinforcement in X direction

$P_y$ : percentage of reinforcement in Y direction

Cracked concrete is highly anisotropic especially for moderate reinforcement ratios [17].

### 2.3.3 Crack Modes

Figure 11 summarizes the types of crack modes that can possibly occur during different types of loading conditions, that is monotonically increasing loads, unloading or alternate loading. Closing of cracks and opening of a new set of cracks in an element which contains closed cracks and also opening of two sets of cracks are especially important when the loads are reversed or unloading occurs.

### 2.3.4 Definition of a "Crack Width"

Referring to Fig. 10, the strain normal to the cracks can be written as:

$$\epsilon_{\perp} = \epsilon_x \cos^2 \gamma + \epsilon_y \sin^2 \gamma - \gamma_{xy} \cos \gamma \sin \gamma$$

where

$$\gamma = \beta - \frac{\pi}{2}$$

as defined in the figure. The cracked concrete carries  $\sigma_v^c$  stresses which are acting parallel to the cracks. These stresses cause strains in the direction normal to the crack because of the Poisson's effect, that is:

$$\epsilon_u^c = -\frac{\nu}{E^c} \sigma_v^c$$

where

$$\sigma_v^c = \sigma_x \sin^2 \gamma + \sigma_y \cos^2 \gamma - 2\tau_{xy} \sin \gamma \cos \gamma$$

A "closed crack" can be assumed if:

$$\epsilon_{\perp} \leq \epsilon_u^c$$



otherwise the crack is open. The difference between the two strains, namely the difference between  $\epsilon_{\perp}$  and  $\epsilon_{\parallel}$ , is defined as "crack width." Note that this crack width is only relative since it is defined in terms of strains.

It is possible to establish the varying value assigned for the shear term  $d_{33}$  defined in Eq. 2.8 as a function of the crack width defined above. If closing of cracks occurs then the uncracked material property matrix, Eq. 2.1a, should be used.

### 2.3.5 Plastic Behavior After Cracking

The elastic behavior of a cracked element is terminated if compressive yielding occurs in the cracked concrete and/or yielding occurs in the reinforcement under tension or compression. Uniaxial perfect plasticity is assumed for both the cracked concrete and the reinforcing steel. Hence the modulus of elasticity for a yielding component material is set equal to zero in the computation of the material property matrices.

### 2.3.6 Plastic Behavior of Uncracked Concrete

The uncracked concrete is in a biaxial state of stress. Associated with the initial stress method (explained in Chapter 3) a special elasto-plastic material property matrix is used. This matrix is developed in Ref. [26]. For ideal plasticity the general form of the elasto-plastic matrix is given as:

$$\underline{D}_{ep} = \underline{D} - \underline{D} \underline{F}'(\sigma) \underline{F}'^T(\sigma) \underline{D} [\underline{F}'^T(\sigma) \underline{D} \underline{F}'(\sigma)]^{-1} \quad (2.10)$$

where

$\underline{D}$  : elastic material property matrix

$$\underline{F}'(\sigma) = \frac{\partial F(\sigma)}{\partial \underline{\sigma}}$$

$F(\sigma)$ : function of the yield surface.

If the Von Mises yield condition and the associated flow rule is assumed for the plasticity of the uncracked concrete under biaxial stresses, then the yield surface  $F(\sigma)$  is defined by:

$$F(\sigma) = \sigma_x^c{}^2 - \sigma_x^c \sigma_y^c + \sigma_y^c{}^2 + 3\tau_{xy}^c{}^2 - \sigma_0^c{}^2 = 0 \quad (2.11)$$

where  $\sigma_0^c$  is the uniaxial yield stress. Also the elasto-plastic matrix specializes to:

$$\underline{D}_{ep}^c = \underline{D}^c - \underline{D}^c \underline{\psi} \underline{\psi}^T \underline{D}^c / (\underline{\psi}^T \underline{D}^c \underline{\psi}) \quad (2.12)$$

where

$$\underline{\psi}^T = \frac{1}{\sigma_0^c} \left[ \left( \sigma_x^c - \frac{\sigma_y^c}{2} \right) \left( \sigma_y^c - \frac{\sigma_x^c}{2} \right) 3\tau_{xy}^c \right]$$

$\underline{D}^c$  is defined by Eq. 2.1 and  $\sigma_0^c$  is defined by Fig. 8a. Note that the term  $[\underline{\psi}^T \underline{D}^c \underline{\psi}]$  is nothing more than a scaling factor.

### 2.3.7 Termination of Plastic Behavior of Concrete

Concrete can sustain compressive strains only up to a certain strain. At that time it crushes. This crushing strain can be determined from uniaxial compression tests of concrete. However, to use that value in the biaxial state of stress, an equivalent strain must be defined. If the Von Mises yield criterion is used this equivalent strain is:

$$\epsilon = \left( \epsilon_x^2 - \epsilon_x \epsilon_y + \epsilon_y^2 + \frac{3}{2} \gamma_{xy}^2 \right)^{1/2} \quad (2.13)$$

Once concrete crushes it cannot sustain any further load and its stiffness is disregarded.

## 2.4 Behavior of the Frame Elements

Axial and bending deformations are allowed for the frame elements. Constant strain distribution is assumed along the length of a frame element. Since the bending deformations involve variations through the depth of the frame element, the method for introducing an adjustment in material properties based on the stress level requires some approximation. One possibility of handling this would be to consider the frame element made up of a number of layers. By retaining the assumption of normals remaining normal it would be possible to allow progressive penetration of cracking and/or plasticity. Such an approach was discarded, however, as being too costly in computation time.

It was decided that a more approximate treatment of the frame elements is adequate for this study. Based on the stress levels at key locations, the behavior of each frame element is defined. The various combinations of strains possible in the frame element are shown in Fig. 12. If both the top and bottom strains are positive as shown in Fig. 12a, then the average of the top and bottom fiber stresses is used to determine cracking. In that case the whole section is assumed to crack. If both the top and bottom strains are negative as shown in Fig. 12b, then the average of the top and bottom stresses is checked against the yield stress. For this type of strain distribution, the cracking check is not made. Yield of the whole section is assumed if the center line value reaches yield. Yielding can continue until the concrete crushes. For the other two remaining strain distributions of Fig. 12, concrete is assumed to crack down to the mid-depth of the section if the tensile stress either at the top (Fig. 12.c) or at the bottom (Fig. 12.d) reaches the cracking stress. Assumed crack modes and the associated transformed areas are shown in Fig. 13.

If an underreinforced section is assumed, the plasticity and crushing of concrete in the compression zone is preceded by yielding of reinforcement in the tension zone. Uniaxial failure limits are assumed for both concrete and reinforcement.

## 2.5 Behavior of the Link Elements

The contact area between the wall and the frame represented by one link is called the tributary area of that link. Strength of a link element in tension and shear can be computed as:

$$\text{Strength in tension } F_t = A \cdot \sigma_{\text{tension}}^c$$

$$\text{Strength in shear } F_s = A \cdot \sigma_{\text{shear}}^c$$

where

$A$  : the tributary area

$\sigma_{\text{tension}}^c$  : tensile strength of concrete

$\sigma_{\text{shear}}^c$  : shear strength of concrete (assumed to be  $2 \sigma_{\text{tension}}^c$ ).

Initially very stiff values are assigned for the spring constants  $k_h$  and  $k_v$  which represent the stiffness of the link element in the directions tangent and normal to the contact area respectively (Fig. 6). A crack between the wall and the frame may be caused either due to shear or to tension. The occurrence of a crack is determined by comparing the strengths  $F_t$  and  $F_s$  with the forces acting between the wall and the frame. It is assumed that a crack can maintain some shear stiffness [27].

Once a crack forms  $k_h$  and  $k_v$  values should be altered depending upon the condition of the crack. If a crack forms due to shear and the normal force is tension then  $k_v$  is set equal to zero and  $k_h$  is set equal to the friction stiffness; if, however, the normal force is compression,

$k_v$  is kept at its initial large value. If a crack forms due to tension first, then again  $k_v$  is set equal to zero and  $k_h$  is set equal to the friction value.

## CHAPTER 3

## METHOD OF SOLUTION

## 3.1 Elastic Analysis

Finite element method used in this investigation is of the displacement or stiffness approach. General features of the finite element method are now well known. The concepts and steps in the development are explained in detail elsewhere [13] [14] and will not be repeated here.

Basically the method begins with dividing the continuous structure into a number of regions or subdomains known as "elements." On the basis of an assumed displacement field, stiffness properties of each element are determined in terms of values of the displacements and their derivatives at selected points called the "nodes." The stiffness characteristics of the whole structure is then constructed from the assembly of the stiffnesses of the individual elements. Finally, the following force-displacement relation is obtained:

$$\underline{P} = \underline{K} \underline{U} \quad (3.1)$$

where

$\underline{P}$ : vector of nodal forces (known)

$\underline{U}$ : vector of nodal displacements (unknown)

$\underline{K}$ : stiffness matrix of the structure (known).

Equation 3.1 is a system of linear simultaneous algebraic equations which express the equilibrium of the structure. The displacement boundary conditions can easily be incorporated by either including or deleting the appropriate degrees of freedom from Eq. 3.1.

If a direct stiffness approach is followed in the assembly of  $\underline{K}$ ,

a compact array of equations is obtained. This array of equations can be efficiently solved because of the banded and symmetric nature of  $\underline{K}$ .

In this research Gauss Elimination method is used for the solution of the equilibrium equations.

After solving  $\underline{u}$ , the strains  $\underline{\epsilon}$  and stresses  $\underline{\sigma}$  within each element can be computed by:

$$\underline{\epsilon} = \underline{B} \underline{u} \quad (3.2)$$

and

$$\underline{\sigma} = \underline{D} \underline{\epsilon} \quad (3.3)$$

where

$\underline{u}$  : nodal displacement vector of the element.

## 3.2 Incremental Analysis

### 3.2.1 General

Initially the structure is uncracked and elastic. This elastic state continues until first cracking or plasticity occurs. By loading the structure in increments and through the use of an iterative procedure it is possible to extend the elastic solution into the study of the propagation of cracks and plasticity of concrete or reinforcement.

When an element cracks or plasticity of any component material occurs, the released "pseudo stresses" or the "initial stresses" (see Section 3.3) should be distributed to the surrounding elements. Within one load increment the distribution of the initial stresses can be achieved in several ways. The following two alternatives can be mentioned:

Method 1: uses the updated, or current elastic stiffness. This procedure can be called "the initial stress method using a variable stiffness."

Method 2: uses the initial stiffness throughout each iterative cycle. This adaptation can be called "the initial stress method using constant stiffness."

Both methods can be used to study crack propagation and plasticity.

### 3.2.2 Cracking

Figures 14 and 15 are schematic illustrations of the methods mentioned in Section 3.2.1 in relation to crack propagation.

Referring to Fig. 14, assume that when the load is incremented from  $P_0$  to  $P_1$  some elements crack and the stiffness of the structure changes from  $K_1$  to  $K_2$ . Initial loads  $\bar{P}_A^{(1)}$  are released. At the same deflected configuration  $U_1$  the structure can only support a load which corresponds to point  $D_1$ . In order to reach the same external load level  $P_1$ , the structure must reabsorb the initial load  $\bar{P}_A^{(1)}$  causing further displacement of the structure by an amount of  $\Delta \bar{U}_A^{(1)}$ . This additional displacement is calculated as:

$$\Delta \bar{U}_A^{(1)} = K_2^{-1} \bar{P}_A^{(1)} \quad (3.4)$$

The inverse sign on  $K_2$  is symbolic only. If now this additional deformation causes cracking of new elements and the stiffness changes to  $K_3$  then new pseudo loads,  $\bar{P}_A^{(2)}$ , are released and the structure deforms further to  $U_3$  by an amount

$$\Delta \bar{U}_A^{(2)} = K_3^{-1} \bar{P}_A^{(2)} \quad (3.5)$$

Assuming that cracking stops at point  $A_3$ , then the next load increment is applied. Note that in the distribution of  $\bar{P}_A^{(1)}$  and  $\bar{P}_A^{(2)}$  the current cracked stiffnesses  $K_2$  and  $K_3$  are used respectively.

Figure 15 illustrates the same cracking process by Method 2. Again



assume that at the load level  $P_1$  some elements crack and the pseudo loads  $\bar{P}_A^{(1)}$  are released. The following iterative scheme is used to distribute the pseudo loads:

$$\Delta \bar{U}_A^{(1)} = K_1^{-1} \bar{P}_A^{(1)} \quad (3.6)$$

$$\Delta \bar{U}_A^{(2)} = \bar{K}_1^{-1} \bar{P}_A^{(2)} \quad (3.7)$$

$$\Delta \bar{U}_A^{(3)} = \bar{K}_1^{-1} \bar{P}_A^{(3)} \quad (3.8)$$

$$\Delta \bar{U}_A^{(4)} = \bar{K}_1^{-1} \bar{P}_A^{(4)} \quad (3.9)$$

etc.

Iteration continues until all the pseudo loads diminish to within a specified limit.

Final displacement  $\Delta \bar{U}_A$  caused by the pseudo loads is obtained as the sum of the displacements  $\Delta \bar{U}_A^{(1)}$ ,  $\Delta \bar{U}_A^{(2)}$ ,  $\Delta \bar{U}_A^{(3)}$ , etc. Assuming again that cracking stops at point  $A_3$ , then the next load increment is applied. If in the next increment further cracking occurs, the iterative scheme described by Eqs. 3.6, 3.7, etc., is repeated but using  $K_3$  as the stiffness properties this time. Note that in Method 2 the stiffness of the structure at the beginning of an increment is used for the distribution of the initial stresses.

The effect of cracking on the load-displacement diagram is non-linear but the cracking process itself is elastic, that is the structure remains elastic before and after cracking [17] [28].

In the real behavior of the structure cracking process continues gradually and the stiffness of the structure changes slowly. The path of deformation of the mathematical model has a stepped configuration as shown in Fig. 16. The approximated path of deformation of the mathematical model

using finite size load increments is also shown on the same figure. Only the points I,  $A_3$  and B are common to both of the paths. The detailed real path is approximated by a less detailed path which includes points I,  $A_1$ ,  $A_3$ ,  $B_1$ ,  $B_3$ , etc.

Referring to Fig. 16, if a single large load increment is applied between points I and  $B_3$ , the analysis may indicate cracking of a number of elements at the same time. In reality these should not occur at the same time but should occur more or less sequentially. The cracked stage achieved by the small load increment process may differ from that found with the large load step. In order to keep the solution to within reasonable limits of accuracy of the mathematical model, care must be experienced in selection of the size of load increment.

### 3.2.3 Plasticity

The distribution of the pseudo-loads due to plasticity again requires an iterative scheme. In this research within a typical load increment Method 1 is used for the plasticity of reinforcement and the cracked concrete, and Method 2 is used for biaxial plasticity. Computation of pseudo stresses and determination of yielding for the cracked concrete and the reinforcement are given in Section 3.3.2. In the case of a biaxial state of stress the determination of the yielding stage is more complex than the uniaxial case, since various combinations of stress are possible causes for yielding to start. All such combinations are expressed by a yield surface (e.g., Eq. 2.11 defines the Von Mises yield surface). Within a typical load increment the following steps should be taken to compute and distribute the initial stresses due to plasticity developing in an uncracked concrete element [26] (see Fig. 17):

- 1) Apply the load increment and determine the elastic stress and strain increments ( $\Delta \underline{\sigma}$ ,  $\Delta \underline{\epsilon}$ ).
- 2) Add the increments to the existing values of stress and strain at the beginning of the increment. Thus current total values are obtained ( $\sigma_1$ ,  $\epsilon_1$ ).
- 3) Evaluate  $F(\sigma)$  from the total value of stresses computed in

Step 2:

a) If  $F(\sigma) < 0$ , the element is elastic, no pseudo stresses are released. Stop the process.

b) If  $F(\sigma) > 0$  and also at the beginning of the increment  $F(\sigma) = 0$  (which means element was at yield at the beginning of the increment) set  $\Delta \underline{\sigma}_1 = \Delta \underline{\sigma}$ ,  $\Delta \underline{\epsilon}_1 = \Delta \underline{\epsilon}$ . Compute  $\Delta \underline{\sigma}_2$  using  $\Delta \underline{\epsilon}_1$  and the elasto-plastic matrix  $D_{=ep}$  (see Eq. 2.12):

$$\Delta \underline{\sigma}_2 = D_{=ep} \Delta \underline{\epsilon}_1 \quad (3.10)$$

where  $D_{=ep}$  is based on the total stresses obtained in Step 2.

Therefore, the pseudo stresses (the stresses which cannot be supported by the elasto-plastic concrete) are computed as:

$$\Delta \underline{\sigma}^- = \Delta \underline{\sigma}_1 - \Delta \underline{\sigma}_2 \quad (3.11)$$

c) If  $F(\sigma) < 0$ , but at the beginning of the increment  $F(\sigma) > 0$  (which means the element was elastic), find the intermediate value of stress and strain at which yield starts ( $\underline{\sigma}_0$ ,  $\underline{\epsilon}_0$ ) by interpolation and compute the incremental stresses and strains which have taken place above the yield point as:

$$\Delta \underline{\sigma}_1 = \underline{\sigma}_1 - \underline{\sigma}_0 \quad (3.12)$$

$$\Delta \underline{\epsilon}_1 = \underline{\epsilon}_1 - \underline{\epsilon}_0 \quad (3.13)$$

Again compute the pseudo stresses  $\Delta\bar{\sigma}$  using Eqs. 3.10 and 3.11.

4) Compute the pseudo loads  $\bar{P}$  (see Section 3.3.4) corresponding to  $\Delta\bar{\sigma}$  and analyze the structure using the initial stiffness at the beginning of the increment which will give a new set of increments,  $\Delta\sigma_1^i$  and  $\Delta\epsilon_1^i$ .

5) Repeat steps 2 through 4 until the pseudo stresses reach sufficiently small values.

Figure 17 is a schematic illustration of the process described above in a two-dimensional space. Note that the yield surface is artificially shifted away from its initial position. In order to prevent this shift the state of stress represented by point 2 should be projected on the yield surface (point 3) during the iterations.

When plasticity occurs the state of stress does not uniquely define the state of strain, it is path dependent. The same state of stress cannot be reached if different paths are followed. Also the process is irreversible, which means there is an energy loss during plastic action.

If within an increment only biaxial plasticity takes place, the initial stiffness of the structure is not altered and the pseudo loads are iterated by the use of the initial stiffness at the beginning of the increment. If, however, within an increment cracking occurs in some elements and concrete plasticity occurs in some other element, then only the element stiffness matrices of the cracked elements are changed; the element stiffness matrices of the uncracked yielding elements are not changed. Hence the structural stiffness matrix reflects only the changes occurring due to cracking.

### 3.2.4 Mathematical Correspondence of Method 1 and Method 2

Mathematically Method 1 corresponds to the solution of nonlinear equations of equilibrium (nonlinear since the computed initial loads are the functions of the state of stress reached) by employing Newton's [13] approach where tangential slope is used. Method 2, however, corresponds to the Modified Newton-Raphson [13] approach with constant slope being used during the iterations.

The convergence of the initial stress method has been illustrated by various practical applications [26] [13] [17] [29]. It has been successfully used to study cracking as well as plasticity problems.

### 3.3 Computation of Pseudo Stresses and Pseudo Loads

Pseudo (or initial) stresses may be released due to cracking or plasticity. In the following paragraphs the definition of the pseudo stresses and the nodal forces (pseudo loads) corresponding to them are given.

#### 3.3.1 Pseudo Stresses Due to Cracking

When an element cracks a sharp change in the material property matrix occurs at the instant the element goes from an uncracked state to the cracked state. Assuming that the element keeps the same deformed configuration at that instant of cracking (see Fig. 18), the cracked element can only support a value of stress which is computed from:

$$\underline{\sigma}_{cr} = \underline{D}_{cr} \underline{\epsilon} \quad (3.14)$$

The difference between the previously attained stress  $\underline{\sigma}$  and the new value of stress  $\underline{\sigma}_{cr}$  is called the "pseudo" or "initial" stress, that is

$$\underline{\bar{\sigma}} = \underline{\sigma} - \underline{\sigma}_{cr} = (\underline{D} - \underline{D}_{cr}) \underline{\epsilon} \quad (3.15)$$

### 3.3.2 Pseudo Stresses Due to Uniaxial Plasticity

When a component material (either concrete or reinforcement) reaches such a state of stress that yielding begins, the element cannot sustain any additional stress, that is stress in excess of the yield stress. Here again the excess stresses released, that is the elastic computed stress less the yield stress, are the pseudo or initial stresses. Yielding may begin at any point within an increment (see Section 3.2.3 for the incremental procedure). Change from an elastic to a plastic state of stress (loading) or from a plastic to an elastic state of stress (unloading) can be determined from the sign of the plastic work increment:

- if  $\Delta W_p \geq 0$  loading occurs, material is plastic,
- if  $\Delta W_p < 0$  unloading occurs, material is elastic.

Figure 19 schematically illustrates the amount of pseudo stresses released due to uniaxial plasticity of the cracked concrete or plasticity of the steel reinforcement.

### 3.3.3 Pseudo Stresses Due to Plasticity of Uncracked Concrete

The computation of the stresses released due to biaxial plasticity of the uncracked concrete is given in Section 3.2.3 in relation to the plastic analysis where Method 2 is employed.

### 3.3.4 Computation of the Pseudo Loads

Forces corresponding to the pseudo stresses can be computed from the equation [26]:

$$\bar{\underline{P}} = \int_A \underline{\underline{B}}^T \bar{\underline{\sigma}} dA \quad (3.16)$$

where  $\underline{\underline{B}}$  is the matrix which relates the nodal displacements to the element

strains (see Appendix A).

It is also possible to compute the pseudo loads directly from the difference of the element stiffness matrices:

$$\underline{\bar{P}} = (\underline{k} - \underline{k}_{cr}) \underline{u} \quad (3.17)$$

where

$\underline{k}$ : uncracked element stiffness matrix

$\underline{k}_{cr}$ : cracked element stiffness matrix

$\underline{u}$ : nodal displacement vector of the element.

---

## CHAPTER 4

## NUMERICAL RESULTS

## 4.1 General

To demonstrate the applicability of the analysis presented in the previous chapters and also to investigate the adequacy of the finite elements suggested a reinforced concrete deep beam, a reinforced concrete panel and a reinforced concrete shear wall-frame system are numerically analyzed. Experimental results are already available.

All the computations are carried on the IBM 360/75 system operated by the Department of Computer Science of the University of Illinois.

## 4.2 Deep Beam

Various investigators have studied the behavior and stress distribution in reinforced concrete deep beams, both theoretically and experimentally. One of the deep beams tested at the University of Illinois [20] was selected and analyzed by the incremental finite element method outlined in the previous chapters.

The geometry and the cross-sectional properties of the selected specimen, designated G24S-11 in Ref. [20], are shown in Fig. 20. The average compressive strength of the concrete used in the model beam was 5600 psi. The modulus of rupture of the concrete is estimated as 580 psi. The specimen had no web reinforcement and contained a single # 4 intermediate grade deformed bar (yield stress = 45.7 ksi, yield strain = 0.170%) as the tension reinforcement. Also a single # 3 intermediate grade deformed bar (yield stress = 48.9 ksi, yield strain = 0.178%) was used as compression reinforcement.



The tension reinforcement had a special anchorage as shown in Fig. 20.

#### 4.2.1 Experimental Behavior

The experimental data provided the following information:

- 1) the details of the geometry and material stress-strain laws,
- 2) cracking pattern,
- 3) variation of concrete and steel strains versus load.

The specimen was tested both statically and dynamically but only the static results are used here as a basis for comparison.

The beam behaved as a tied arch in which the tension steel acted as a tie and the concrete above and outside the cracks served as the arch rib. Both vertical and inclined cracks formed and at advanced stages of loading they became well developed. The inclined cracks advanced approximately 45 degrees toward mid-span and then rose almost vertically to the compression zone. Final failure of the beam occurred by the yield of tension reinforcement (yield load  $P_y = 27.8$  kips).

#### 4.2.2 Behavior Predicted from the Analysis

The layout of the finite element array used to model the beam is shown in Fig. 21. Due to symmetry only one half of the beam is analyzed. Discretization required 42 quadrilateral elements and 56 nodes. The load is applied uniformly over the nodes 29, 36 and 43 and a single support is used at node 14. (shown on Fig. 21) which provides a couple arm of 8 inches. Elastic material properties used in the analysis are:

$$E^C = 3,540,000.0 \text{ psi for concrete}$$

$$E^S = 27,300,000.0 \text{ psi for the reinforcement}$$

$$\nu = 0.10 \text{ for concrete}$$

Realizing that the surface of the crack in the concrete is not smooth it is assumed that cracked concrete maintains 25% of its full shear capacity. This phenomenon is termed aggregate interlock.

First cracking started almost in a vertical direction in element 7 at the load of 15 kips and propagated through the structure as illustrated by the sequential plots of cracks at each load level as shown in Figs. 22 and 23. The experimental crack pattern is reproduced in Fig. 24. There is a good agreement between the experimental and analytical crack patterns, both in location and direction (Figs. 23, 24).

The load is applied in increments of 5 kips up to failure. Load versus displacement diagrams obtained from the analysis and the experiment are compared in Fig. 25. The points corresponding to a single load level show the increase of displacement due to propagation of the cracks. Good agreement between the experimental and analytical behavior is found. From the test it was observed that the flattening of the load displacement diagram was initiated by yielding of the tension reinforcement. This type of behavior was very well predicted by the analysis. Figure 26 shows the comparison of the load versus steel strains. The initial slopes of both the experimental and the analytical curves are steep. This stage corresponds to the elastic behavior before cracking. After formation of cracks in the tension zone, stresses carried by the concrete are transferred to the reinforcement which causes the steel strains to increase and produces a change in the slope of the curves. Inelastic behavior starts by yielding of the reinforcement where the strains increase more rapidly with load. It is observed that the load versus steel strain curves have similar shapes as the stress-strain curve for the tension reinforcement.

#### 4.2.3 Variation of Stresses

From the output of the analysis it is possible to trace the variation of stresses at any section of the beam at any load level. In Figs. B.1 through B.4 such a sequential plot is given for section A-A which is designated in Fig. 21. The diagrams exhibit stepped configuration because the stresses are assumed to be constant within an element. The solid lines show the distribution of stresses at the beginning of the indicated load level and the dotted lines show the distribution at the end. From the variation of  $\sigma_x$  stresses it is possible to observe shifting of the neutral axis towards the compression zone when cracking occurs in the tension zone. With the increase of the loads compressive  $\sigma_x$  blocks grow larger and larger to balance the stresses developed in the tension reinforcement.  $\sigma_y$  stresses don't show considerable change except for the cracked elements. A decrease in  $\sigma_y$  stresses is noticed due to cracking. Section A-A lies in a constant moment region where zero shear stresses should exist according to the beam theory. Small magnitude and slight variation of the shear stresses is in agreement with the above consideration.

#### 4.3 Shear Panel

One of the shear panels tested at the University of Colorado [17] was analyzed. Two panels were combined to form a beam-like specimen which was tested as a simply supported beam with mid-point load as shown in Fig. 27a. The selected specimen was designated as W2 in Ref. [17]. The three vertical ribs shown in Fig. 27a transmit the concentrated forces at the support points and at the load point to the panels. They also provide lateral stability to the panels. The geometry and the cross-sectional properties of the selected specimen are given in Fig. 27a through Fig. 27c.

The following data was listed for the materials used in specimen W2:

Average compressive strength of concrete 3387 psi

Modulus of elasticity of concrete 2900 ksi

Tensile strength of concrete 483 psi

Yield strength of the reinforcement 51.2 ksi

Modulus of elasticity of the reinforcement 27300 ksi

Because of symmetry only one half of the specimen had to be analyzed. Poisson's ratio for concrete is assumed to be 0.10.

The failure mechanism reported from the tests was a flexural failure where yielding of the tension reinforcement occurred first and plasticity of concrete in the compression zone followed. The analysis also predicted the same type of failure. The analytical and the experimental load-displacement diagrams are compared in Fig. 28. The agreement between the computed and the experimental results is considered good.

Two types of finite element meshes are used. They are shown in Figs. 29 and 30. Mesh 1 required 35 quadrilateral elements and 48 nodes. Mesh 2 required 63 quadrilateral elements and 80 nodes. In both meshes the failure of the specimen started by the yielding of the tension reinforcement. When the finer mesh was used (Fig. 28, curve b) yielding occurred at a lower load than with the coarse mesh (Fig. 28, curve a). The analysis indicated plasticity developed in the concrete in the compression zone when the finer mesh was used, while no plasticity was detected in the concrete when the coarse mesh was used. This difference can be explained by the ability of the finer mesh to better reproduce stress concentrations than the coarse mesh.

Three types of load intervals were tried in the three different solutions ( $\Delta P_1 = 2$  kips,  $\Delta P_2 = 4$  kips,  $\Delta P_3 = 8$  kips). Load-displacement

diagrams obtained from  $\Delta P_1$  and  $\Delta P_2$  are shown in Fig. 28 (curves a and c). The numerical values of the displacements at points A, B, C, D (designated in Fig. 28) are as follows:

| <u>Load P<br/>(kips)</u> | <u>Displacement<br/>at Point</u> | <u>for <math>\Delta P_1</math></u> | <u>for <math>\Delta P_2</math></u> | <u>for <math>\Delta P_3</math></u> |
|--------------------------|----------------------------------|------------------------------------|------------------------------------|------------------------------------|
| 10                       | A                                | 0.01073 in.                        | 0.01073 in.                        | 0.01073 in.                        |
| 14                       | B                                | 0.02326 in.                        | 0.02335 in.                        |                                    |
| 18                       | C                                | 0.03815 in.                        | 0.03829 in.                        | 0.03769 in.                        |
| 22                       | D                                | 0.05678 in.                        | 0.05710 in.                        |                                    |

No cracking took place at point A. At point C the number and location of elements cracked during the application of load by  $\Delta P_1$  or  $\Delta P_2$  increments is exactly the same (elements 29, 30, 32, 33, 34 and 35 cracked). However, an additional element (element no. 28) was cracked when the increment used was  $\Delta P_3$ . It is concluded that the effect of the size of load increment on the values of displacements and on the sequence of cracking is slight.

Curves a and d shown on Fig. 28 compare the load-displacement behavior when two different shear stress transfer values are used to transfer stress across a crack (12.5% shear and no shear, respectively). The two diagrams compare well except in the value of the failure load. In the no shear case, failure requires a higher load than the 12.5% shear case. Figure 31 compares the cracked regions at  $P = 24$  kips. The number of cracked elements in the no shear case is less than the 12.5% shear case, thence the transfer of stresses from concrete to the tension reinforcement occurs at a higher load.

Experimental and analytical crack patterns are compared in Fig. 32. Good agreement exists between the two patterns.

#### 4.4 Reinforced Concrete Shear Wall-Frame System

##### 4.4.1 General

The shear wall-frame system used in this analysis (designated as Specimen A-1 in Ref. [21]) is adapted from a series of prototype models which were experimentally tested at the University of Tokyo in 1964 [21]. Two one-story shear wall-frame systems were cast together to form a beam-like specimen as shown in Fig. 33 and tested as a simple beam which is loaded at mid-point with a 2000 ton capacity Universal-type testing machine.

The geometry and the cross-sectional details of the selected specimen are shown in Fig. 33. Physical properties of the materials used are given in Fig. 34. The experimental data did not contain information about the tensile strength of concrete hence it is computed from the compressive strength:

$$\sigma_{\text{rupture}} = (1.25 \sim 1.75) \sigma_{\text{split}}$$

where

$$\sigma_{\text{split}} = (6 \sim 7) \sqrt{f'_c}$$

$f'_c$ : compressive strength of concrete in psi. Substituting the numerical values in the above formulas the modulus of rupture is obtained as  $\sigma_{\text{rupture}} \cong 40 \text{ kg/cm}^2$  (570 psi).

Two systems of finite elements are used for the discretization:

Solution 1: Quadrilateral elements for the wall and the frame, link elements for the connection of the wall to the frame.

Solution 2: Quadrilateral elements for the wall, flexural elements for the frame, link elements for the connections of the wall to the frame.

The beam-to-column connections of the test specimen are quite stiff due to the presence of crowded reinforcement. Analytical model

simulates this by using stiffened quadrilateral elements at those locations (elements 1, 8, 21, 28).

#### 4.4.2 Behavior of the Specimen During the Test

The load-displacement diagrams obtained from the test are reproduced in Figs. 35, 36 and 37. Figure 35 shows the complete load-displacement behavior where the relative displacement between the mid-span and the right or left support is used. Figure 36 is a plot of load versus horizontal displacement of the right and left supports. Figure 37 shows the initial portion of the load versus mid-span displacement.

During the test, the specimen was first loaded up to 110 tons, unloaded and reloaded this time to failure. Final crack appearance after the failure of the specimen is reproduced in Fig. 38. After opening of large diagonal cracks at 127 tons of load, the resistance of the test specimen increased until 197 tons of load. At that time a shear-compression failure occurred at the upper compression columns. No separation between the wall and the frame is reported.

#### 4.4.3 Solution 1

The general layout of the analytical model is given in Fig. 39. Figure 40 shows the location and numbering of the link elements. There are 64 quadrilateral and 28 link elements used for the idealization. Each link element shown on Fig. 40 represent a certain contact area depending upon its location. In this layout four magnitudes of contact areas are identified; which are:

- 1) Horizontal sides, non-corner. Link Elements 9, 10, 11, 12, 13, 23, 24, 25, 26, 27.

- 2) Horizontal sides, at corner. Link elements 8, 14, 22, 28.
- 3) Vertical sides, non-corner. Link elements 2, 3, 4, 5, 6, 16, 17, 18, 19, 20.
- 4) Vertical sides, at corner. Link elements 1, 7, 15, 21.

Analysis identified first cracking of element 15 at a load of 100 tons. From there on the loads are incremented by 10 tons. A cracked element is assumed to transfer some amount of shear stress across the cracks; two extreme cases being zero shear transfer and full shear transfer. Depending upon the width of the crack the value of the shear stiffness assigned to a cracked element will vary between those two extreme cases. Four solutions are run with different values of shear stiffness:

Case 1: in this solution a cracked element is assumed to transfer no shear stress across a crack.

Case 2: 12.5% of the full shear stress is assumed to be transferred across a crack.

Case 3: 25% of the full shear stress is assumed to be transferred.

Case 4: full shear stress is assumed to be transferred across a crack.

The load versus displacement diagrams obtained from the above mentioned cases are given in Fig. 41. All of the four diagrams exhibit similar behavior. However, there is a difference in the size of the cracked regions as illustrated in Fig. 42. As the value of the shear stiffness assumed for a cracked element increases, the number of the cracked elements increase. The cracked region corresponding to no shear case (Case 1) is confined to a smaller area; however, in the case of full shear transfer (Case 4) the cracked region is wide spread. This is mainly caused by the ability of the cracked element used in the latter case (Case 4) to transfer shear stresses



through the cracks and thereby cause cracking of the neighboring elements.

Figures 43, 44 and 45 illustrate the appearance of the analytical cracks at three different load levels. Assumed shear factor for these plots is 0.125. There is a close agreement between the crack pattern obtained from the test (Fig. 38) and the one obtained from the analysis (Fig. 45), both in location and in direction of the cracks.

A comparison between the analytical and the experimental load-displacement diagrams for a shear factor of 0.125 is given in Fig. 41. (curves b and f). Vertical displacement of node 9 is used for this plot. (Fig. 37 shows a similar comparison for the initial portions of the load-displacement diagrams) Analytical and experimental load versus horizontal displacement (horizontal displacement of node 105) diagrams are compared in Fig. 46. The agreement between the analytical and the experimental load-displacement behavior is very good up to a load of 140 tons. From there on the analytical diagrams run with a steeper slope, indicating a stiffer analytical model than the test specimen. The same stiff behavior is observed in all the four cases corresponding to different values of shear stiffness assumed for a cracked element (Fig. 41). Thus it can be concluded that the cause of this stiff behavior is not due to the transfer of shear stresses across the cracks. A possible explanation is given in the following paragraphs.

As the cracks spread in the structure and propagate towards the compression zone, a cumulation of compressive and shear stresses occur in the compression zone. The elements of this zone are subject to high local bending moments caused by the frame action. Now the solution becomes sensitive to the behavior of this region.

Consider a flexural element as shown in Fig. 47a. Under the

action of a bending moment  $M$ , it would deform to the curved shape  $A'B'C'D'$  as shown in Fig. 47b. However, if the same bending moment is applied to a quadrilateral element it would deform to the trapezoidal shape as shown in Fig. 47c. Thus a quadrilateral element while trying to respond to a flexural action, will spend much of its energy in shear-type deformation as implied by the trapezoidal shape. Therefore, a stiff behavior is expected from the quadrilateral element under the action of the flexural stresses. Furthermore, the flexural stresses are suppressed and initiation of plasticity postponed.

From the above discussion it follows that the stiff behavior of the analytical model (after the load of 140 tons) can be attributed to the poor behavior of the quadrilateral elements in the critical compression zone (designated in Fig. 48). This poor behavior of the quadrilateral elements can be avoided if the number of the elements corresponding to the critical zone is increased. This can be achieved with a graded mesh which may look like the one shown in Fig. 48.

Except for a few closed shear cracks (link elements 2, 3, 11, 12, 21), no separation took place between the wall and the frame during the course of loading. The forces acting on the link elements are given in Fig. B.12.

Sequential plots of the variation of global stresses ( $\sigma_x$ ,  $\sigma_y$ ,  $\tau_{xy}$ ) at a vertical section A-A (designated in Fig. 39) as a function of the applied forces are given in Figs. B.5 through B.9.

#### 4.4.4 Solution 2

General layout of the analytical model is given in Fig. 33. The location and the numbering of the link elements is given in Fig. 34. In this solution, instead of the quadrilateral elements, flexural elements are

used for the frame. Discretization required 24 flexural elements, 40 quadrilateral elements and 28 link elements. Again four magnitudes of contact areas are identified for the link elements (see Section 4.4.3).

Analysis identified first cracking of element 15 at a load of 100 tons. From there on the loads are applied in increments of 10 tons up to failure.

A cracked quadrilateral element is again assumed to transfer 12.5% of the shear stress across the cracks. The crack pattern obtained from the analysis at a load of 140 tons is shown in Fig. 49. There is a close agreement between the analytical and experimental (Fig. 38) crack patterns.

Load-versus displacement responses obtained from this analysis and the experiment are compared in Figs. 50 and 51. Agreement between the experimental and the analytical behavior is very good up to 140 tons of load at which time the analysis indicated failure by yielding of reinforcement and plastic behavior of the concrete in the elements adjacent to the single support (elements 20, 58, 64, 63). This local failure is caused mainly by the concentration of stresses due to the excessive rotation of the rigid corner element (element 28). Final failure of the specimen occurred first by yielding of the reinforcement in elements 15, 16, 17, 18, 19, 20, which is followed by yielding of the concrete in the compression zone and yielding of the elements aligned with the main diagonal.

The early failure of the analytical model can be attributed to the abrupt weakening of the flexural elements in the critical compression zone due to excessive yielding. If a slicing or layering procedure [18] is followed for these flexural elements a gradual change of stiffness occurs and this provides the additional strength to the analytical model which is

necessary to prevent the occurrence of the early failure. Figure 52 illustrates such a layered flexural element.

The moments acting at the reference axis of the flexural elements are plotted in Figs. 53 and 54. It should be observed that high flexural action takes place directly under the applied loads (elements 9, 10) and also near the supporting point (elements 26, 27). Numerical values of the normal forces, shear forces and the bending moments acting at the member reference axis are given in Table B.2.

Variation of the global stresses ( $\sigma_x$ ,  $\sigma_y$ ,  $\tau_{xy}$ ) at the section A-A (designated in Fig. 39) are given in Figs. B.10 and B.11.

Similar to the experimental behavior no link element failures occurred except a few shear cracks (link elements 11, 12, 13, 2, 3) which had a very insignificant effect on the general behavior.

It can be concluded that if flexural elements are used to represent the frame in a shear wall-frame system:

- a) a layering procedure is suggested for the elements which are subjected to high flexural action,
- b) a better support should be used to prevent a local failure.

## CHAPTER 5

## SUMMARY AND CONCLUSIONS

A discrete element method for the elastic and inelastic analysis of a reinforced concrete shear wall-frame system has been developed. This method utilizes finite element technique as a tool of computation. An incremental procedure is used to study the nonlinear behavior due to cracking and plasticity. Within an increment of load the pseudo (or initial) stresses which are released due to cracking and plasticity are distributed to the surrounding elements of the structure by either using the initial unchanged stiffness at the beginning of the increment (Method 2), or the current updated stiffness (Method 1). The analysis also incorporates transfer of some amount of shear across the cracks. Only monotonic loading up to failure is considered.

A computer program has been developed to permit high speed computation of the resulting equations.

Three types of structures (a deep beam, a shear panel and a shear wall-frame system) are numerically analyzed and the results obtained are compared with the available experimental results. The analysis provided a means to follow the complete structural behavior under monotonically increasing loads.

Aggregate interlock or the ability of a cracked element to transfer shear is included in the analysis. A constant value of shear stiffness is assumed for all the cracked elements. It is anticipated that a better physical insight can be given to the problem of shear transfer if the value of the assigned shear stiffness is adjusted as a function of the crack width or

some other such similar function. In all the examples solved good agreement is obtained between the analytical and the experimental crack patterns both for coarse and for fine meshes used. The analytical nonlinear load-displacement behavior caused by cracking compared well with the available test results. The analysis can predict with acceptable reliability a failure mechanism which occurs due to bending action (for an under-reinforced section) where yielding of the reinforcement occurs first and compression plasticity of concrete follows (see the deep beam and shear panel examples).

If built-up quadrilateral elements are used for both the frame and the wall in a shear wall-frame system (see Solution 1 of the shear wall-frame example) initiation of plasticity is postponed in the critical compression zone due to the stiff behavior of the quadrilateral elements in the rectangular mesh used. In advanced stages of loading the solution becomes sensitive to the behavior of the limited number of elements located in the critical compression zone (Fig. 48) where stress concentrations occur due to the propagated cracks. To improve the analytical results the following are suggested:

1) use of a new grid with non-rectangular elements to provide a finer mesh in the critical compression zone (e.g., mesh suggested in Fig. 48). This type of a mesh provides improved stress values in the region where high stress gradients occur.

2) use of a four node (same as rectangular element) isoparametric element. The evaluation of the element stiffness matrix of such an isoparametric element requires the integration of a triple matrix product of the following form

$$\int_A \underline{\underline{B}}^T \underline{\underline{D}} \underline{\underline{B}} dA$$

which is approximated by a summation

$$\sum_{i=1}^m \sum_{j=1}^n \omega_{ij} (\underline{B}^T \underline{D} \underline{B}) (x_i, y_j)$$

where each  $\omega_{ij}$  is the integration weighing factor and  $x_i$  and  $y_j$  are the integration points selected for the numerical integration. Each term of the above summation represents in effect the contribution of the stiffness of a subregion to the overall element stiffness. If a procedure is followed such that cracking or yielding criterion is evaluated at the integration points and each time a crack or yielding occurs the material property matrix  $\underline{D}$  is updated to include the effect of the change, then it is possible to obtain a gradually cracking or yielding element. Here it should be noted that only the subregion which corresponds to that integration point is considered cracked or yielded. Peak stresses occurring within such an element results with the partial failure of the element at the same load level where the quadrilateral element still would not have failed. This partial failure results in a more flexible element, thus a more flexible overall behavior.

If flexural elements are used for the frame, however, early failure of the structure occurred (see Solution 2 of the shear wall-frame example). This is attributed to the early weakening of the flexural elements. A layering procedure is suggested for the flexural elements positioned at the critical compression zone.

From the study of the behavior of the link elements it was concluded that the analyzed reinforced concrete shear wall-frame system can be considered as a single integral unit rather than a wall and a frame.

Another version of the program used in this research may include alternating or cyclic loading. This type of loading is of interest in

order to establish the stiffness properties of the analyzed shear wall-frame system under seismic loads. Under cyclic loading a degradation of stiffness occurs, that is, the stiffness of the structure decreases as a function of the maximum deformation imposed in previous cycles. Therefore, analytical prediction of the complete load-displacement behavior is necessary to determine the nonlinear response of the structure under repeated loads such as resulting from earthquakes.

In the idealization of the stress-strain diagram of the concrete, compressive strength provided from the tests of cylinders was used as the maximum stress ( $\sigma_0^c$ , see Fig. 8a). The area covered by the idealized diagram is larger than the experimental diagram, indicating that more energy is required for the idealized material for its failure. Use of an idealized diagram which has a balanced area with the experimental diagram is suggested in order to avoid the additional imposed energy requirements. This can be achieved by lowering the maximum value of the stress and decreasing the initial modulus of elasticity. However, difficulty arises in interpreting the counterpart of the above adjustment in the case of biaxial state of stress.

The assignment of shear stiffness to a cracked element was made arbitrarily in the absence of the test data in this area. Experimental information is necessary about the amount of shear transferred across a crack as a function of the crack width or whatever other variables are being used. Also experimental information about how well an open crack closes may be helpful if the type of the problem to be solved is such that closing of cracks is expected (such as cyclic loading).

The analysis included the nonlinearities caused by cracking and plasticity only. However, it is realized that nonlinear behavior may occur



due to bond failure also. In all the examples solved such a nonlinearity did not occur either due to the provisions taken (e.g., the anchor plates in the deep beam example) or the types of the structures analyzed where bond failure was not critical. If cracking of an already cracked element occurs (e.g., under cyclic loading) bond failure may occur due to the destruction of the element. Hence the analysis should incorporate suitable bond elements in case bond failure is expected.

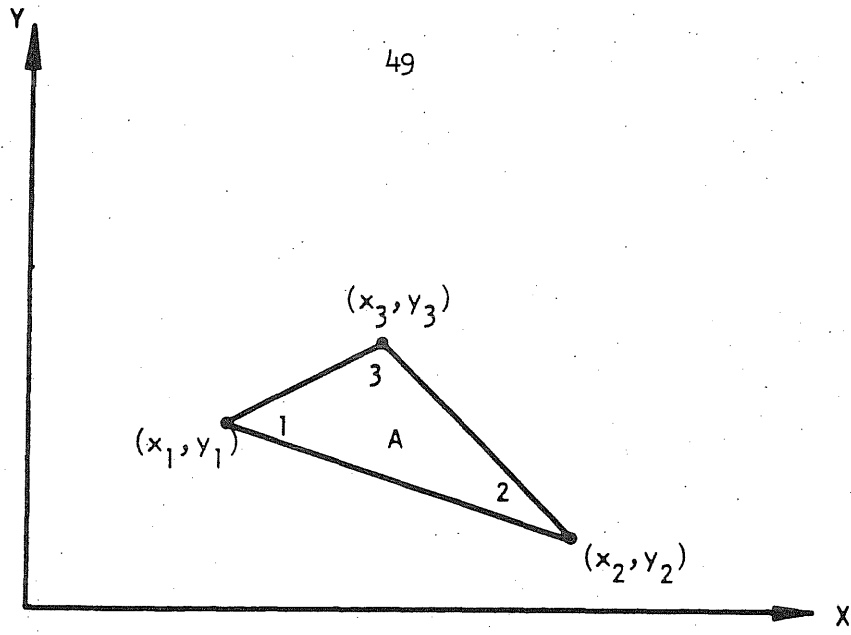


Figure 1, Constant Strain Triangle

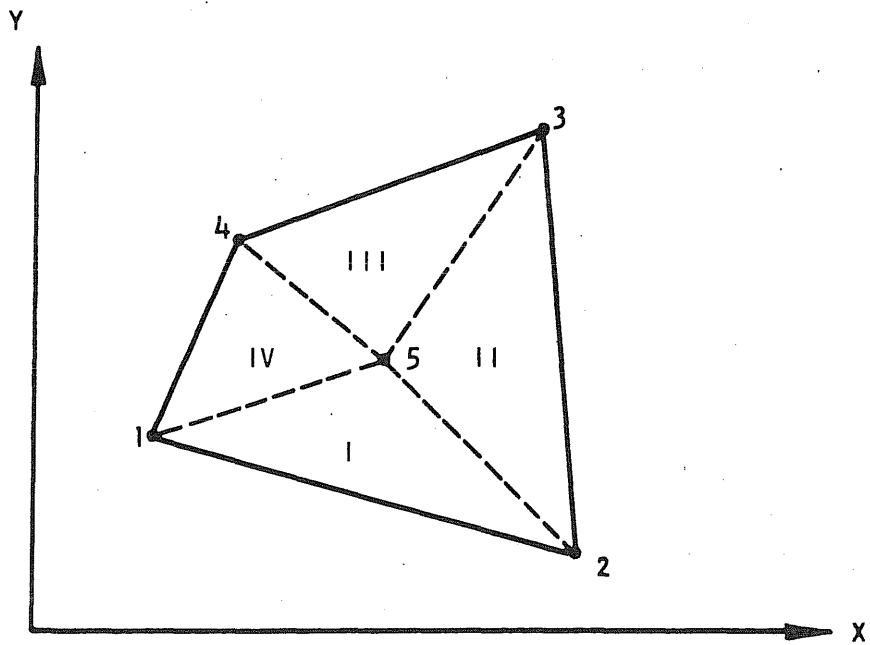
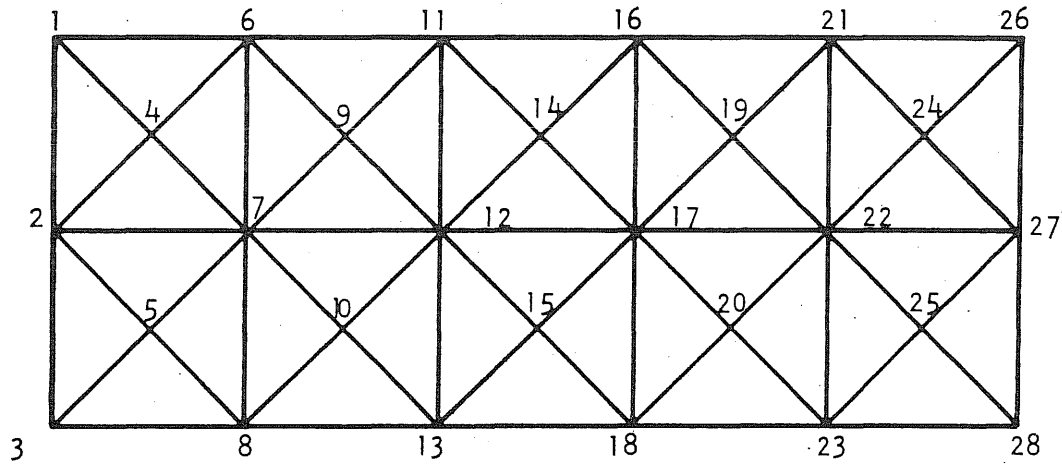
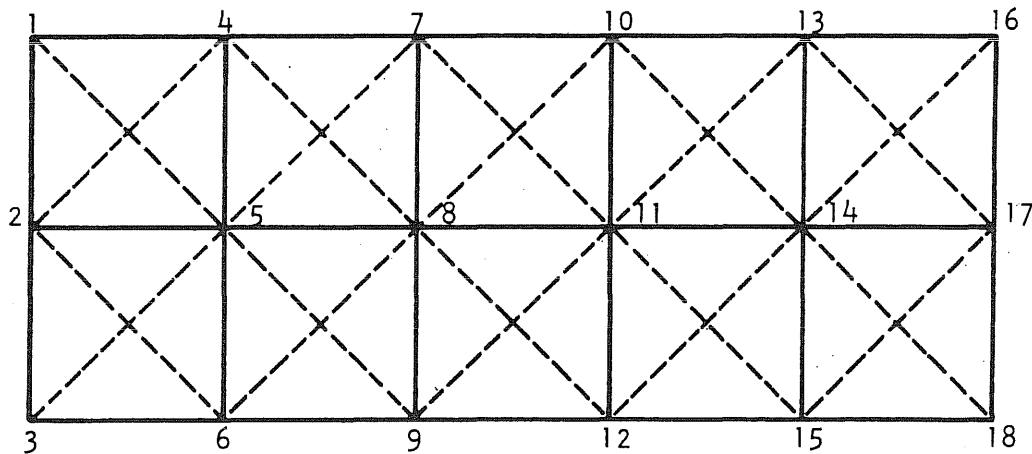


Figure 2, Quadrilateral Element Composed of Four Constant Strain Triangles

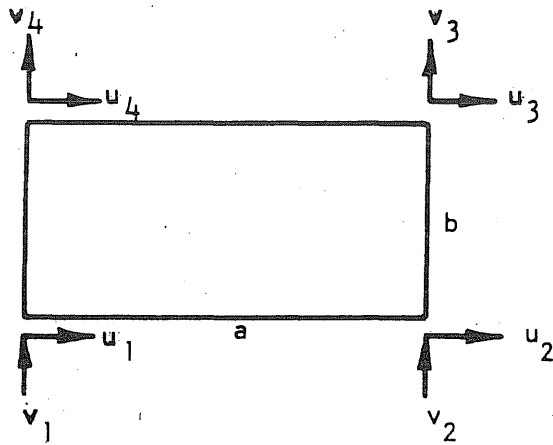


Triangular Elements (40 CST)  
 Number of Nodes = 28  
 Band Width =  $(5 + 1)2 = 12$



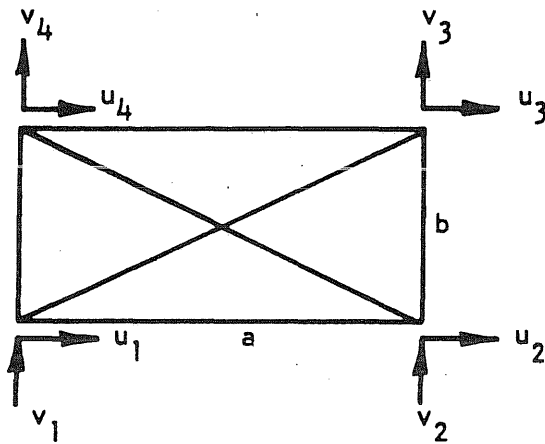
Quadrilateral Elements (10 Q)  
 Number of Nodes = 18  
 Band Width =  $(4 + 1)2 = 10$

Figure 3, Comparison of Mesh Details



- a) Rectangular Element  
Trace of the Stiffness Matrix

$$(8.652) 10^6 \text{ lb/in}$$



- b) Built-up Quadrilateral Element  
Trace of the Stiffness Matrix

$$(7.920) 10^6 \text{ lb/in}$$

Properties Common to Both Elements:

$$a = 5.0 \text{ in}$$

$$b = 3.0 \text{ in}$$

$$\text{Modulus of Elasticity} = (2.4) 10^6 \text{ psi}$$

$$\text{Poisson's Ratio} = 0.0$$

$$\text{Thickness} = 2.0 \text{ in}$$

Figure 4, Stiffness Comparison of the Built-up Quadrilateral and Rectangular Elements

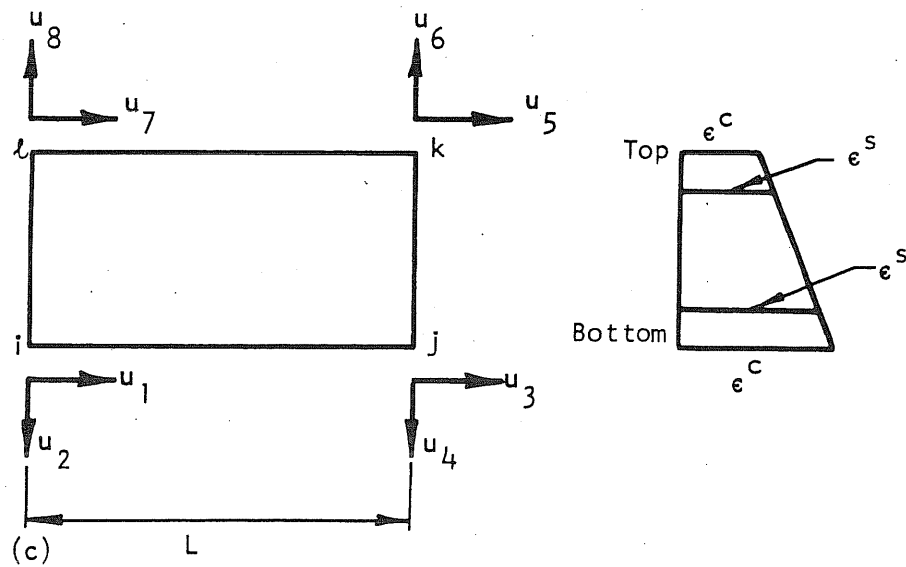
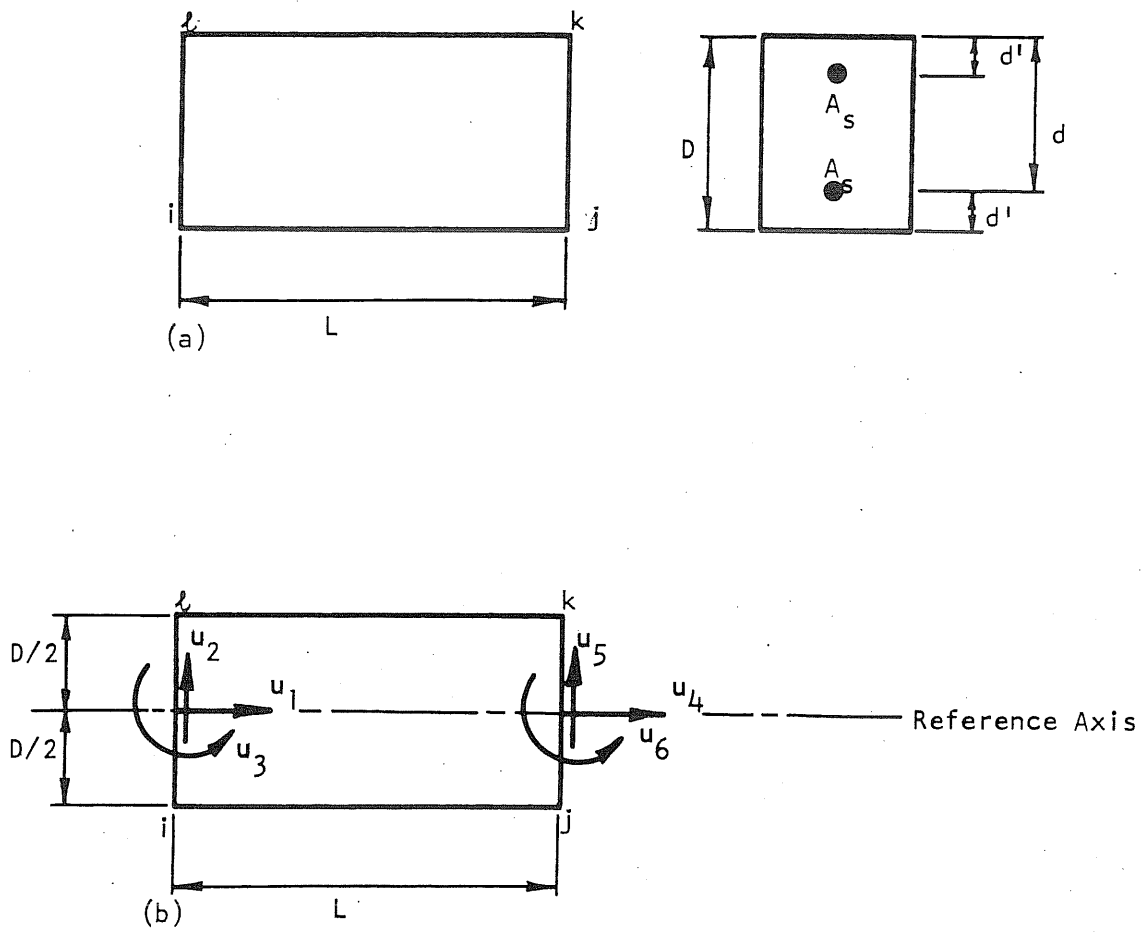
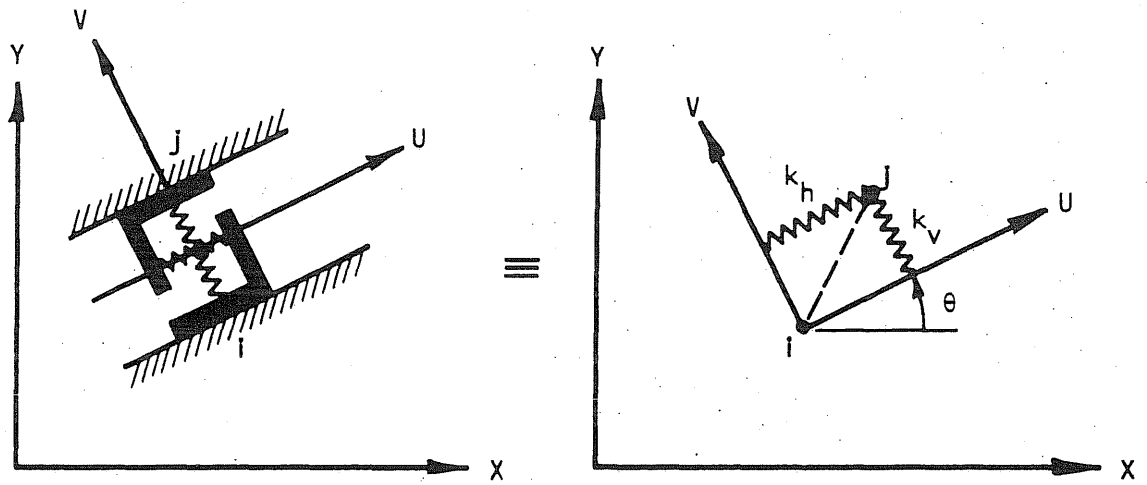


Figure 5, Frame Elements



a) Fictitious Link

b) Spring Constants for the Link

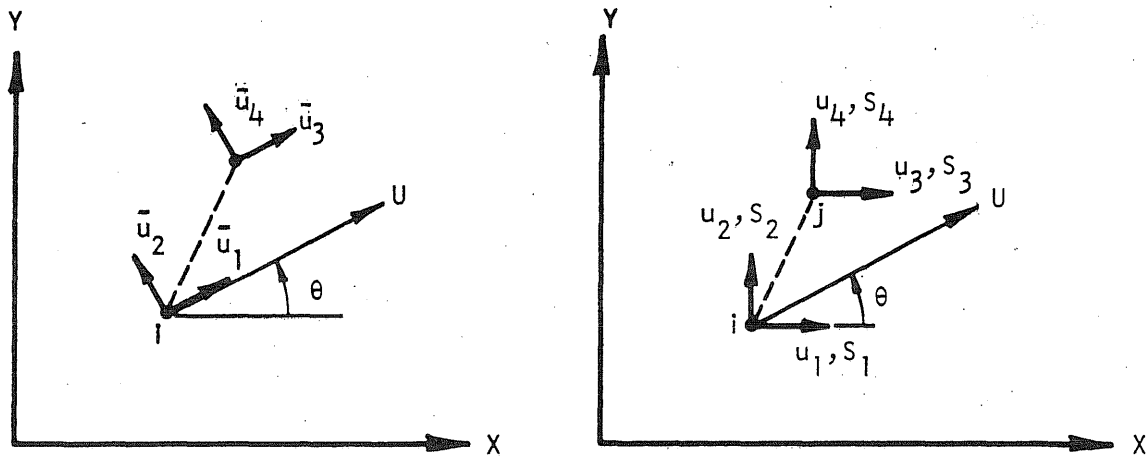
c) Displacements in UV  
Coordinatesd) Displacements in XY - Global  
Coordinates

Figure 6, Link Elements

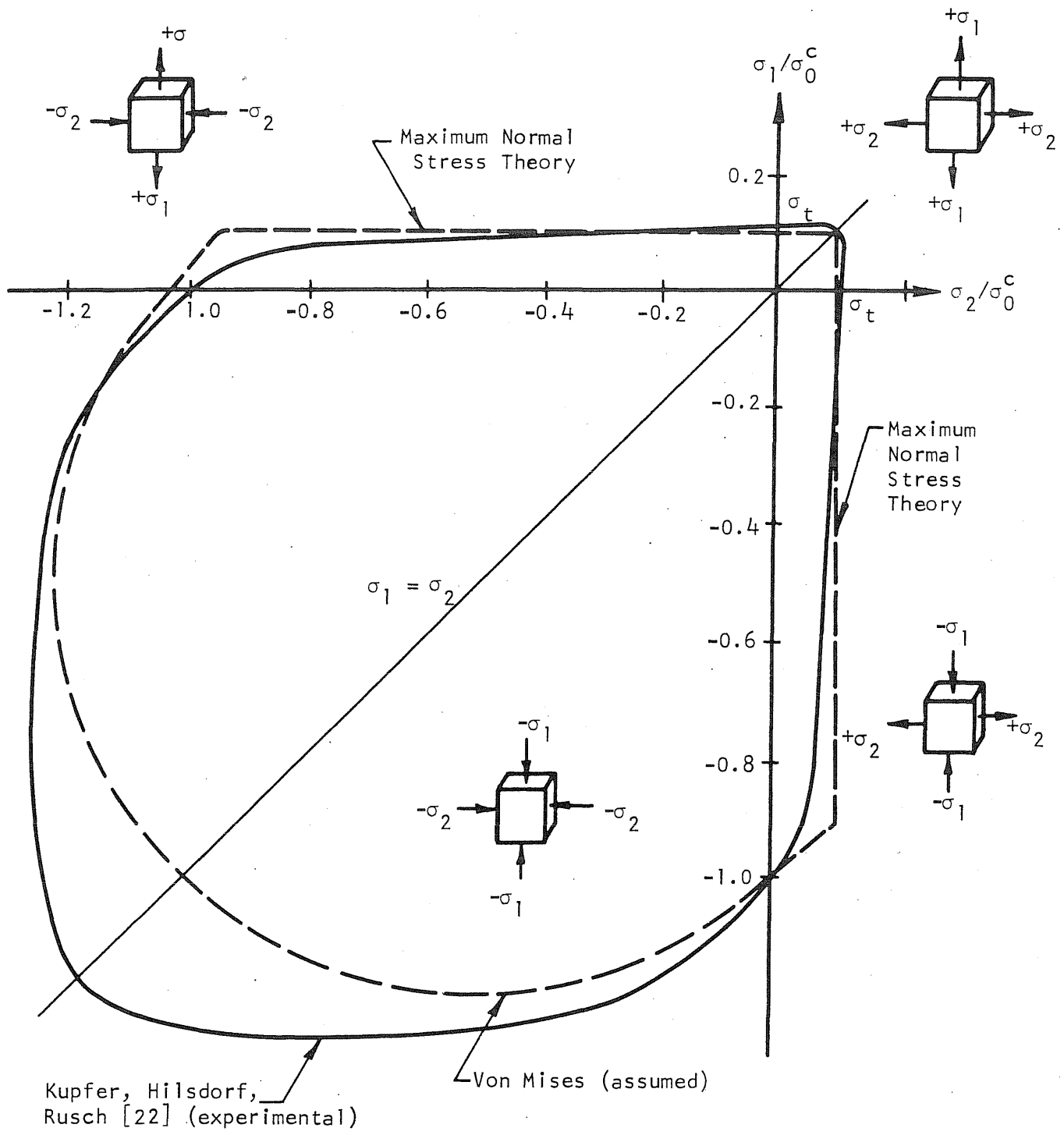
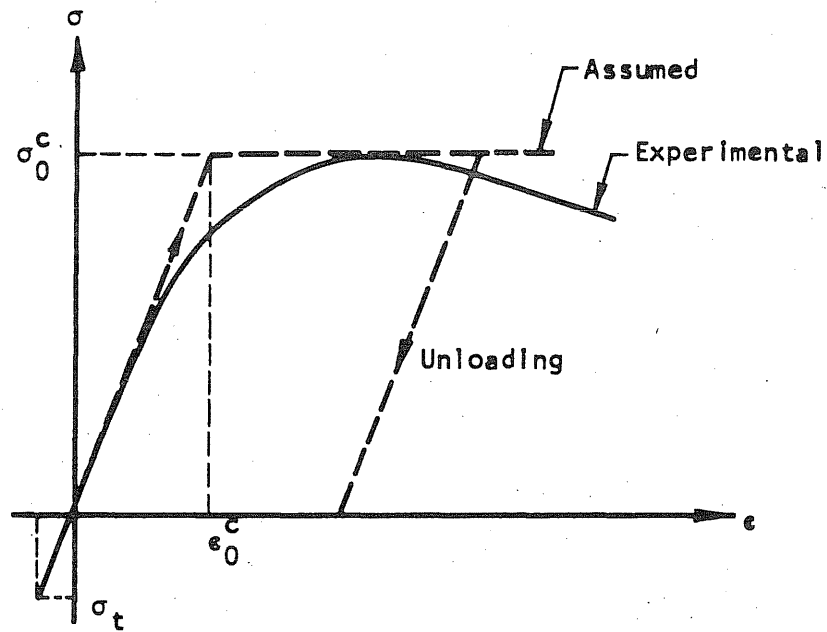
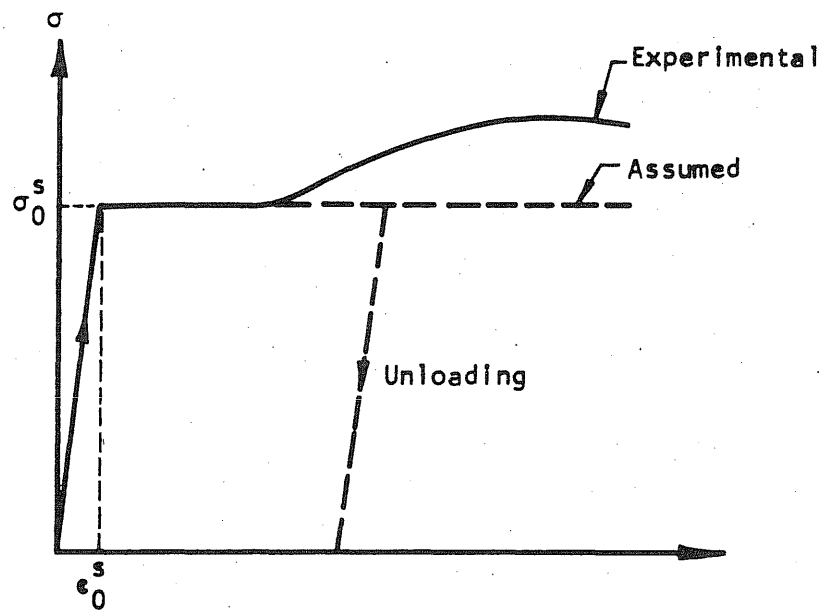


Figure 7, Biaxial Strength of Concrete



a) Uniaxial Stress-Strain Relationship for Concrete



b) Stress-strain Relationship for the Reinforcement

Figure 8, Stress-Strain Diagrams



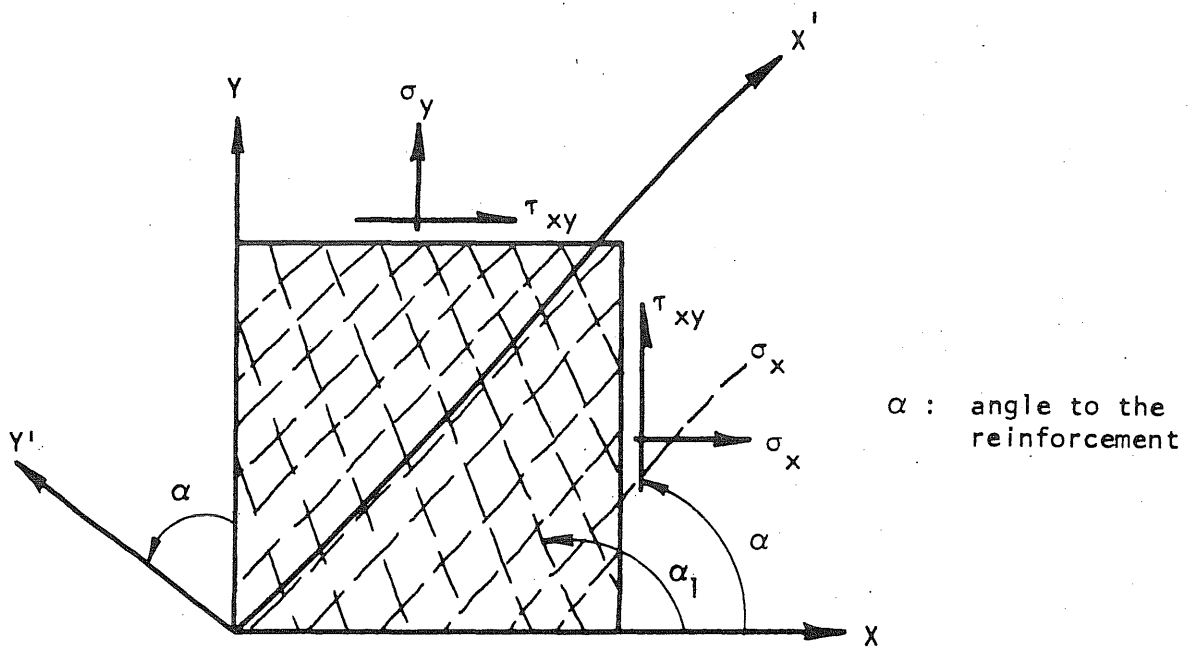


Figure 9, Distribution of the Reinforcement

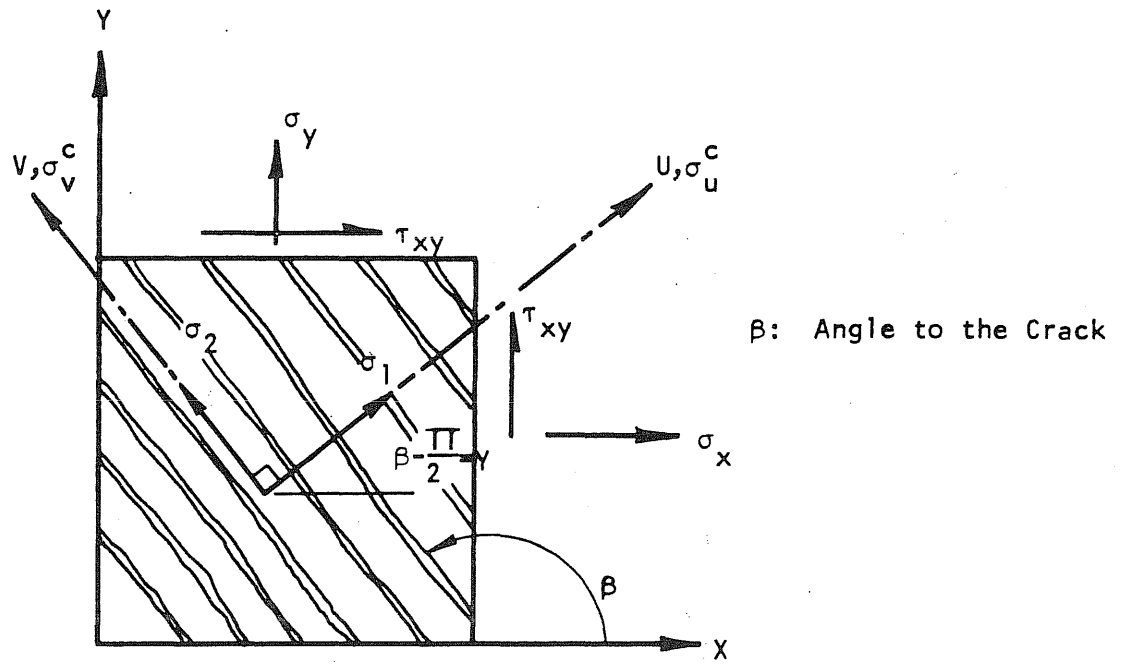


Figure 10, Principal Stresses and Cracking

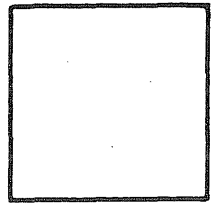
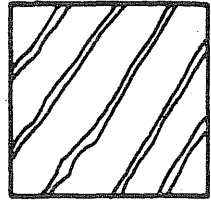
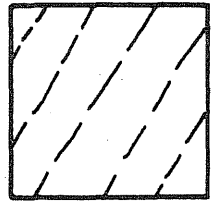
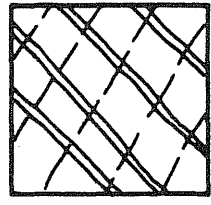
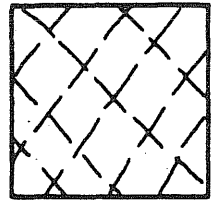
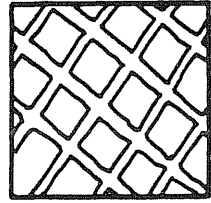
|   | Mode | Description of the Mode                                 |
|---|------|---|
|    | 0    | Uncracked Concrete                                      |
|    | 1    | Cracks in One Direction                                 |
|    | 2    | First Set of Cracks Closed                              |
|  | 3    | First Set of Cracks Closed, Second Set of Cracks Opened |
|  | 4    | Both Sets of Cracks Closed                              |
|  | 5    | Two Sets of Cracks Open at the Same Time                |

Figure 11, Crack Modes for Wall Elements

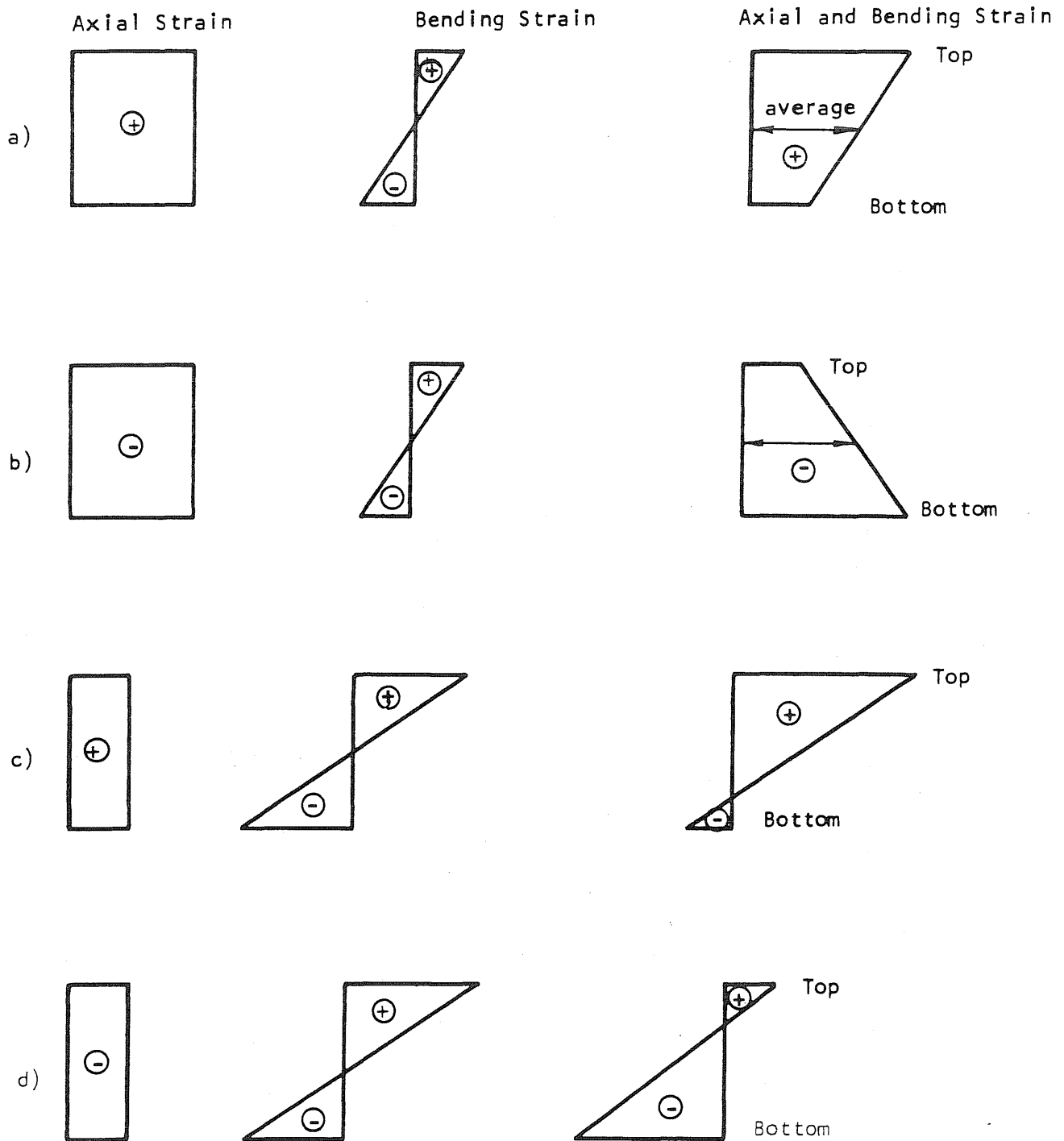


Figure 12, Assumed Strain Distributions for the Flexural Elements

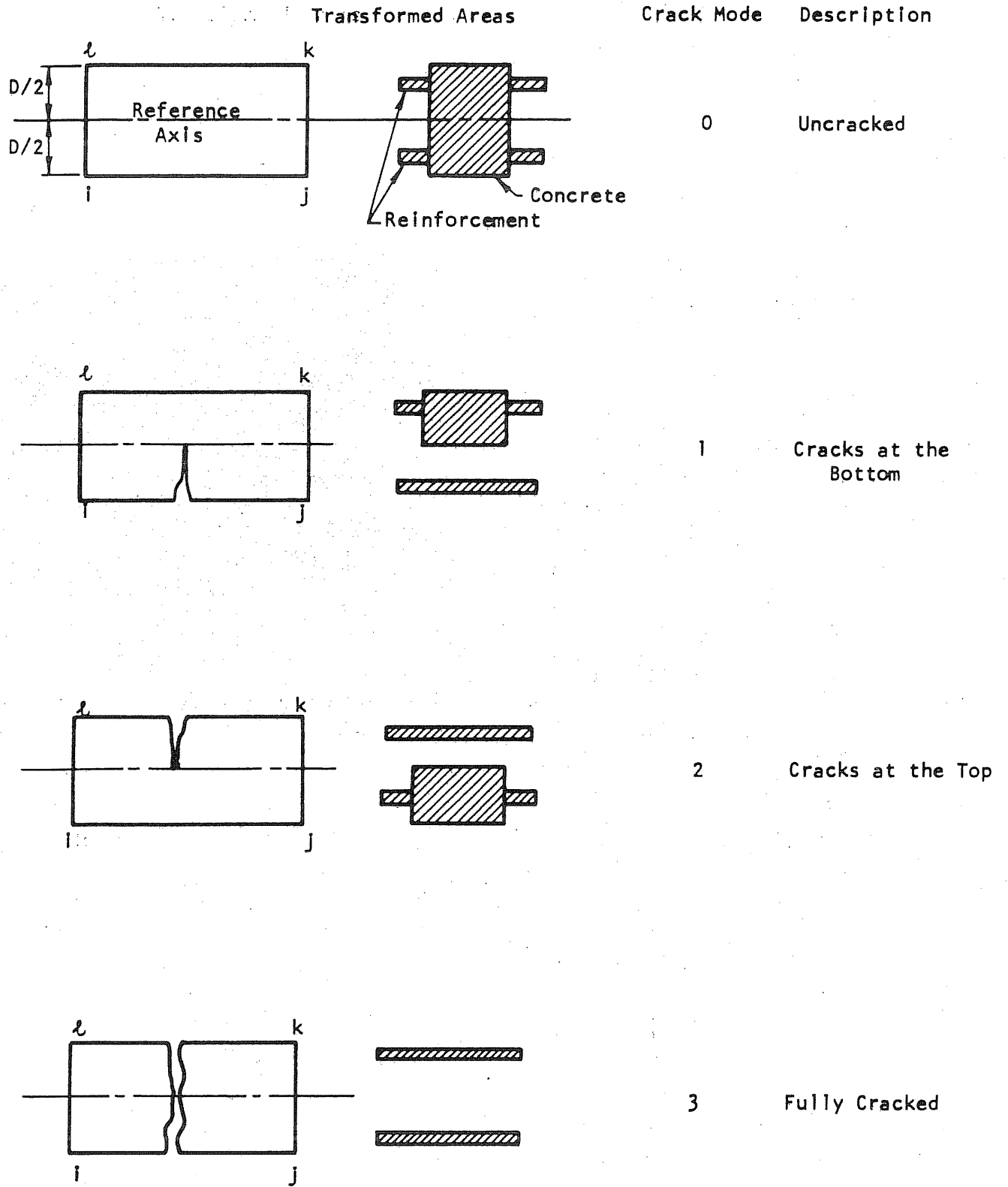


Figure 13, Assumed Crack Modes for the Flexural Elements

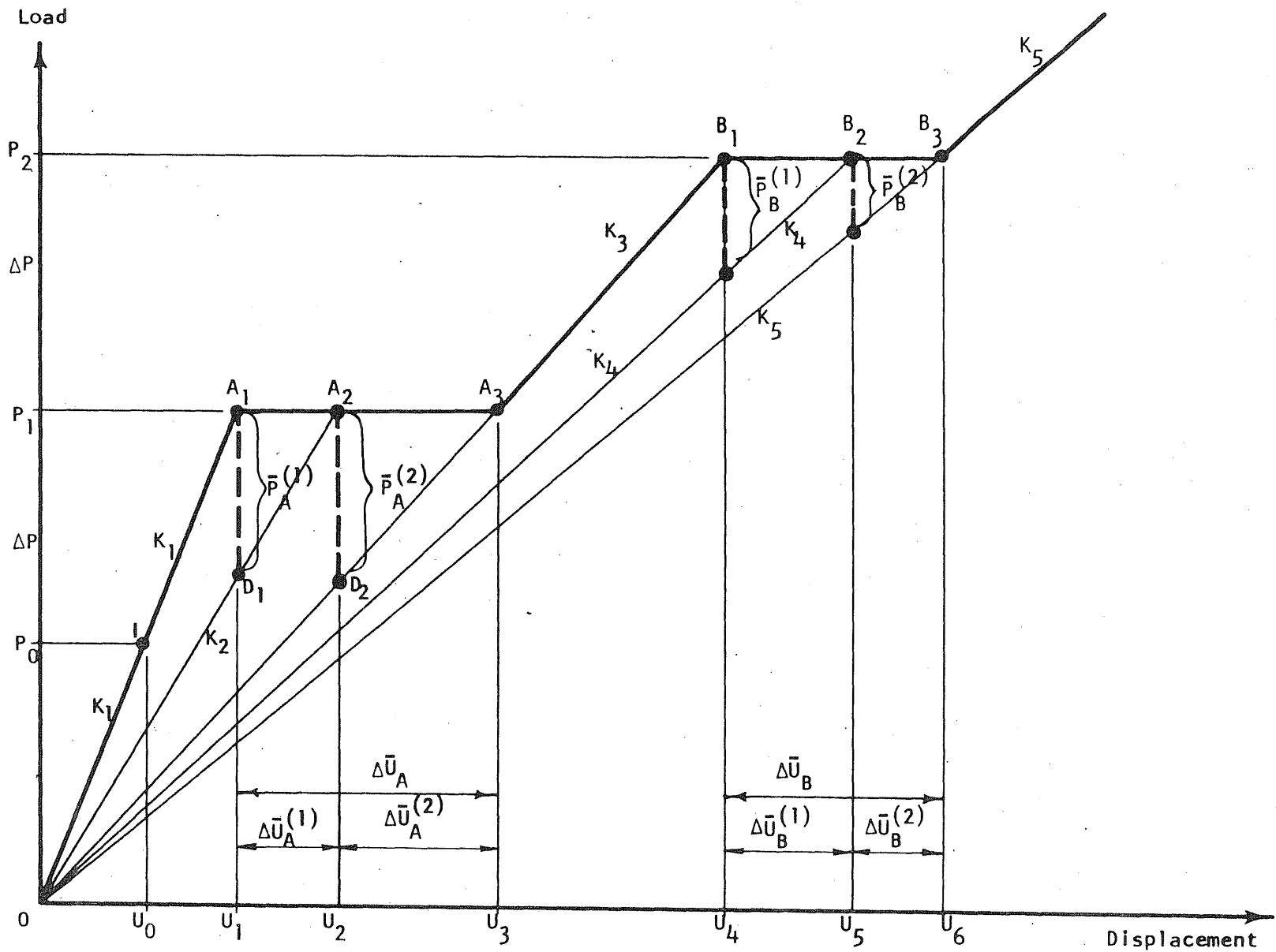


Figure 14, Schematic Diagram to Illustrate Crack Propagation  
 (Method 1: Initial Stress Method Using Variable  
 Stiffness Within an Increment)

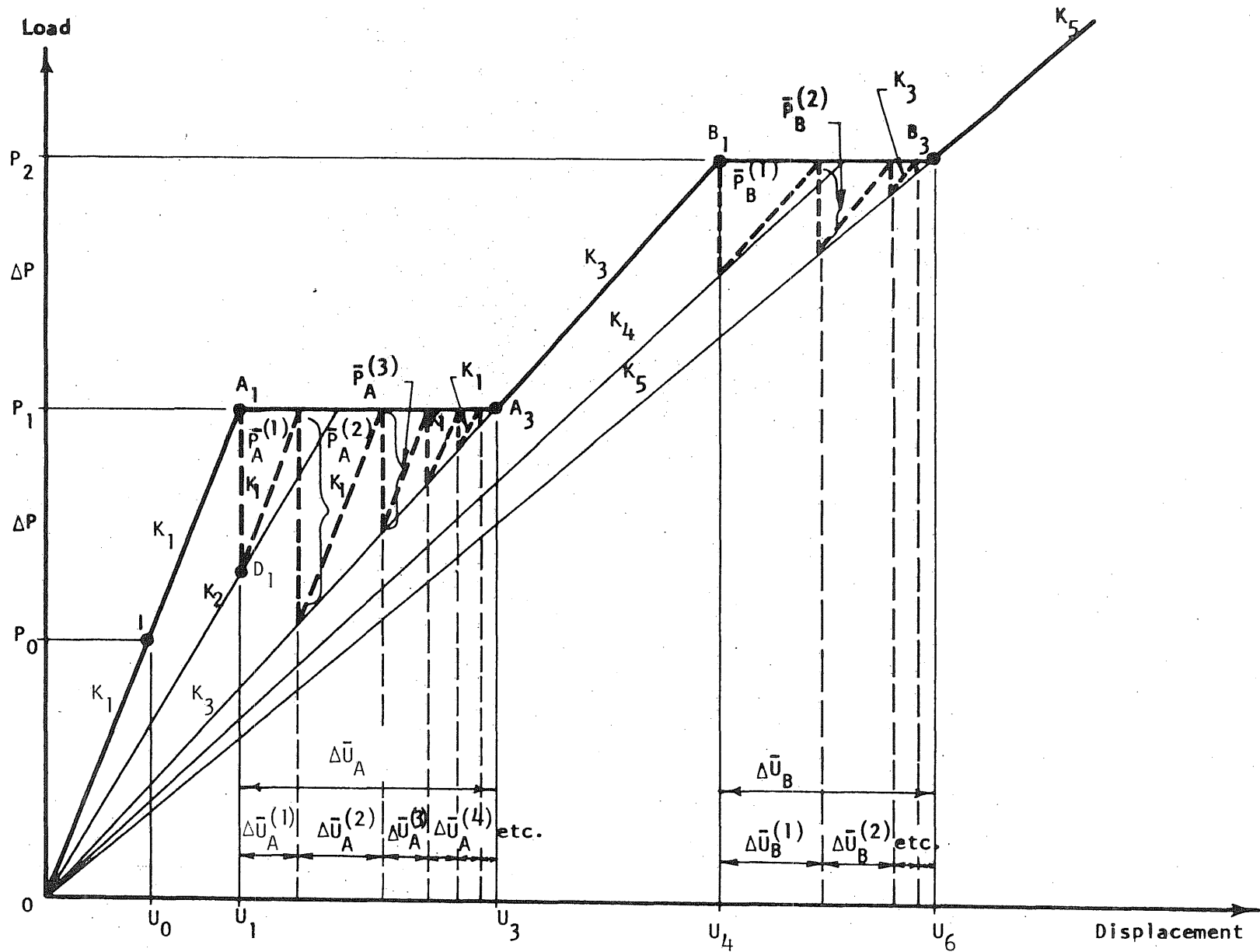


Figure 15, Schematic Diagram to Illustrate Crack Propagation  
 (Method 2: Initial Stress Method Using Constant  
 Stiffness Within an Increment)

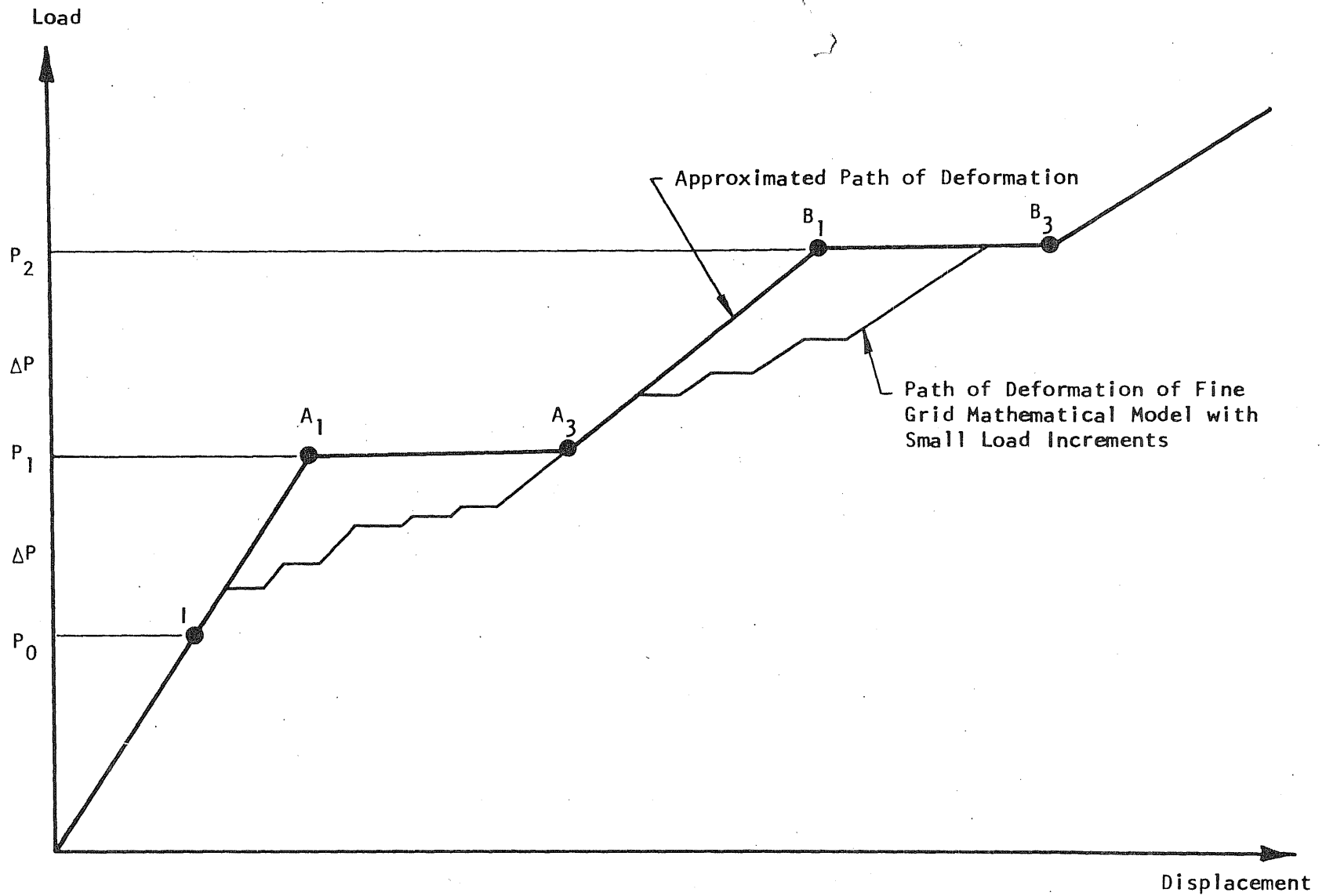


Figure 16, Comparison of Paths of Deformation

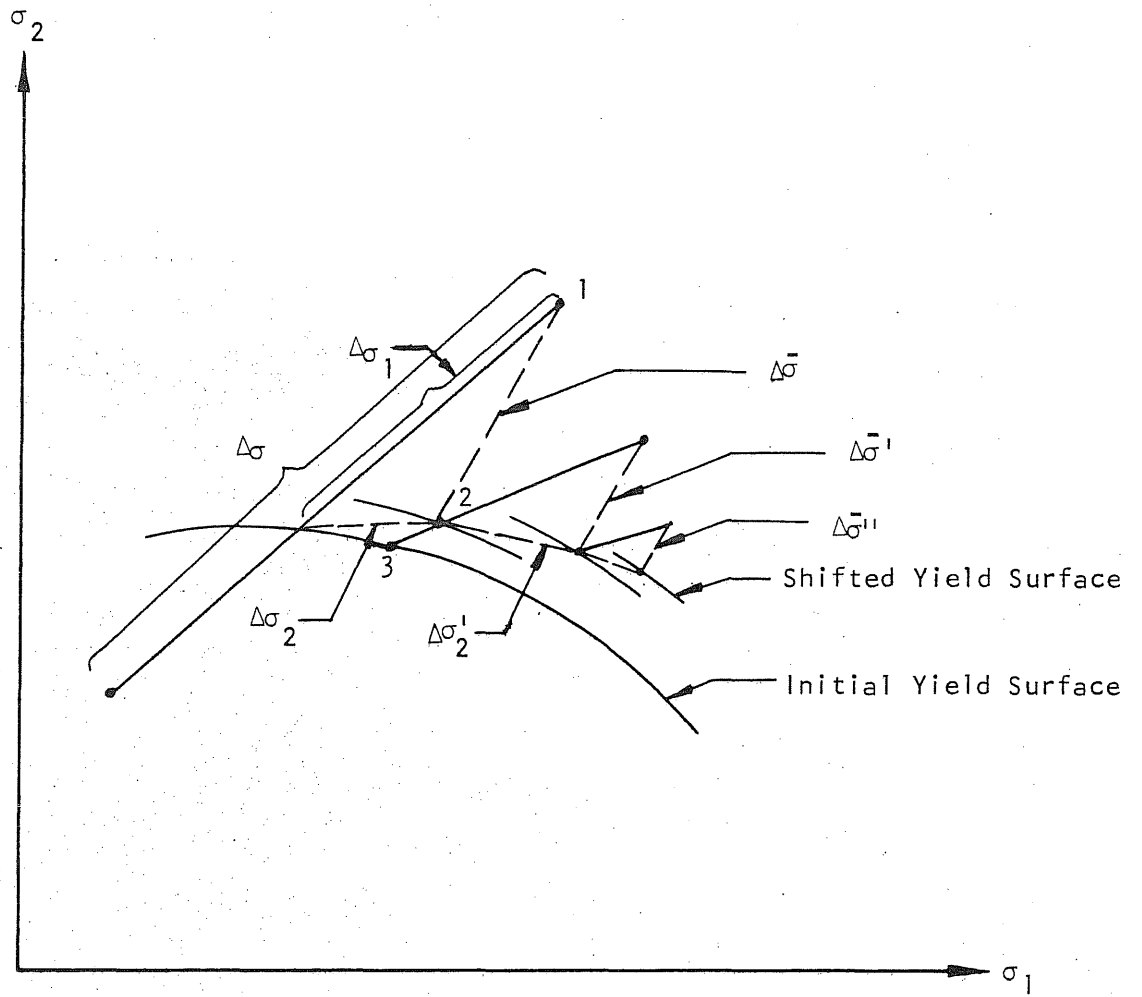
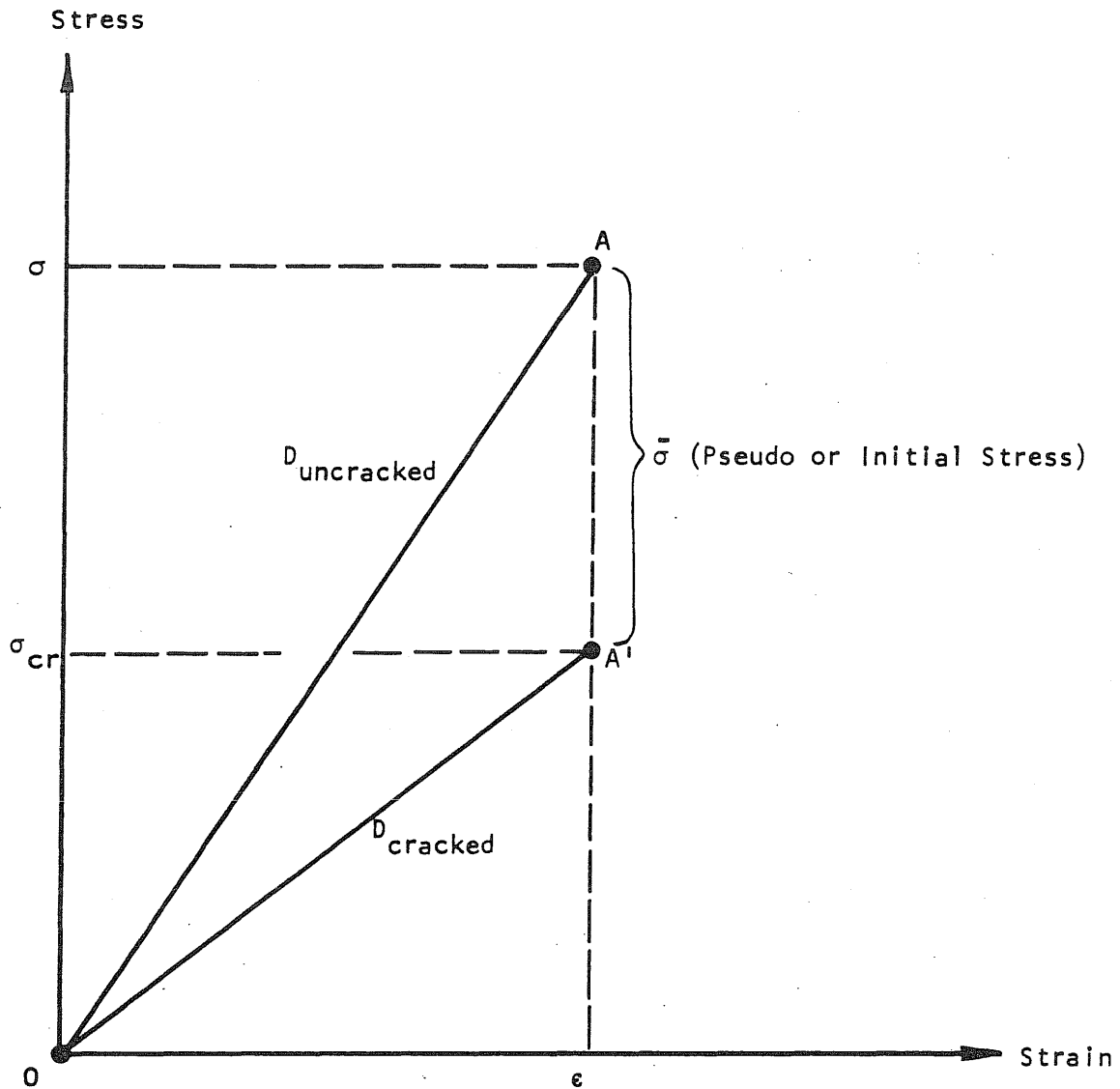


Figure 17, Schematic Illustration of the Distribution of Pseudo Stresses Due to Biaxial Plasticity of Concrete





Note: The lettering of stress and strain quantities are symbolic only.

Figure 18, Pseudo Stresses Released Due to Cracking

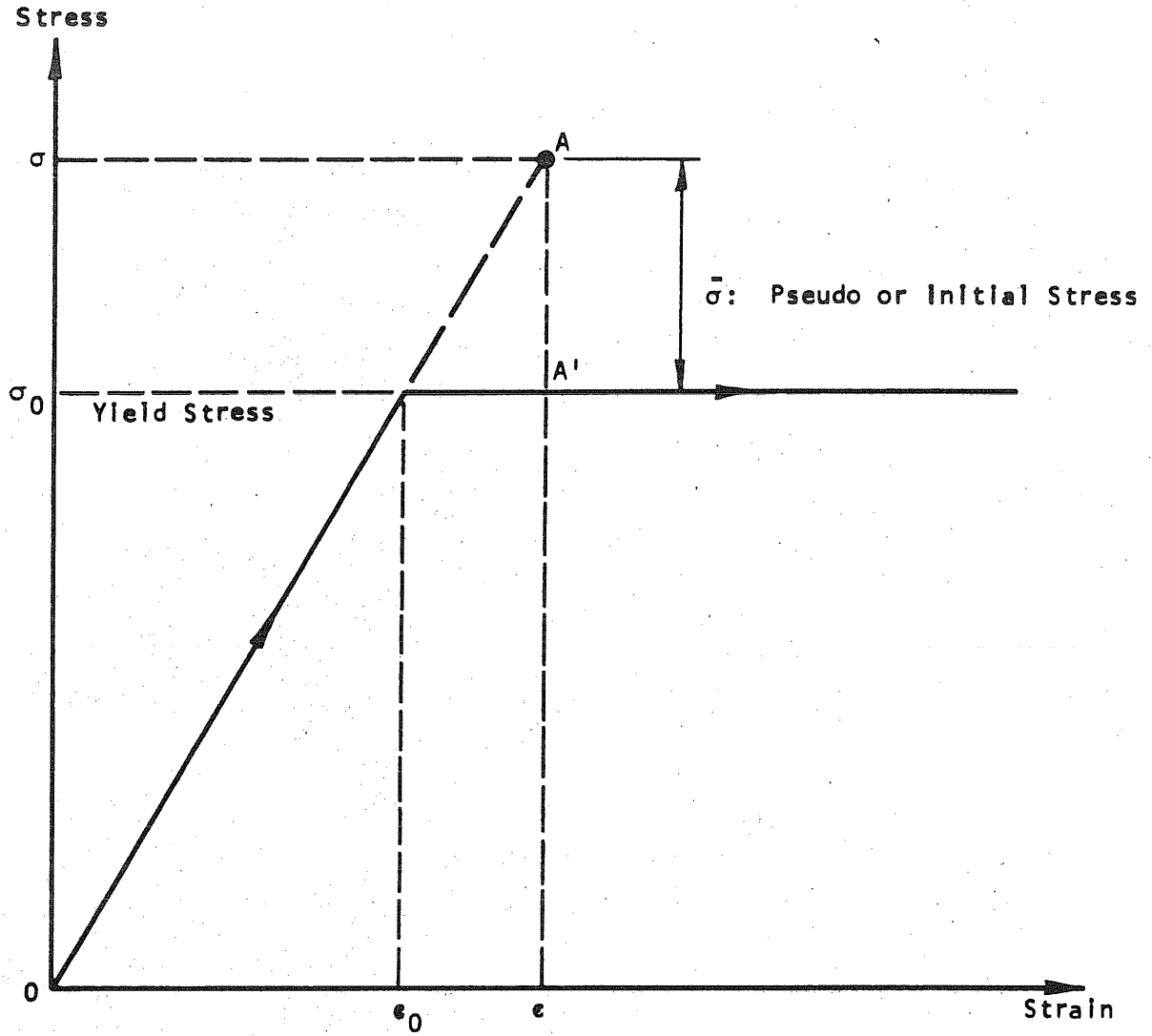


Figure 19, Schematic Illustration of the Pseudo Stresses Released Due to Uniaxial Plasticity of a Component Material (Cracked Concrete or Reinforcement)

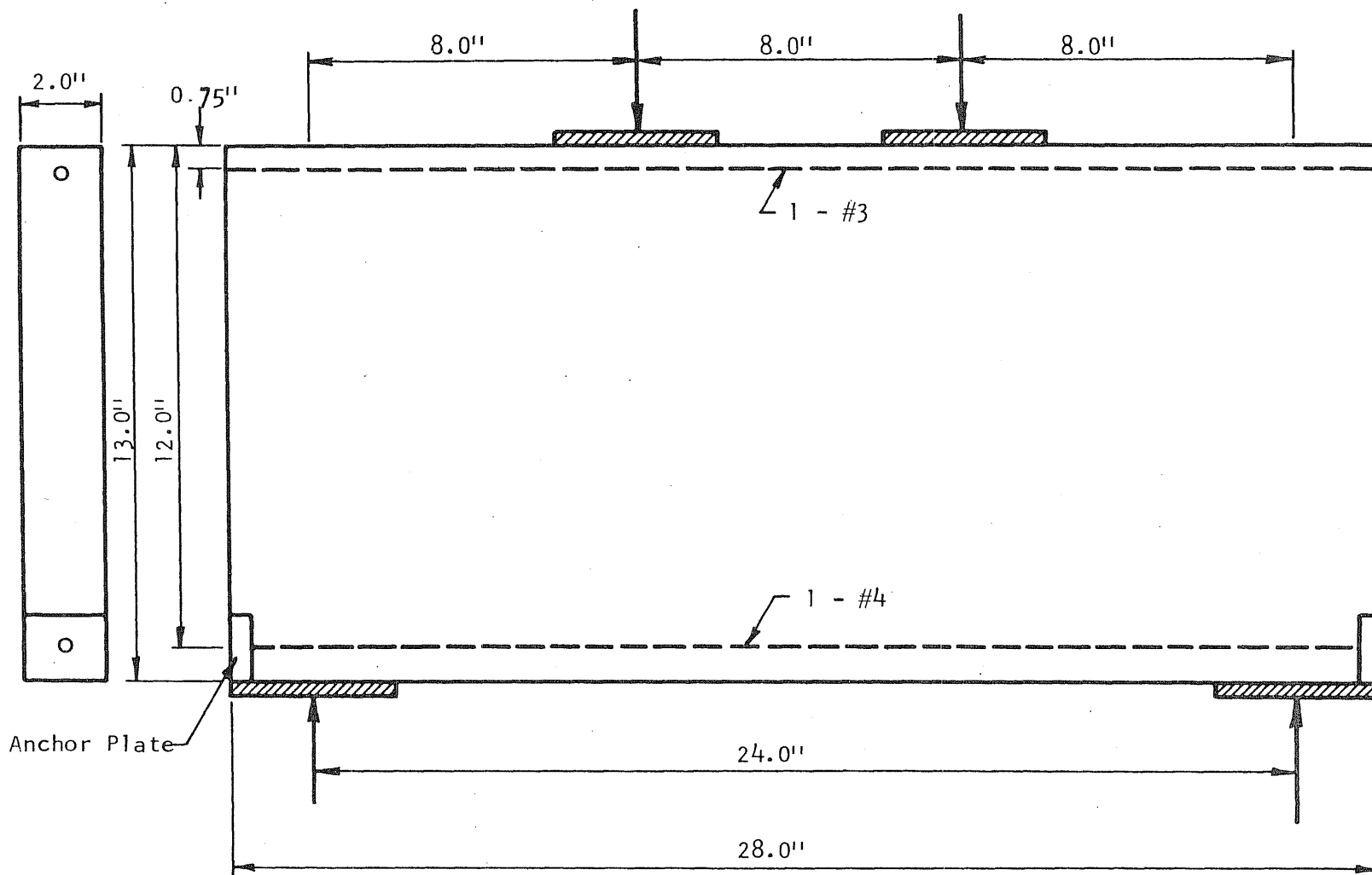


Figure 20, Deep Beam G24S-11 [20]

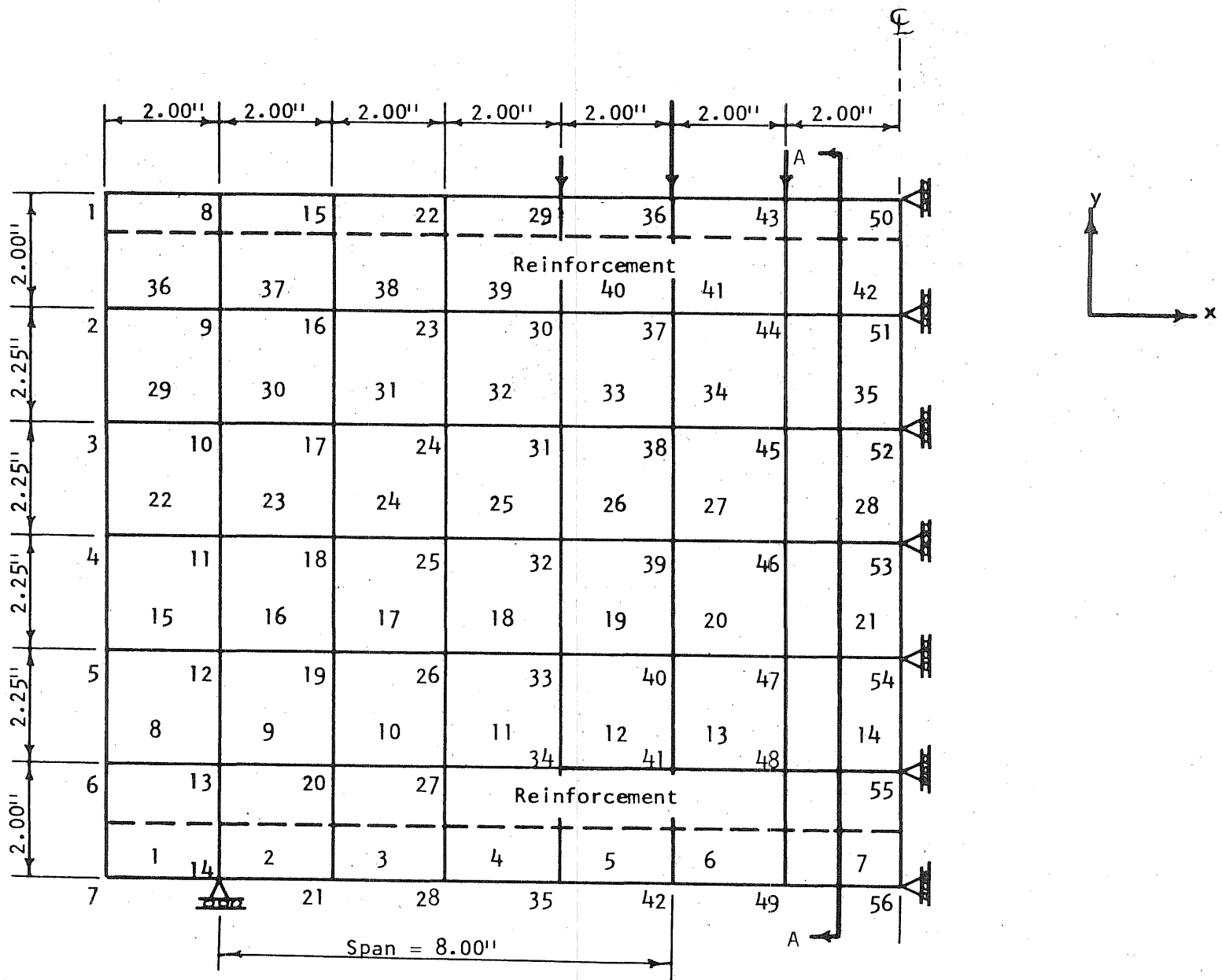
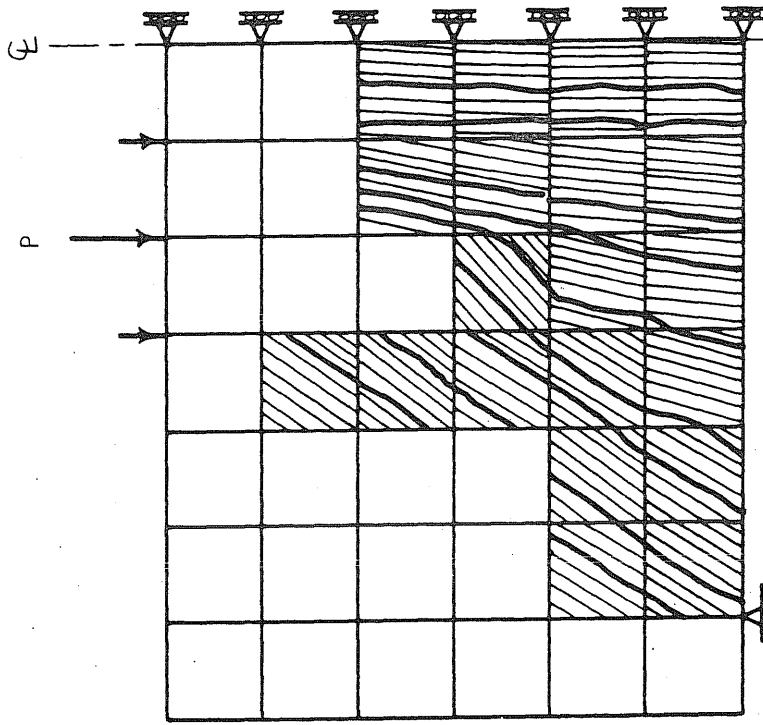
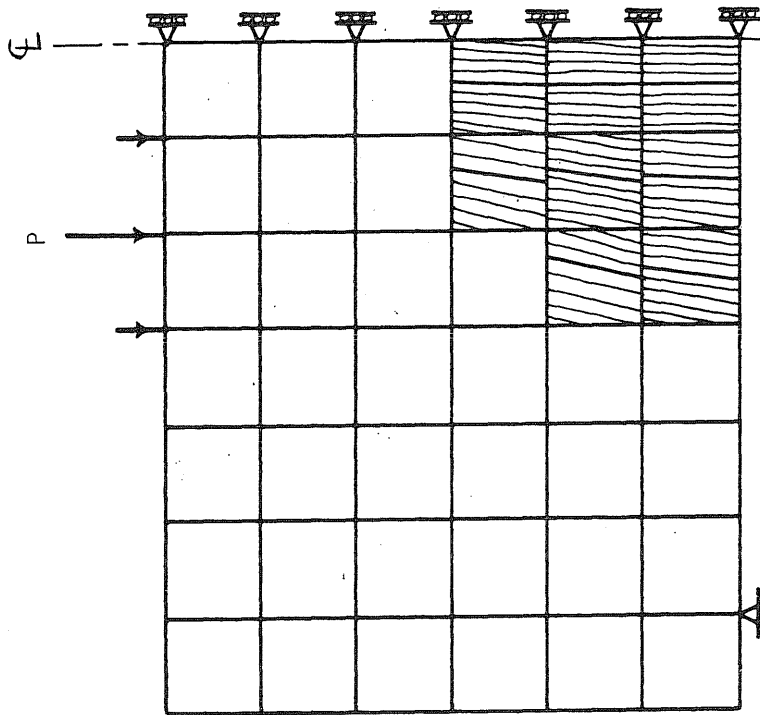


Figure 21, Discretized Model (Specimen G24S-11)



@ P = 20 kips



@ P = 15 kips

Figure 22, Crack Propagation (Specimen 324S-11)

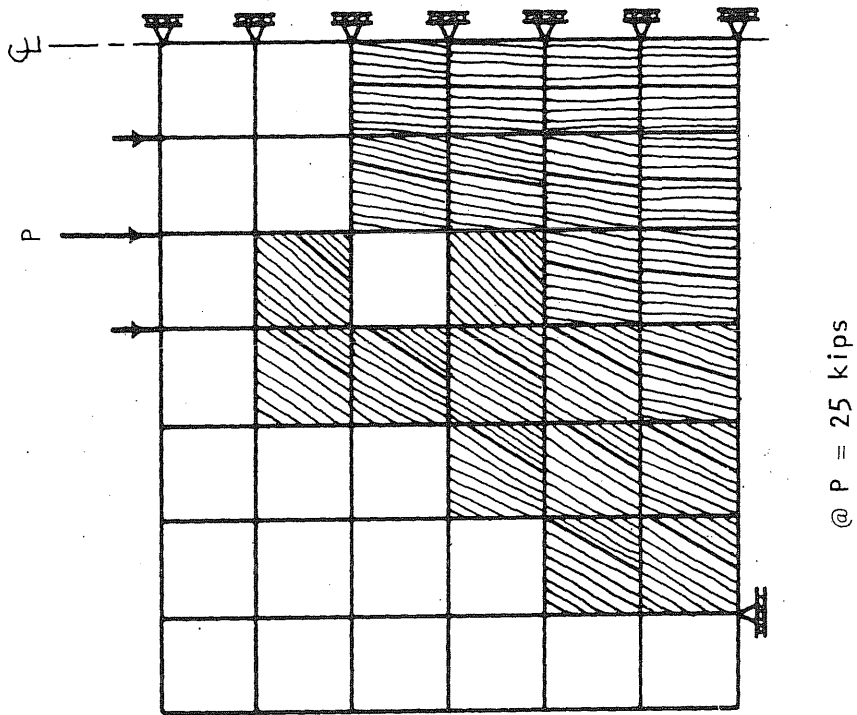
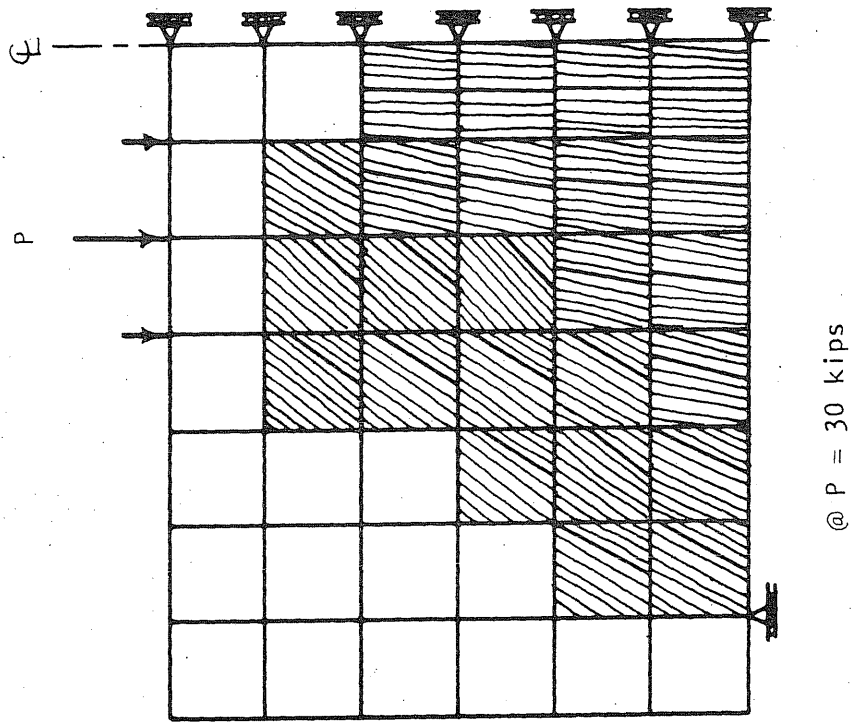


Figure 23, Crack Propagation (Specimen G24S-11)

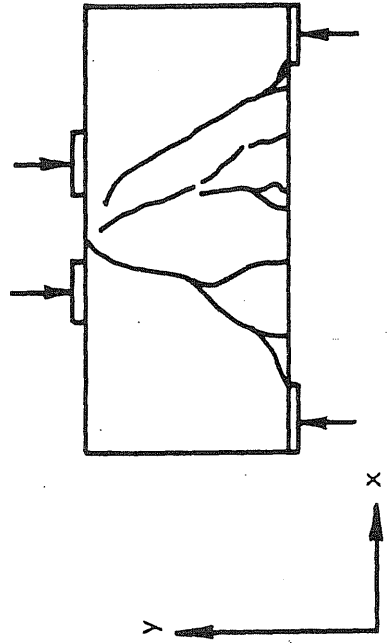


Figure 24, Experimental Crack Pattern (Specimen G24S-11) [20]

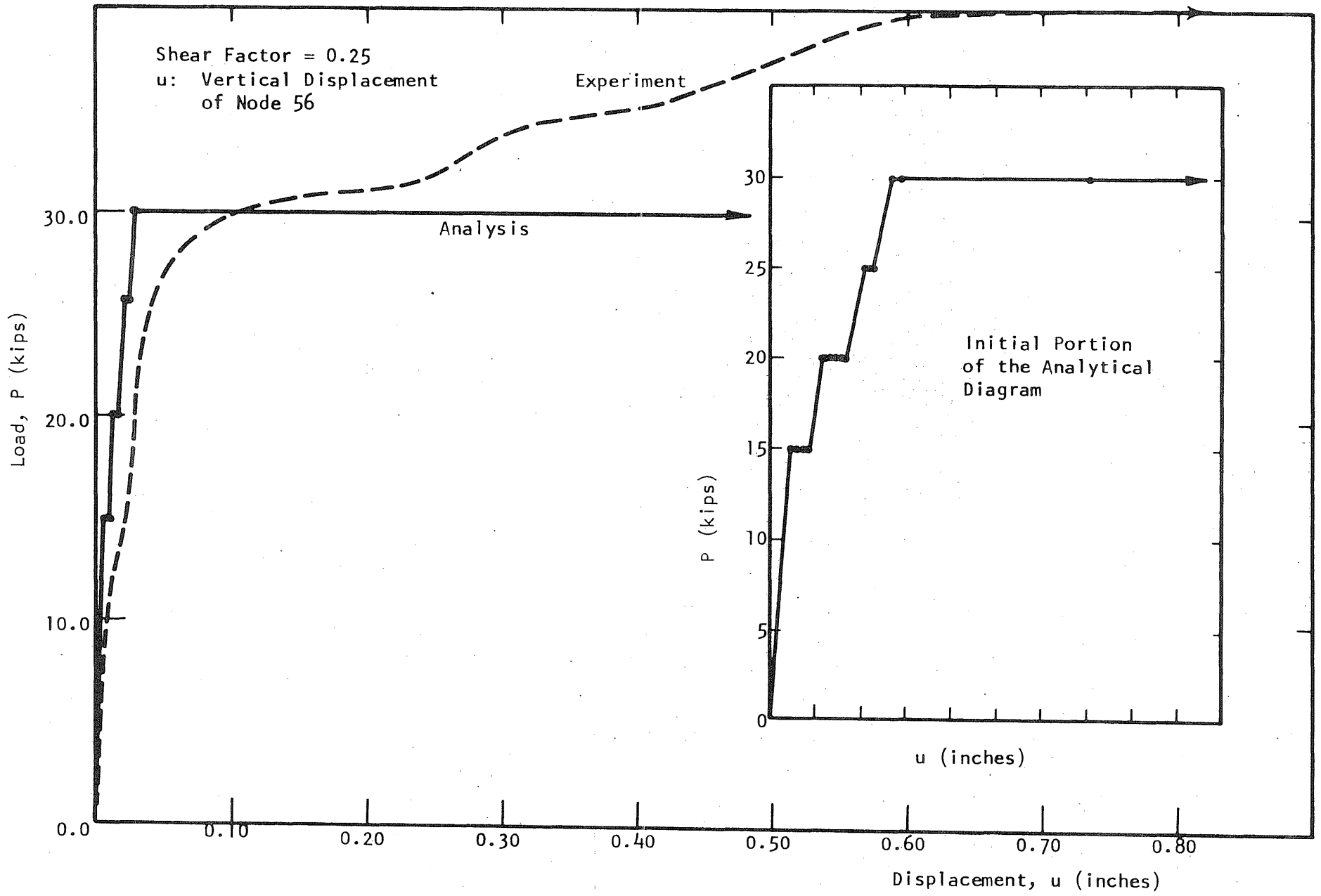


Figure 25, Comparison of Analytical and Experimental Load-Displacement Diagrams (Specimen G24S-11)



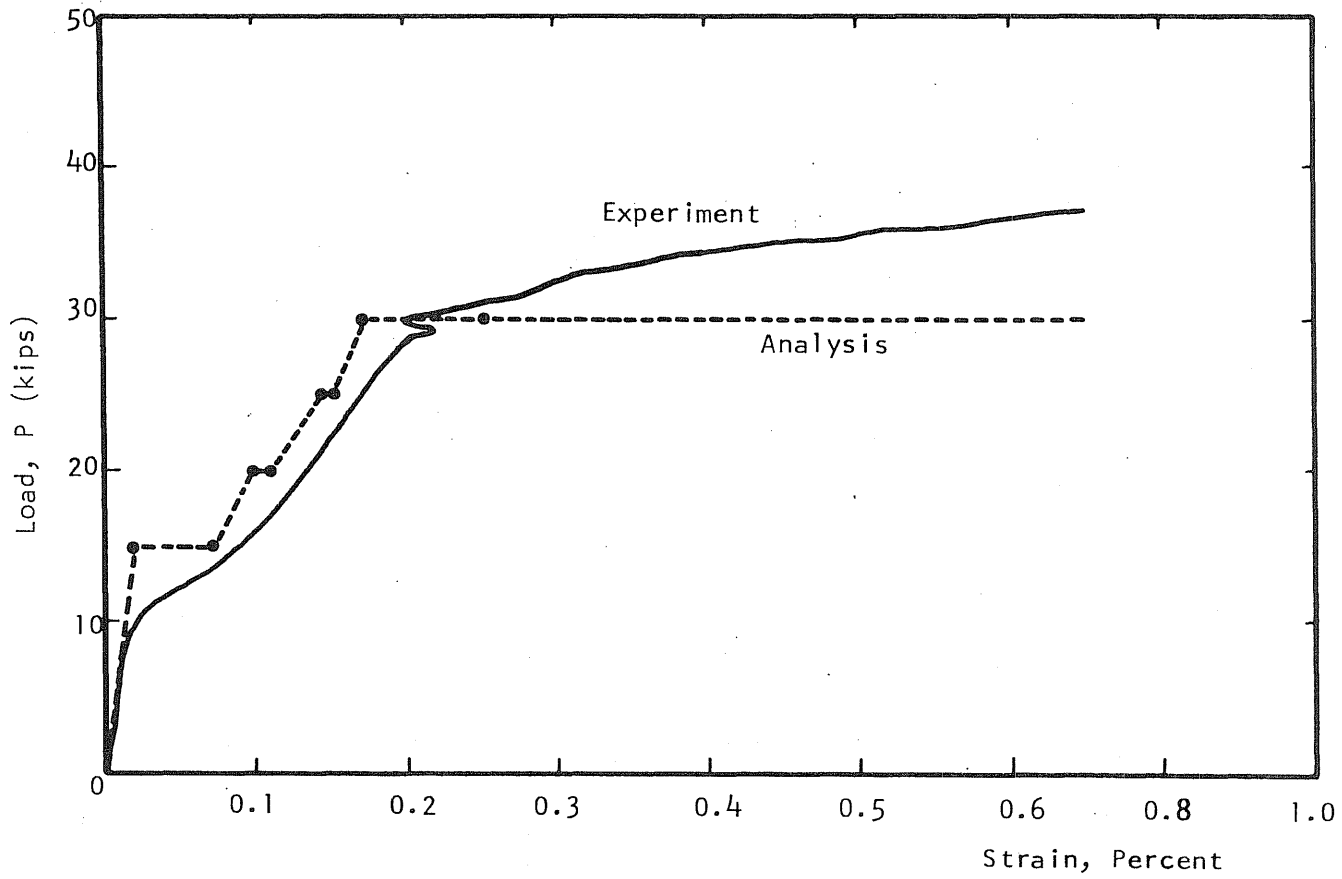
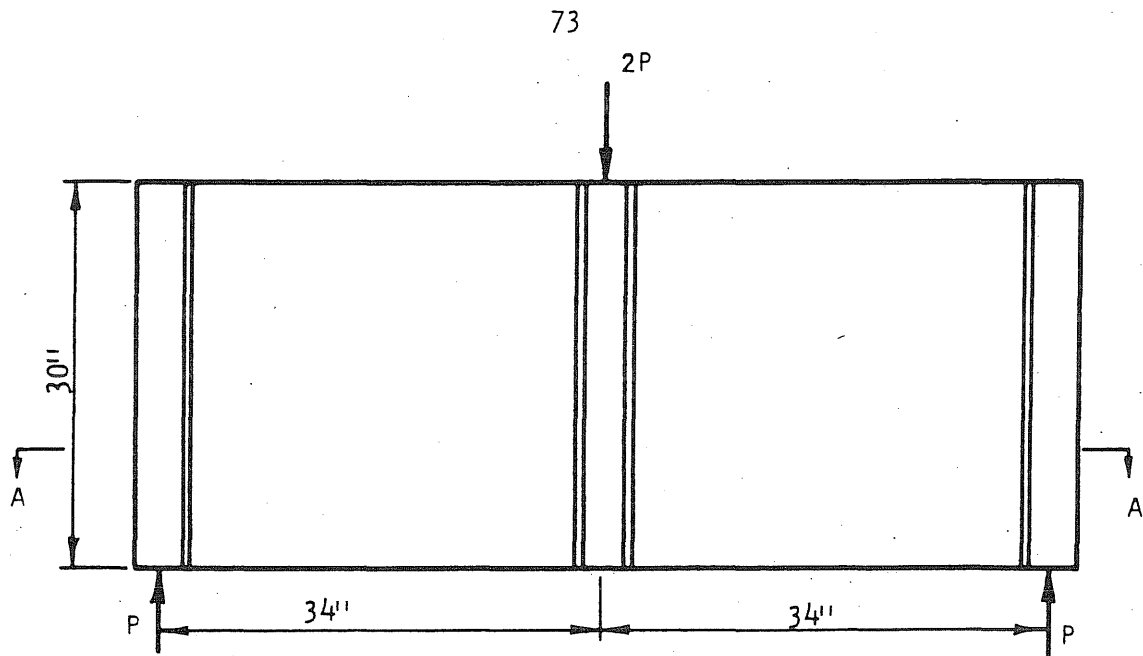
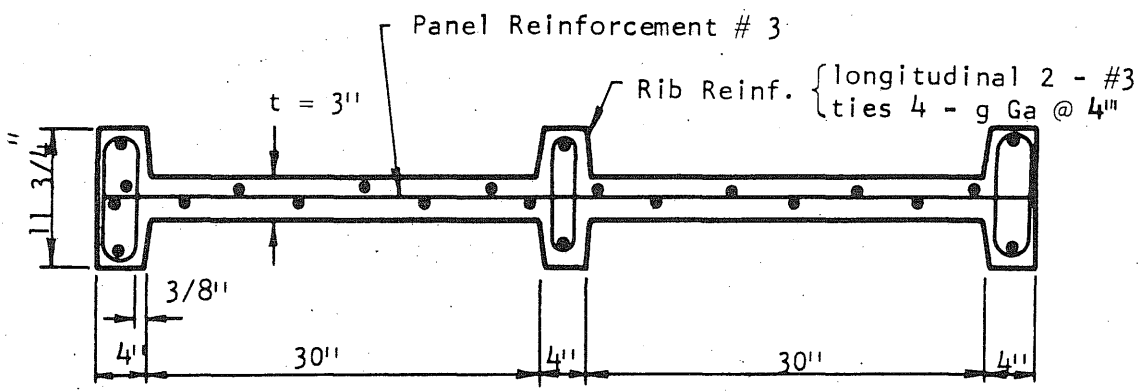


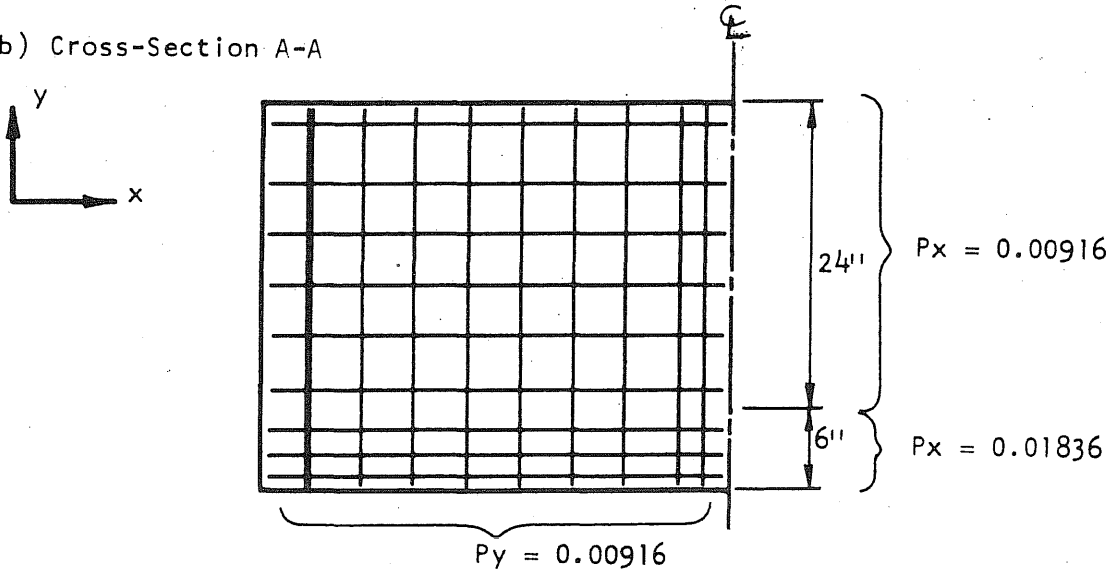
Figure 26, Comparison of Load Versus Tension Steel Strains (Specimen G24S-11)



a) Specimen



b) Cross-Section A-A



c) Reinforcing Ratios

Figure 27, Geometry and the Cross-Sectional Properties of Specimen W2 [17]

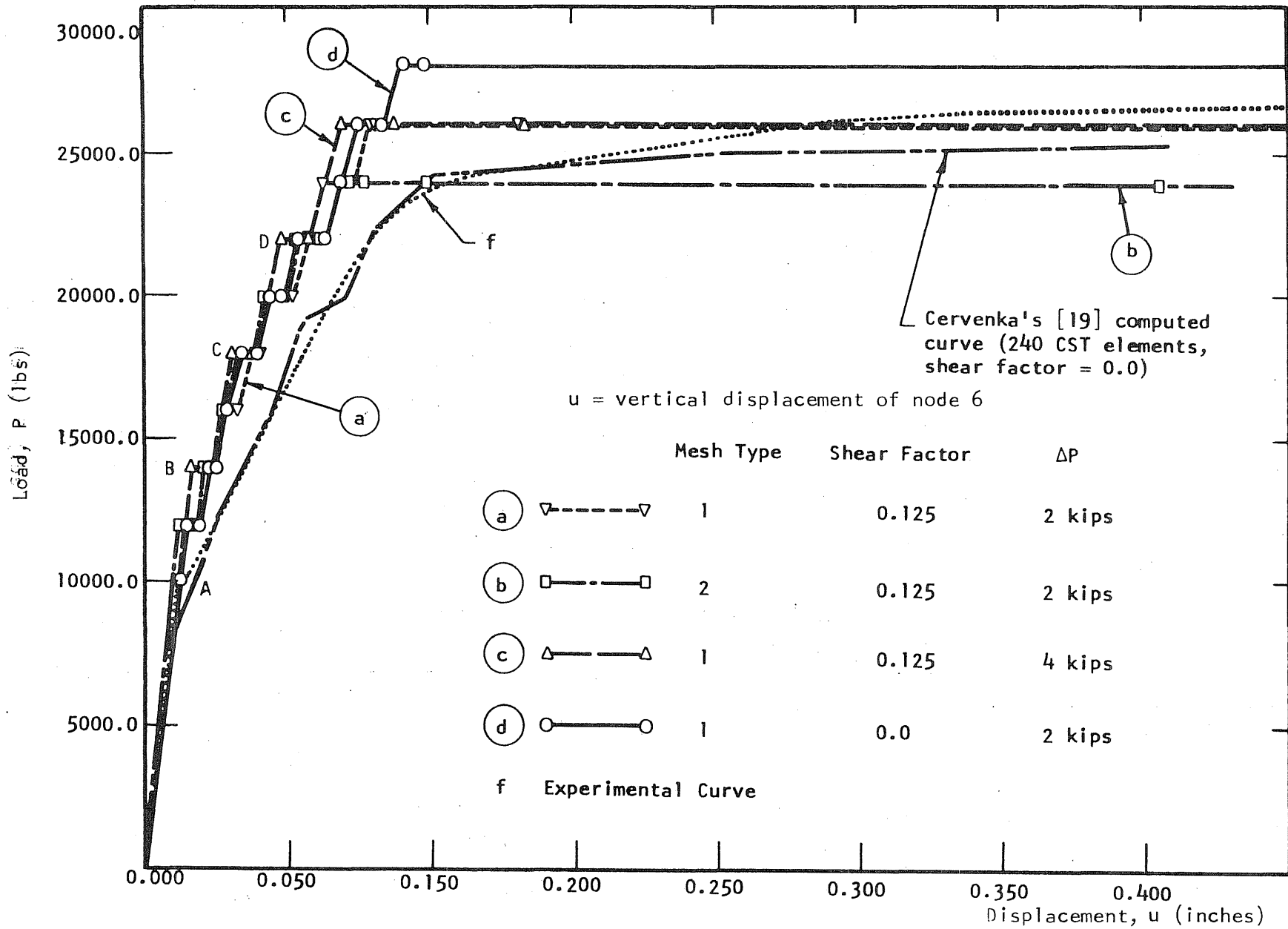


Figure 28, Comparison of the Load-Displacement Curves (Specimen W2)

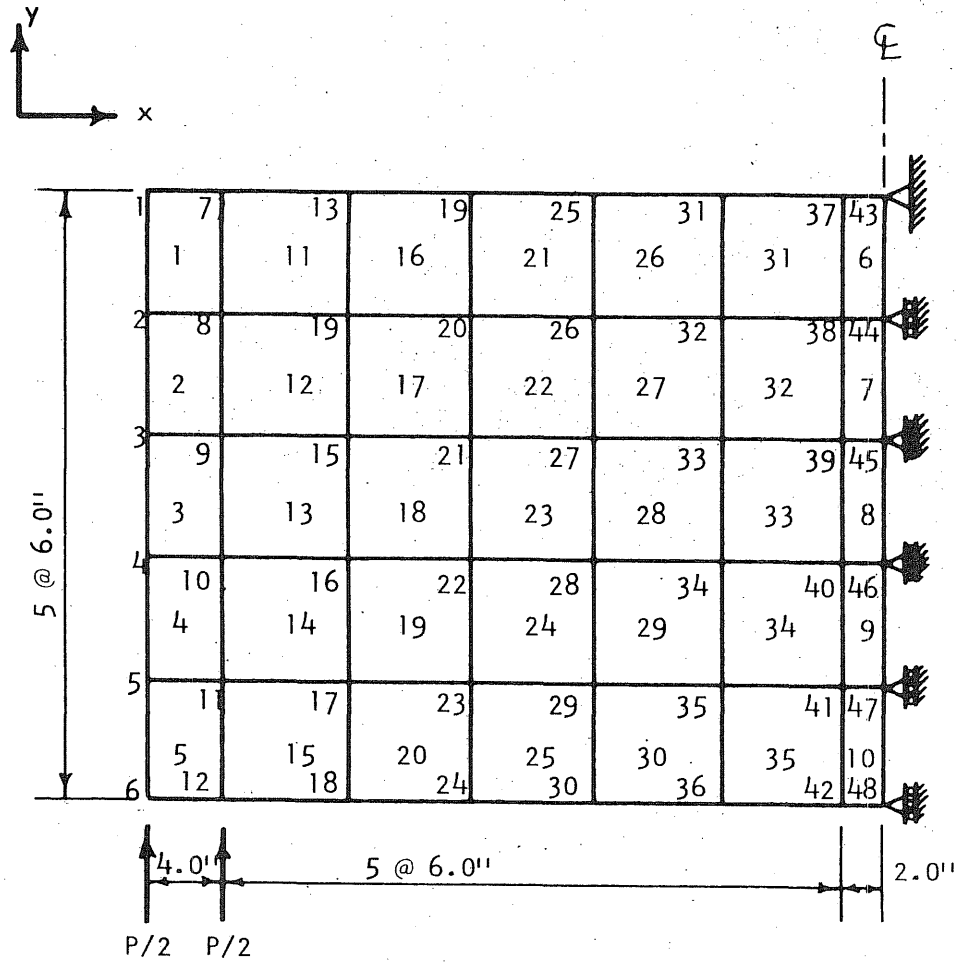


Figure 29, Layout of Mesh 1 (Specimen W2)

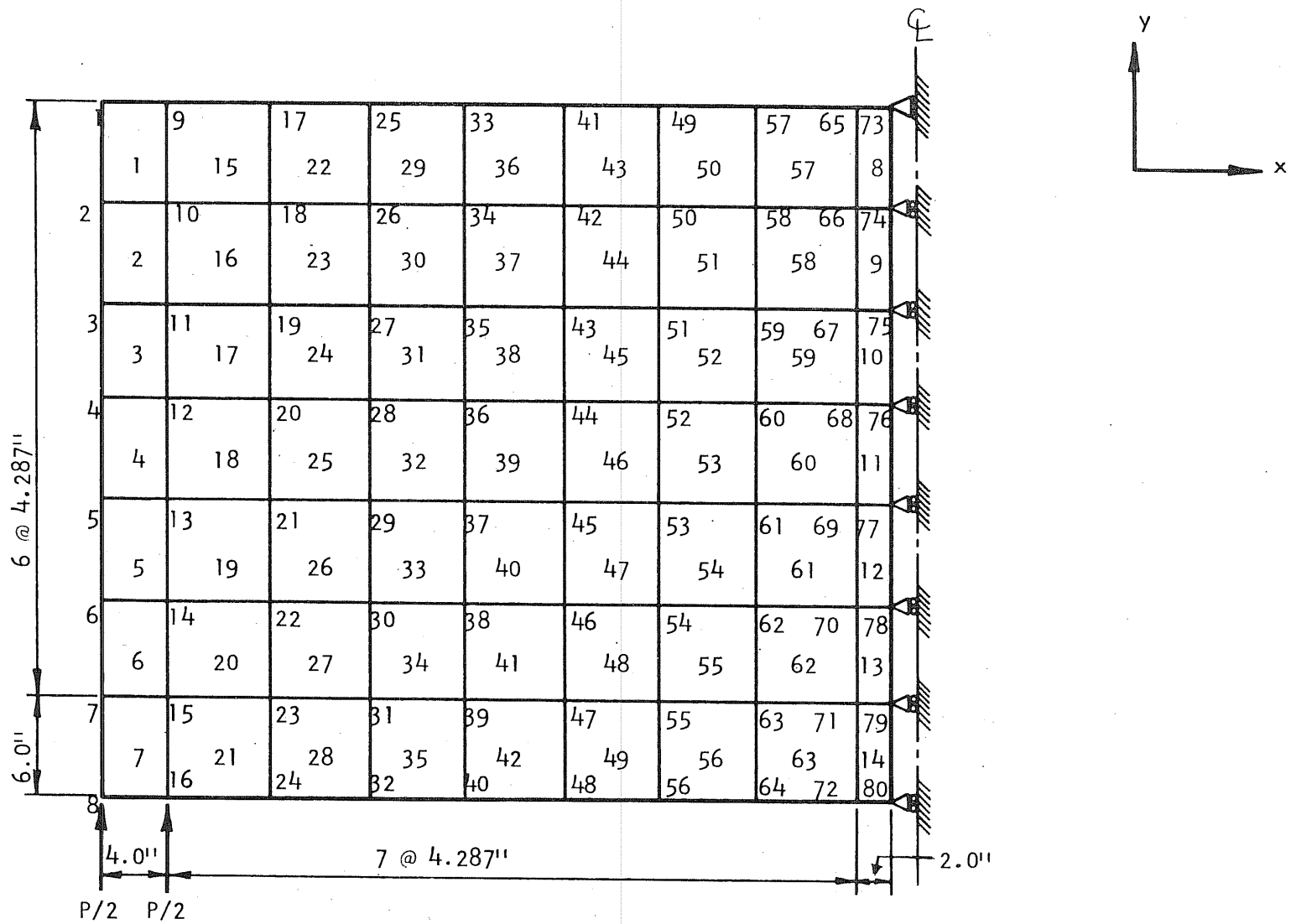


Figure 30, Layout of Mesh 2 (Specimen W2)

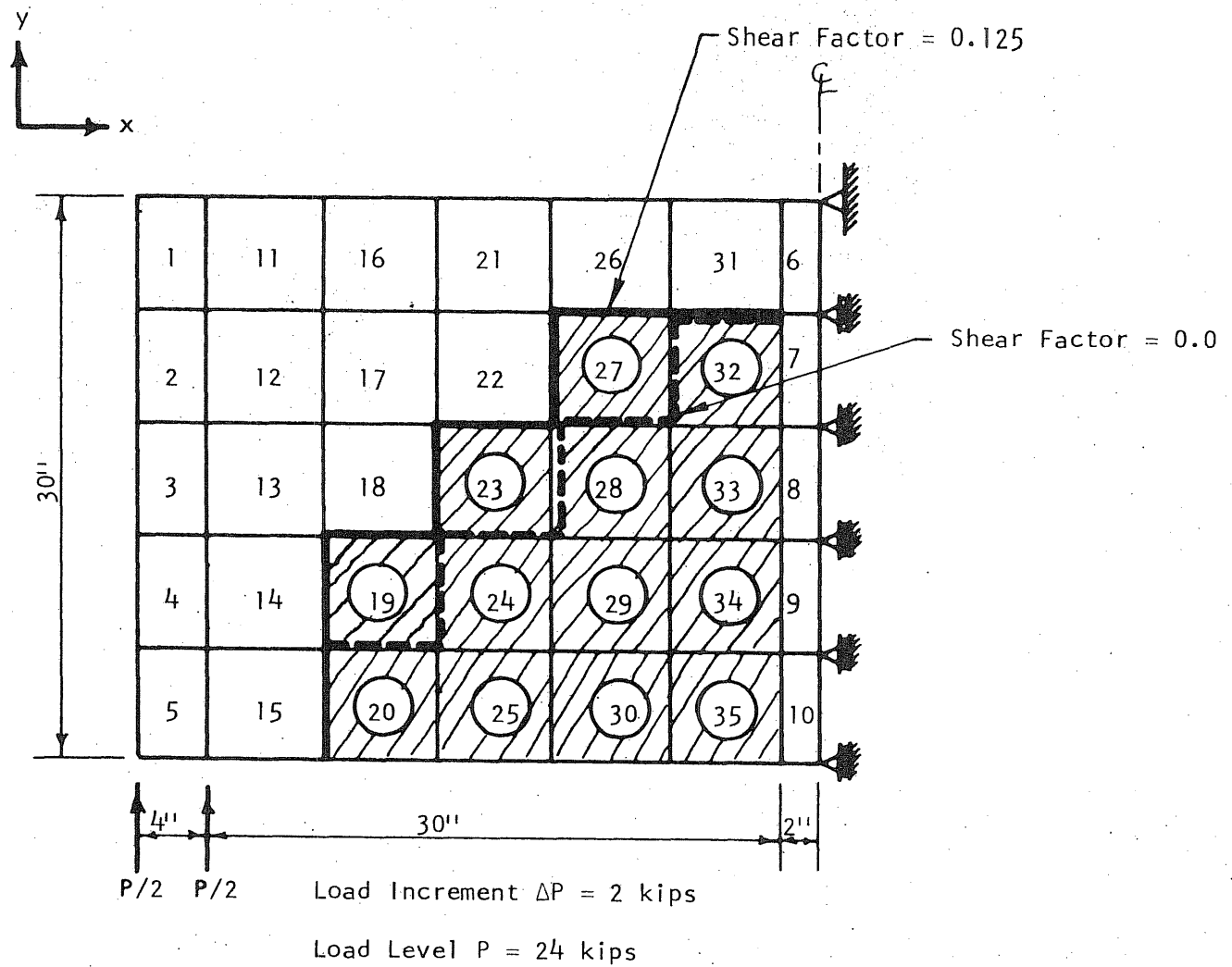
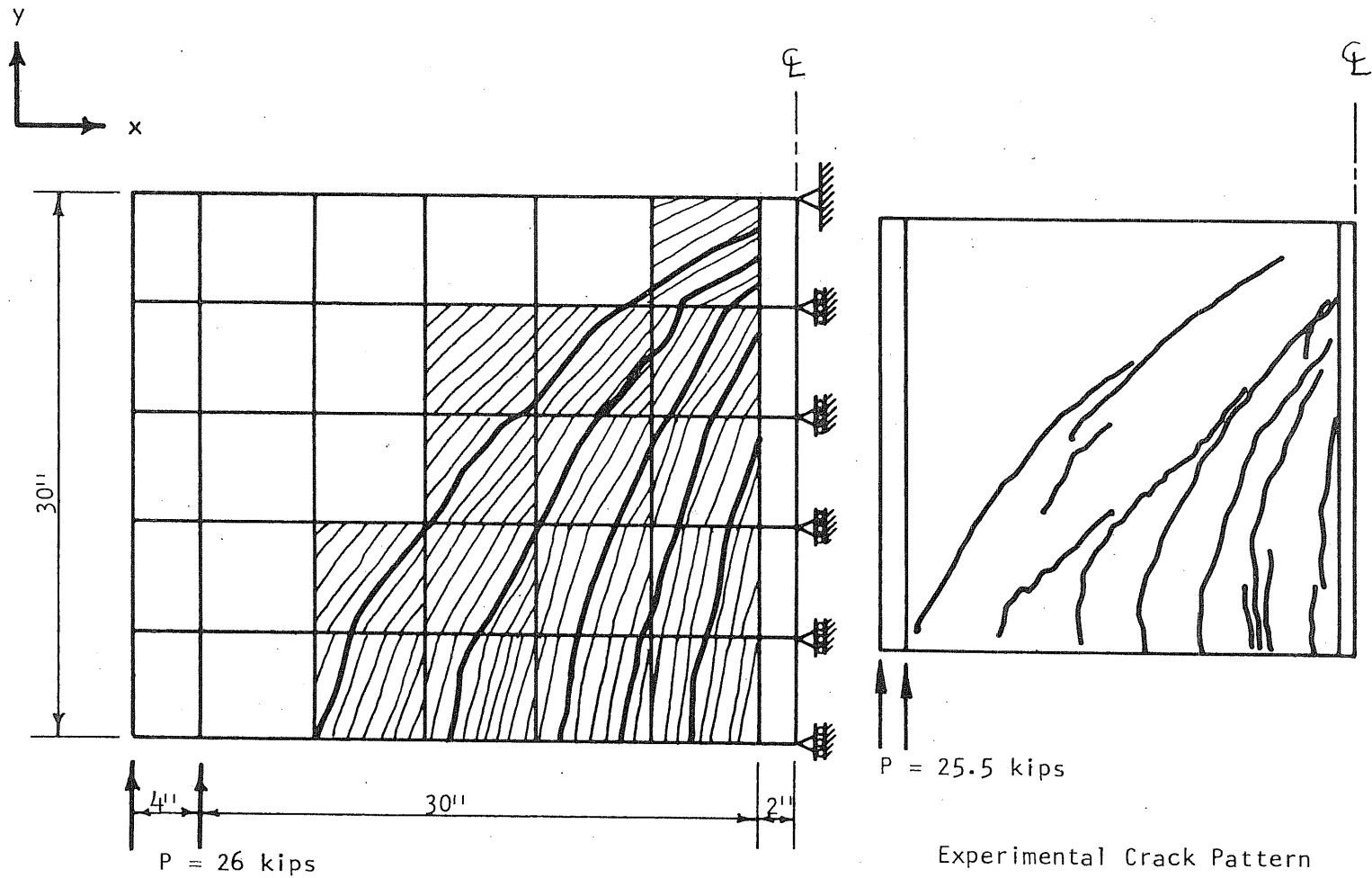


Figure 31, Region of Cracking for Two Different Values of Shear Factor (Specimen W2, Mesh 1)



Analytical Crack Pattern  
(Shear Factor = 0.125)

Experimental Crack Pattern

Figure 32, Comparison of the Experimental and Analytical Crack Patterns  
(Specimen W2, Mesh 1)

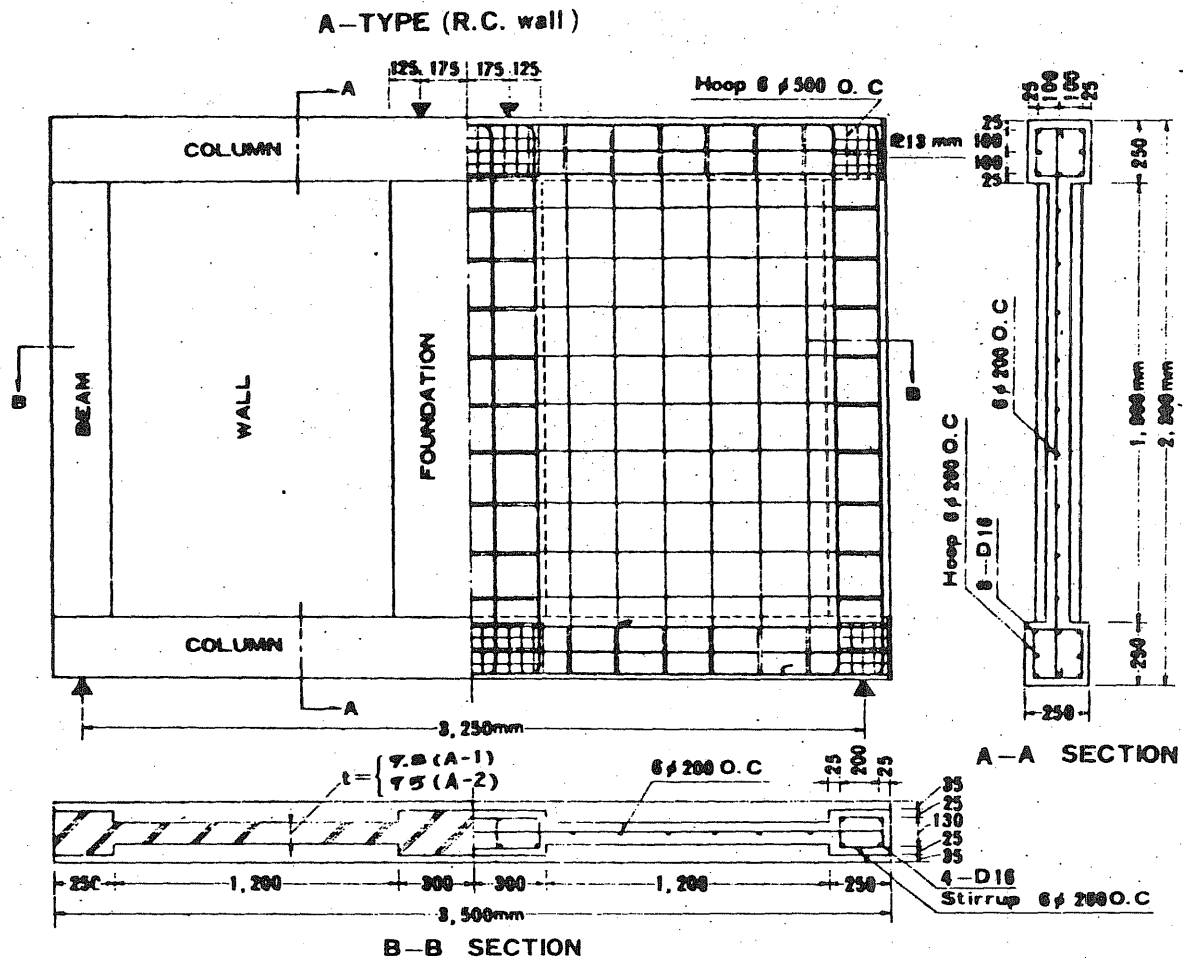


Figure 33, Details of Specimen A-1 [21]



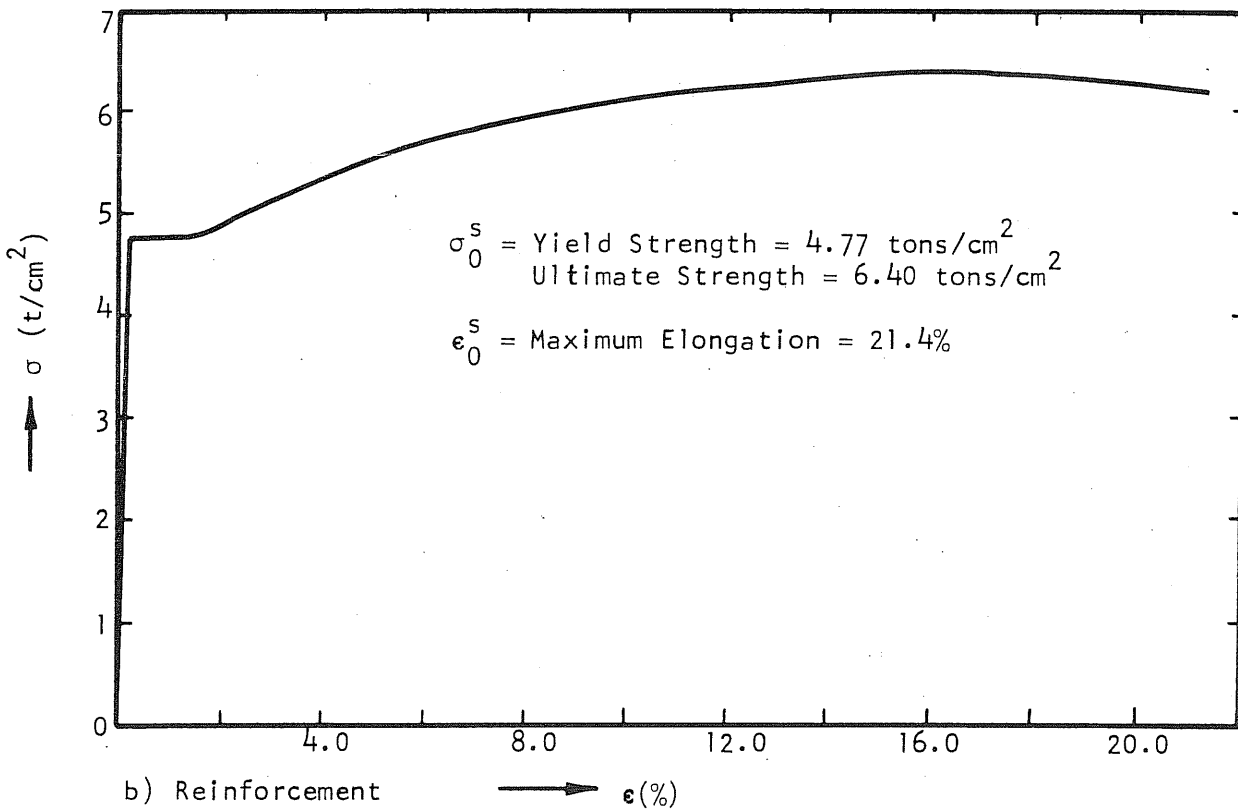
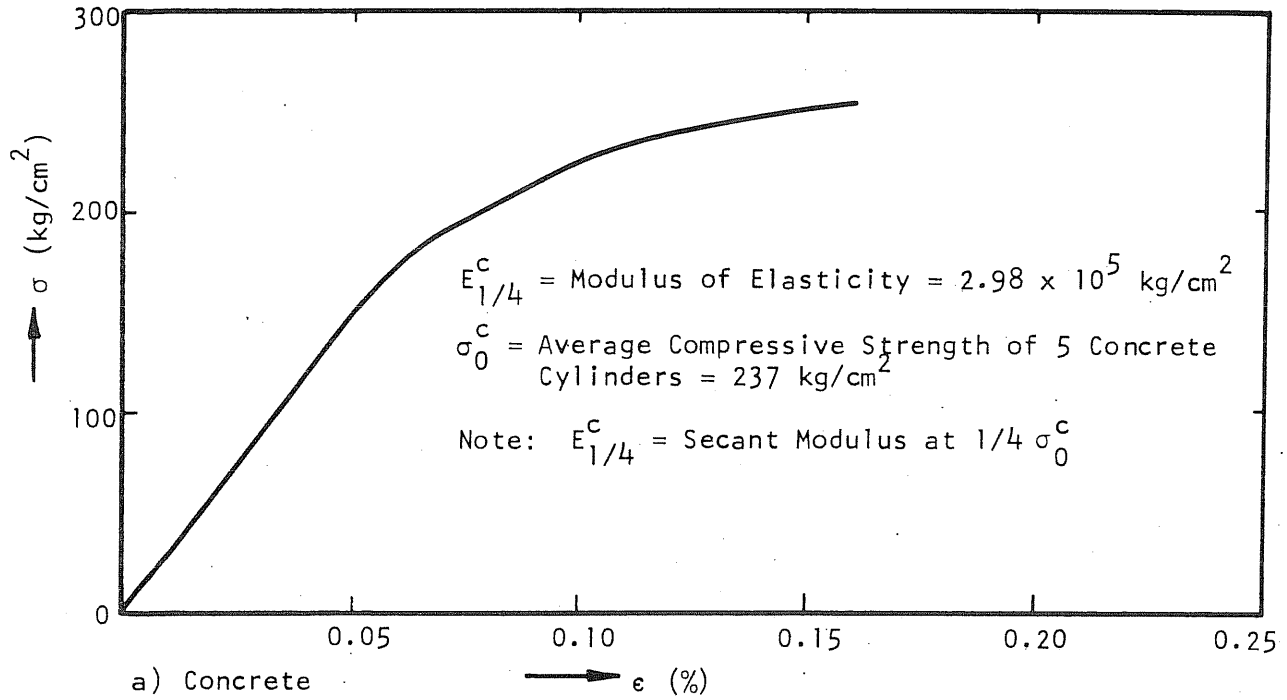


Figure 34, Physical Properties of the Materials Used in Specimen A-1 [21]

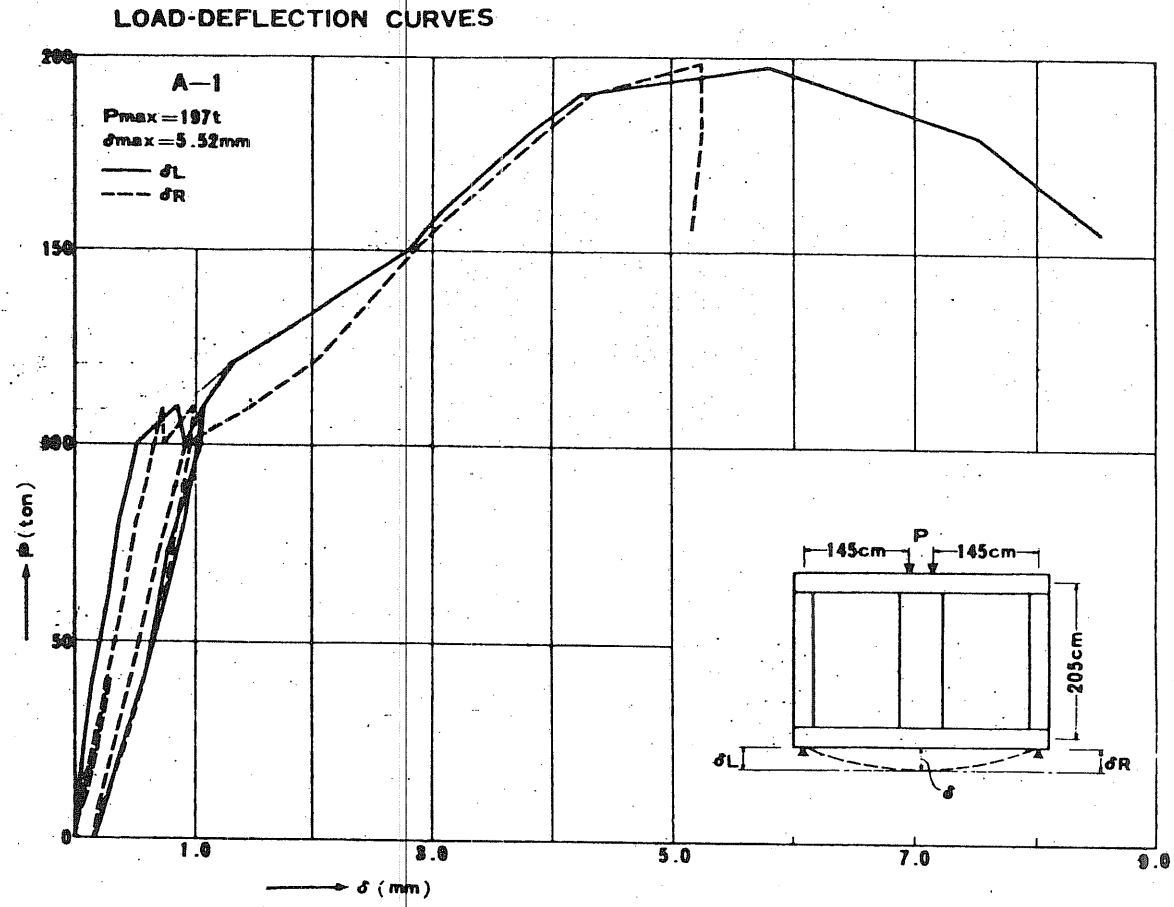


Figure 35, Load Versus Relative Vertical Displacement of the Supports [21]

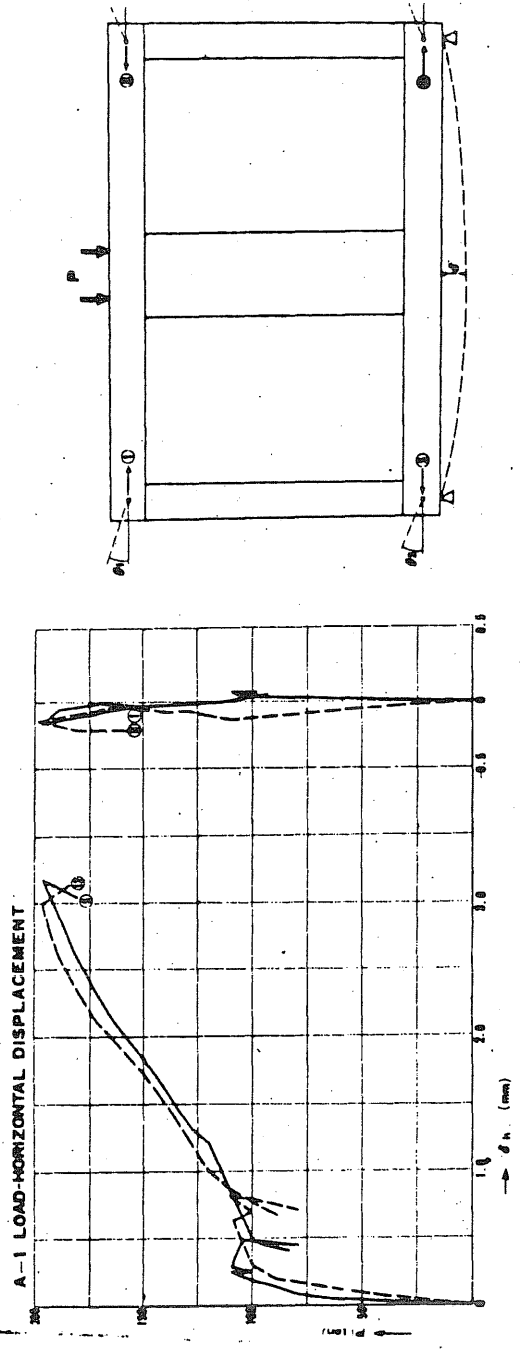


Figure 36, Load Versus Horizontal Displacement of the Supports [21]

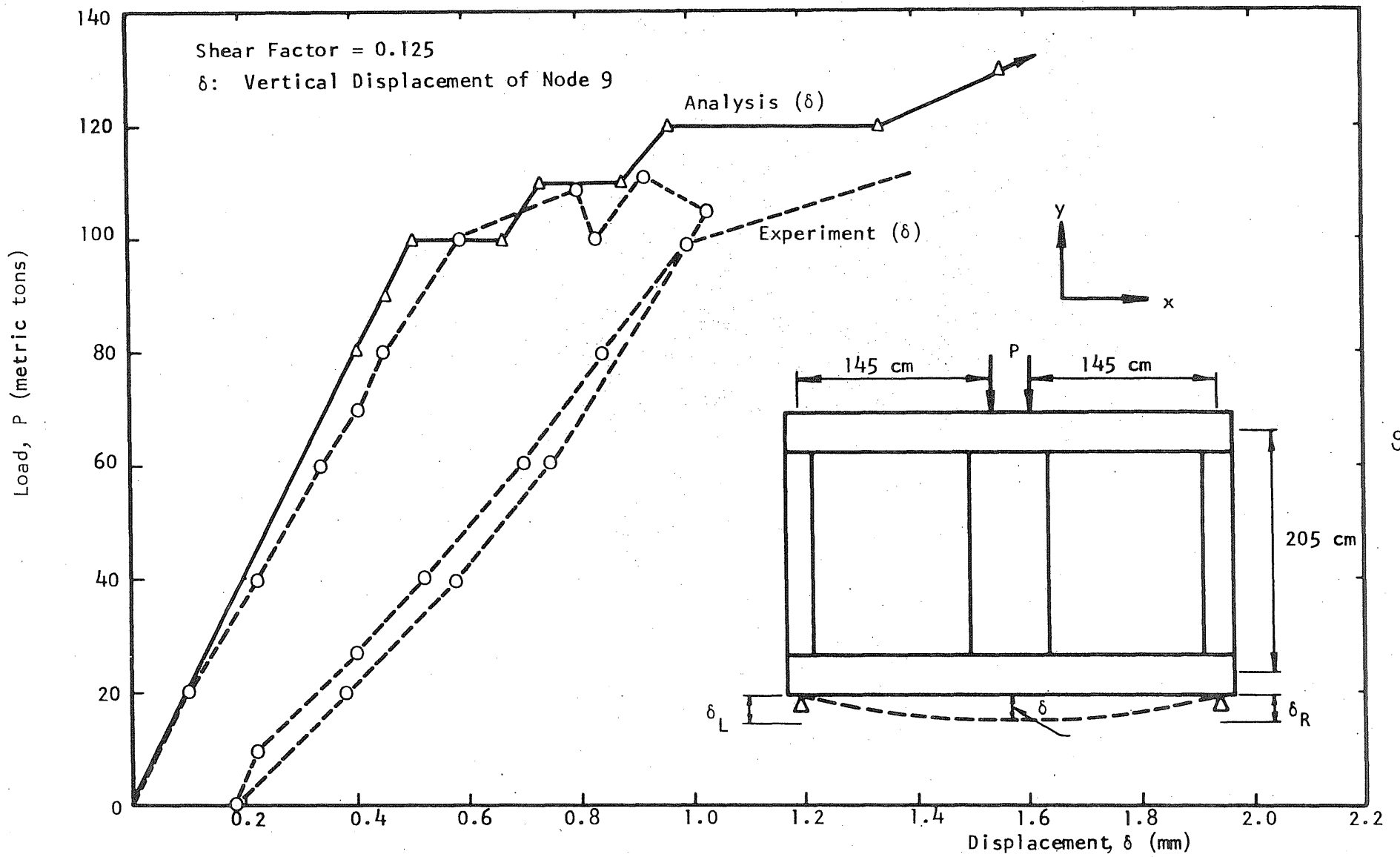


Figure 37, Comparison of the Load-Displacement Curves  
 (Specimen A-1, Solution 1)

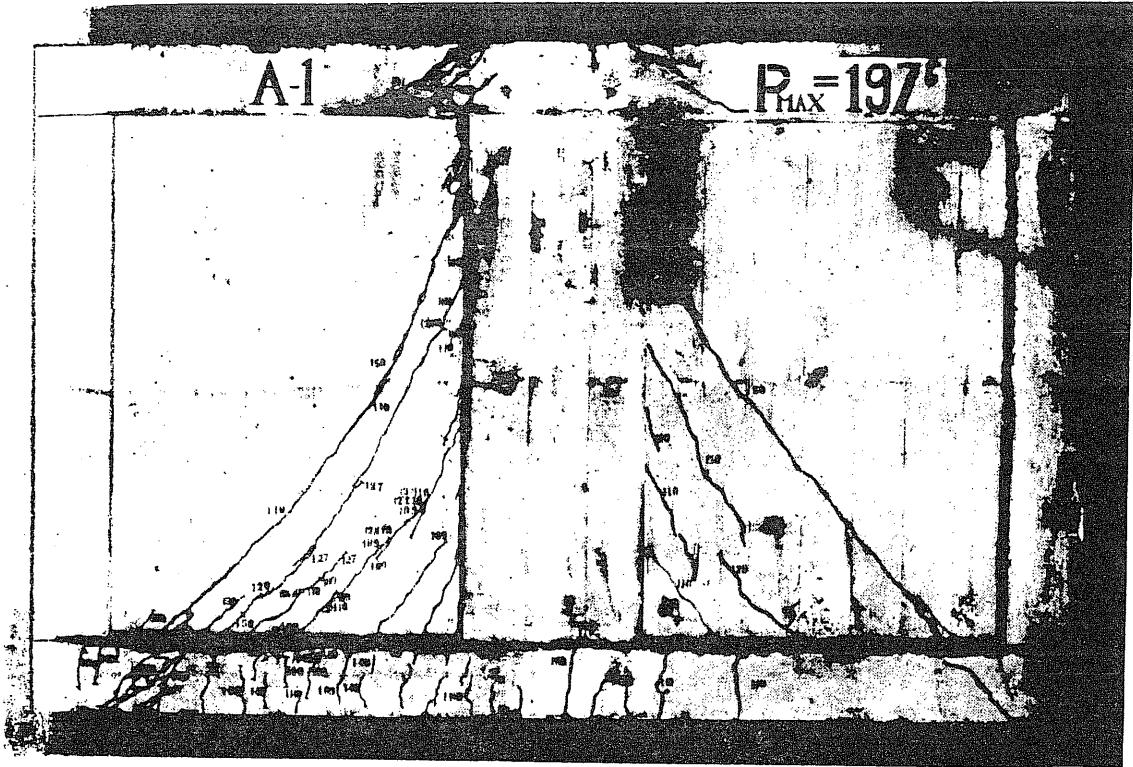


Figure 38, Experimental Crack Pattern (Specimen A-1) [21]

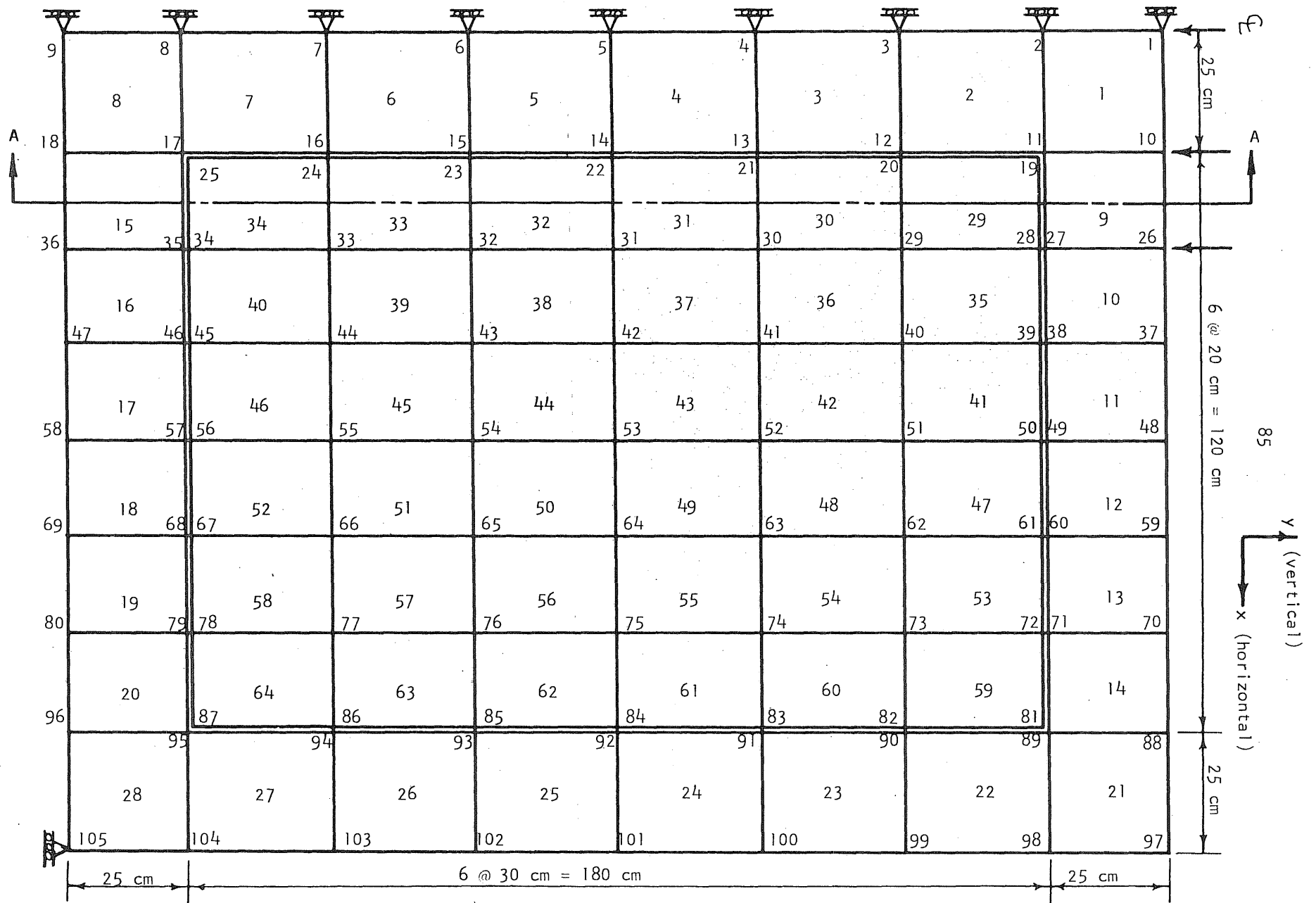
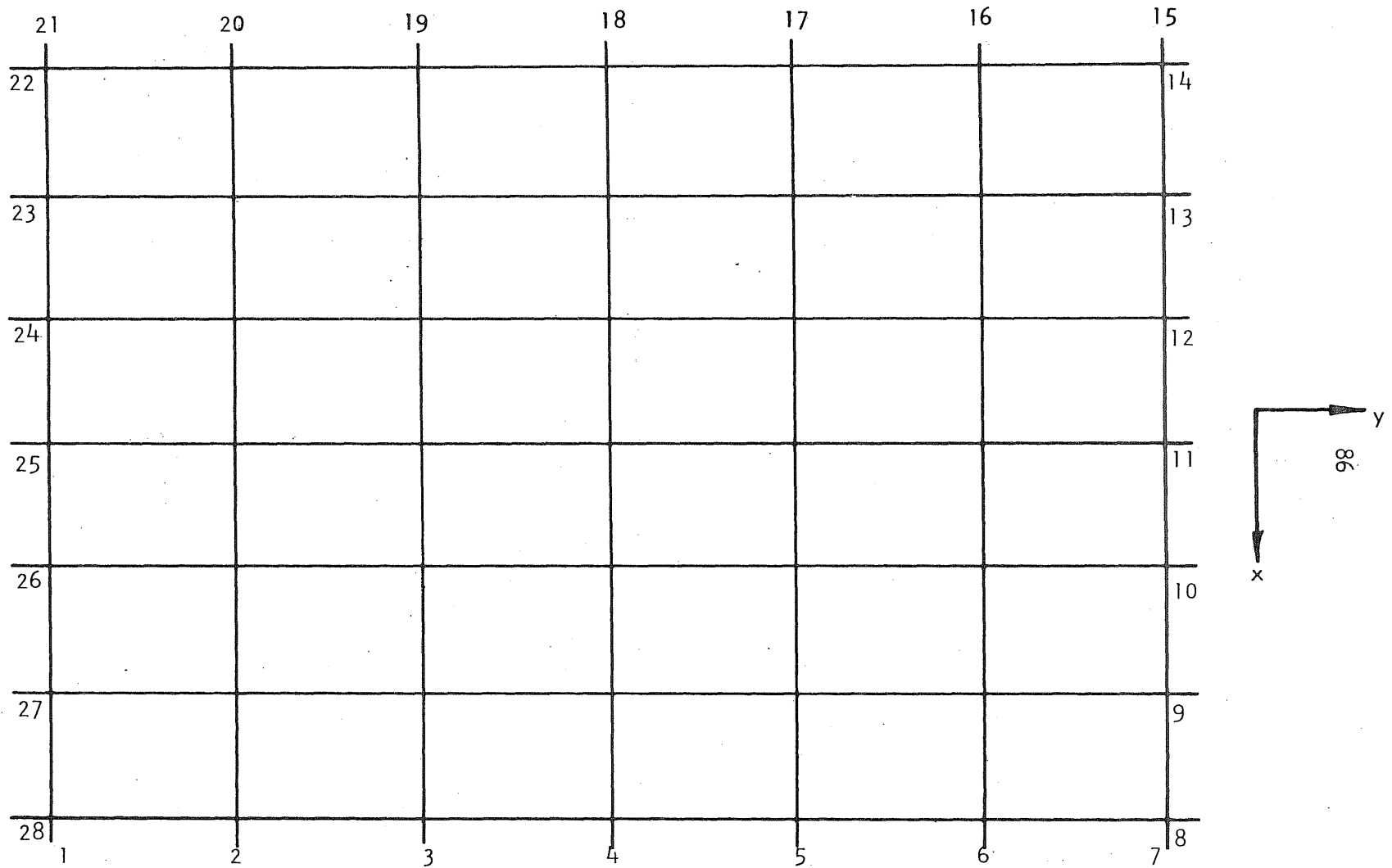


Figure 39, Discretized Model (Specimen A-1)



Note: Each number of this figure represents a link element. Examples: Link element 2 shown on this figure connects nodes 94 and 86 shown on Fig. 39. Also link element 1 and 28 connect nodes 95 and 87.

Figure 40, Link Elements (Specimen A-1)

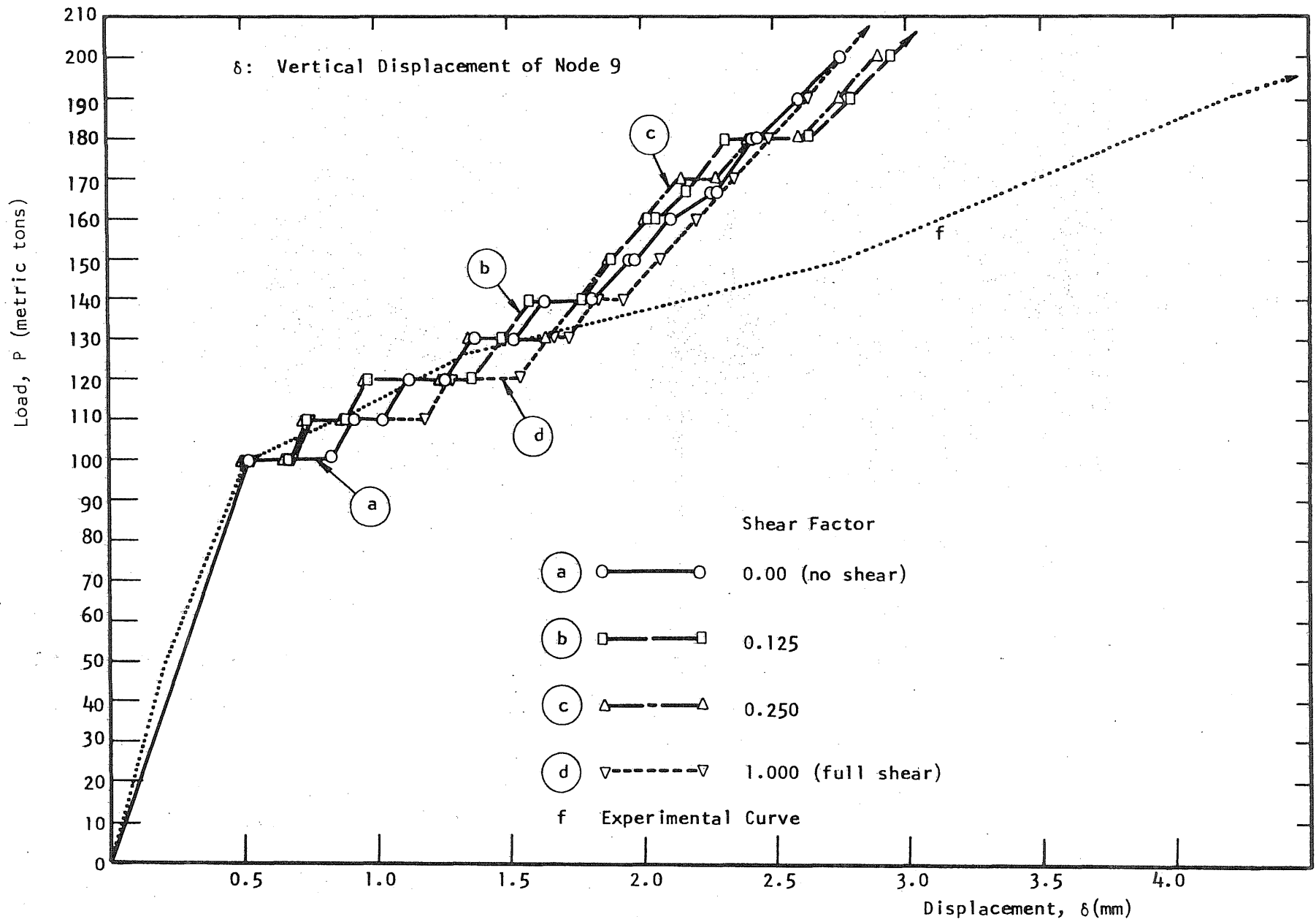


Figure 41, Comparison of Load-Displacement Curves (Specimen A-1, Solution 1)



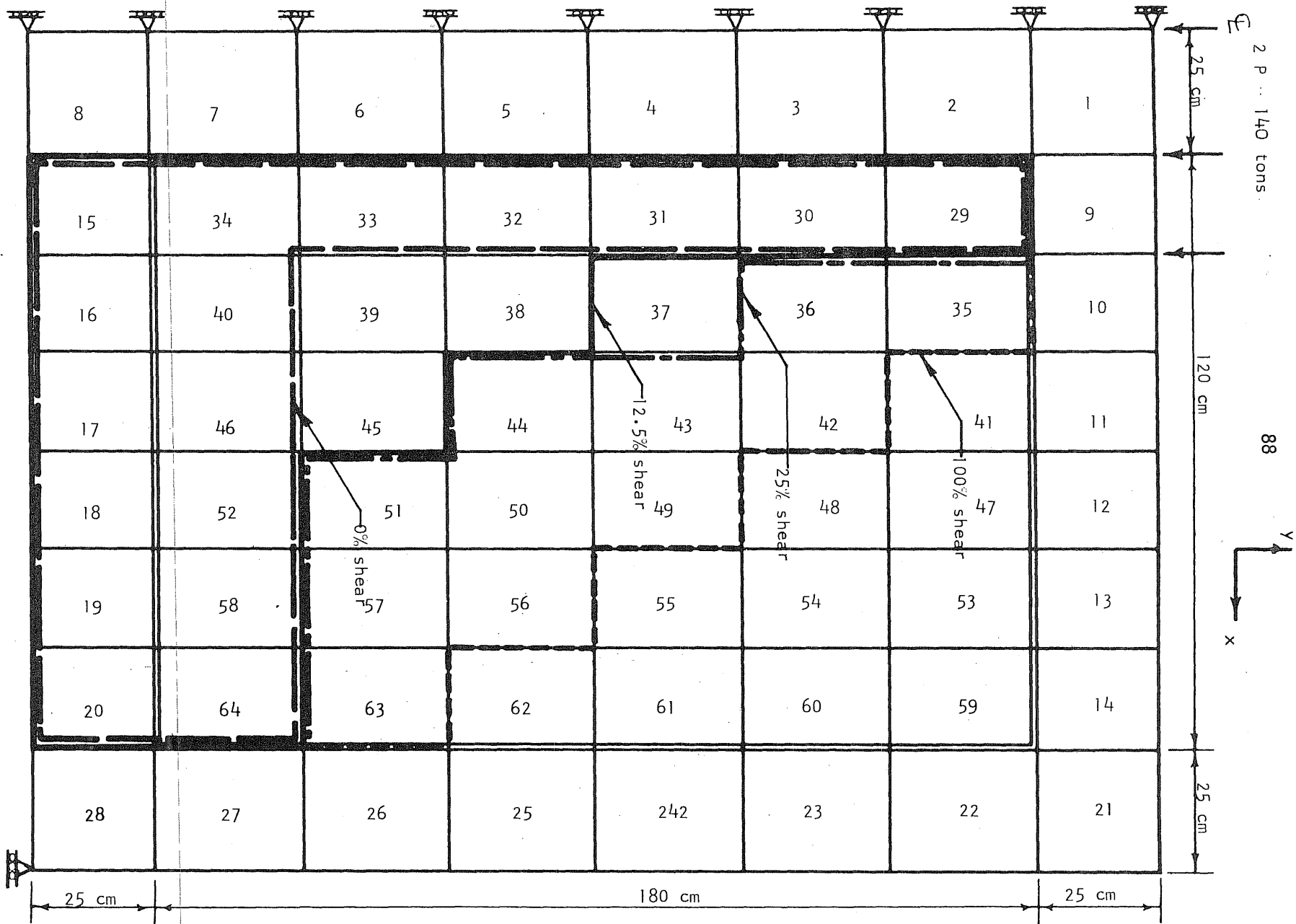


Figure 42 Effect of Shear Transfer on Cracking (Specimen A-1, Solution 1)

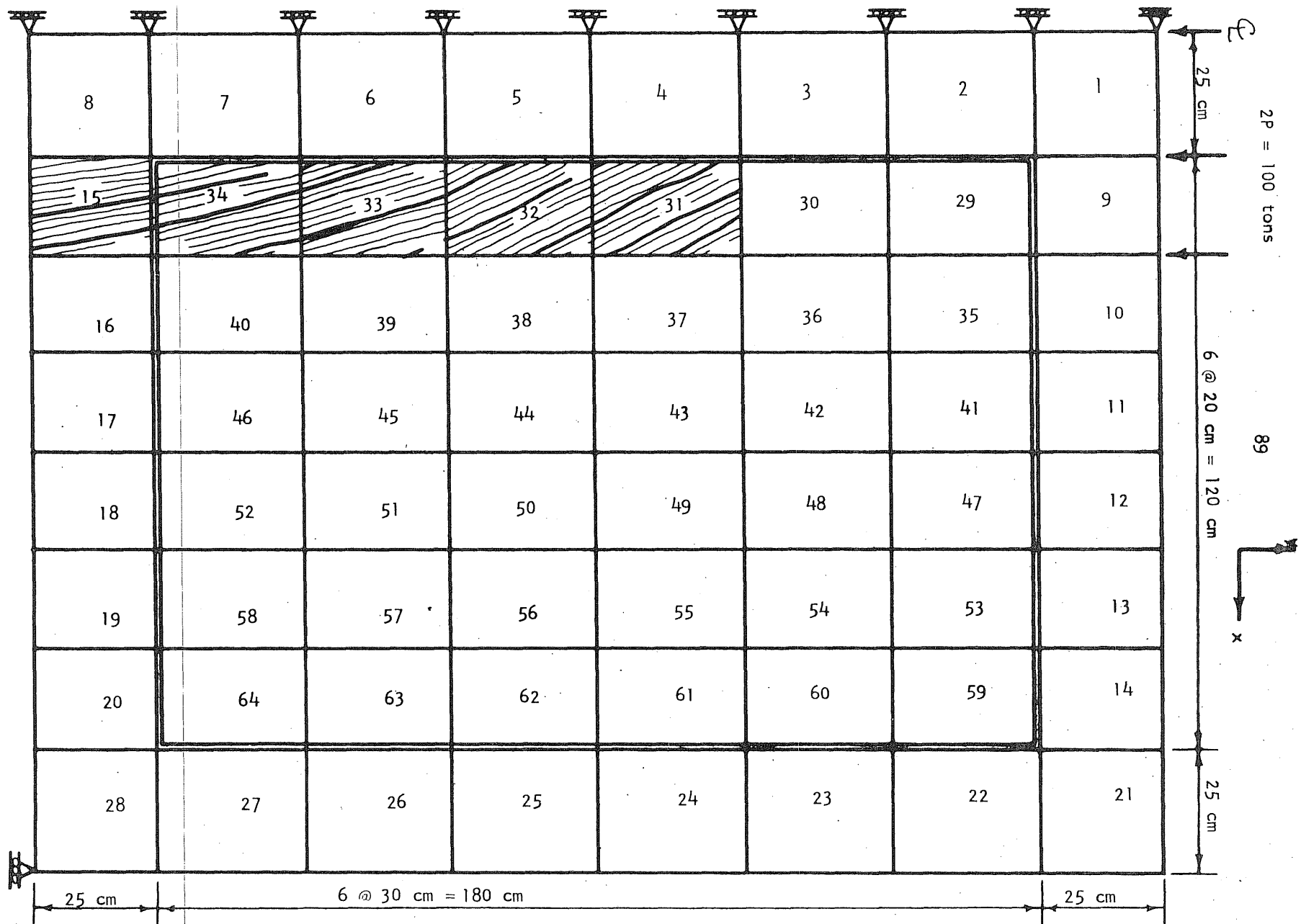


Figure 43, Crack Pattern at 100 tons of Load (Specimen A-1, Solution 1)



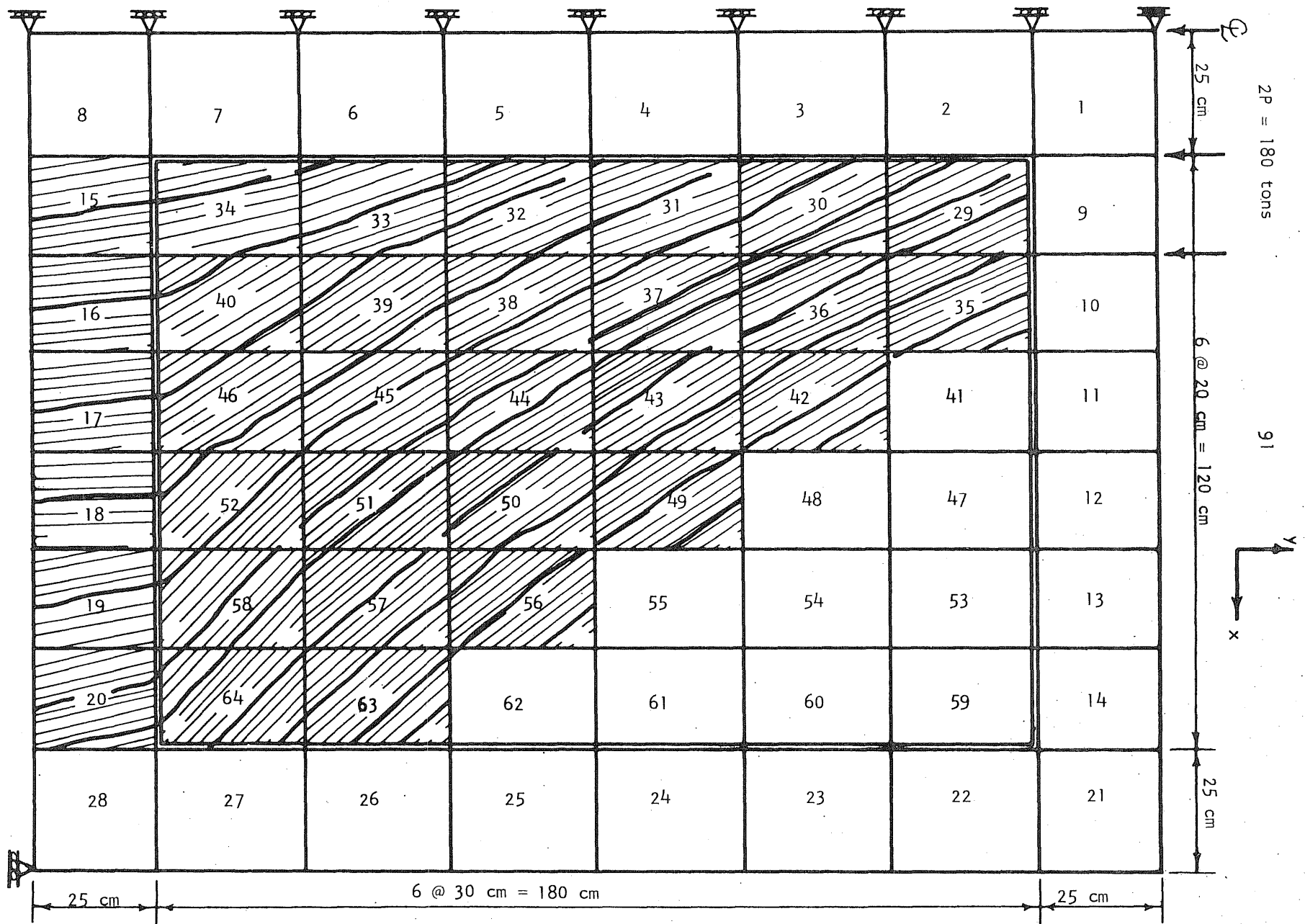


Figure 45, Crack Pattern at 180 tons of Load (Specimen A-1, Solution 1)

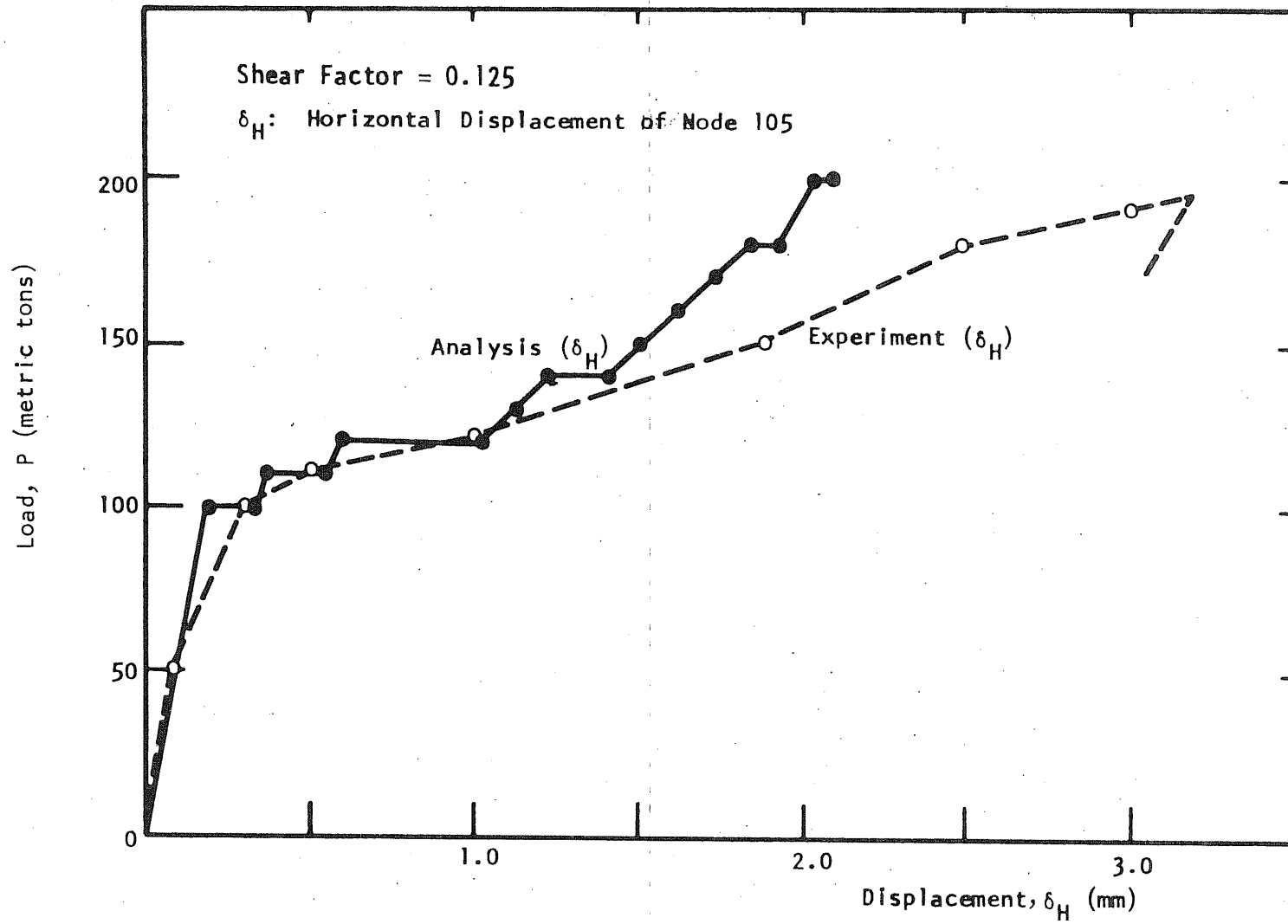
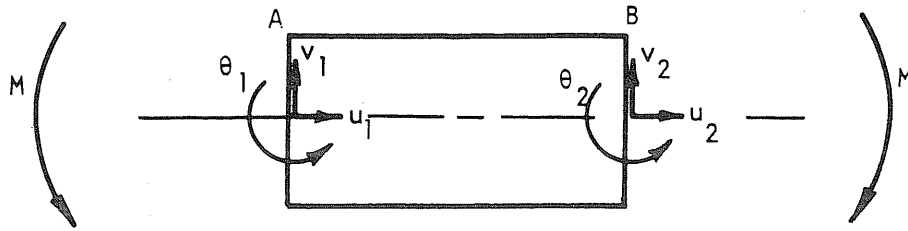


Figure 46, Comparison of the Load Displacement Curves  
 (Specimen A-1, Solution 1)



a) Flexural Element

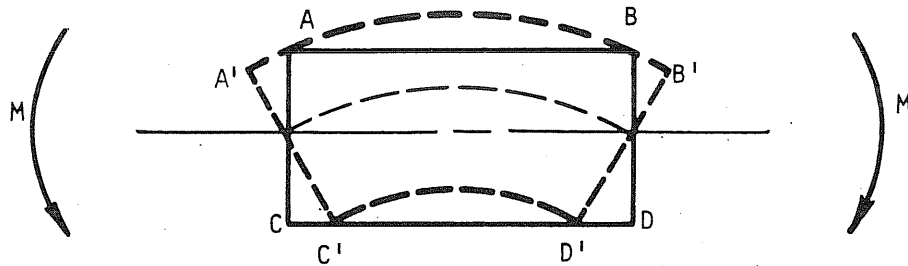
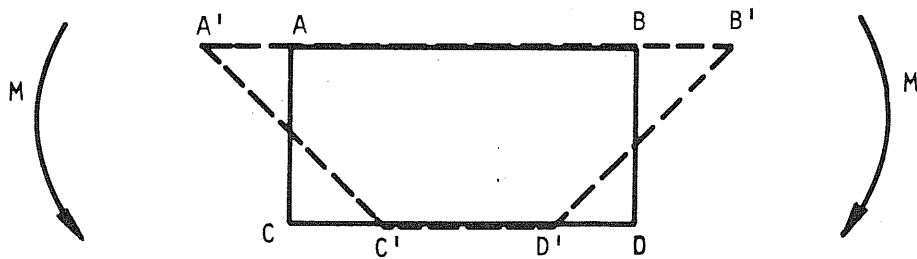
b) Deformed Shape of the Flexural Element  
(Cubic Displacement Function)c) Deformed Shape of the Quadrilateral Element  
(Linear Displacement Function)

Figure 47, Flexural Deformations

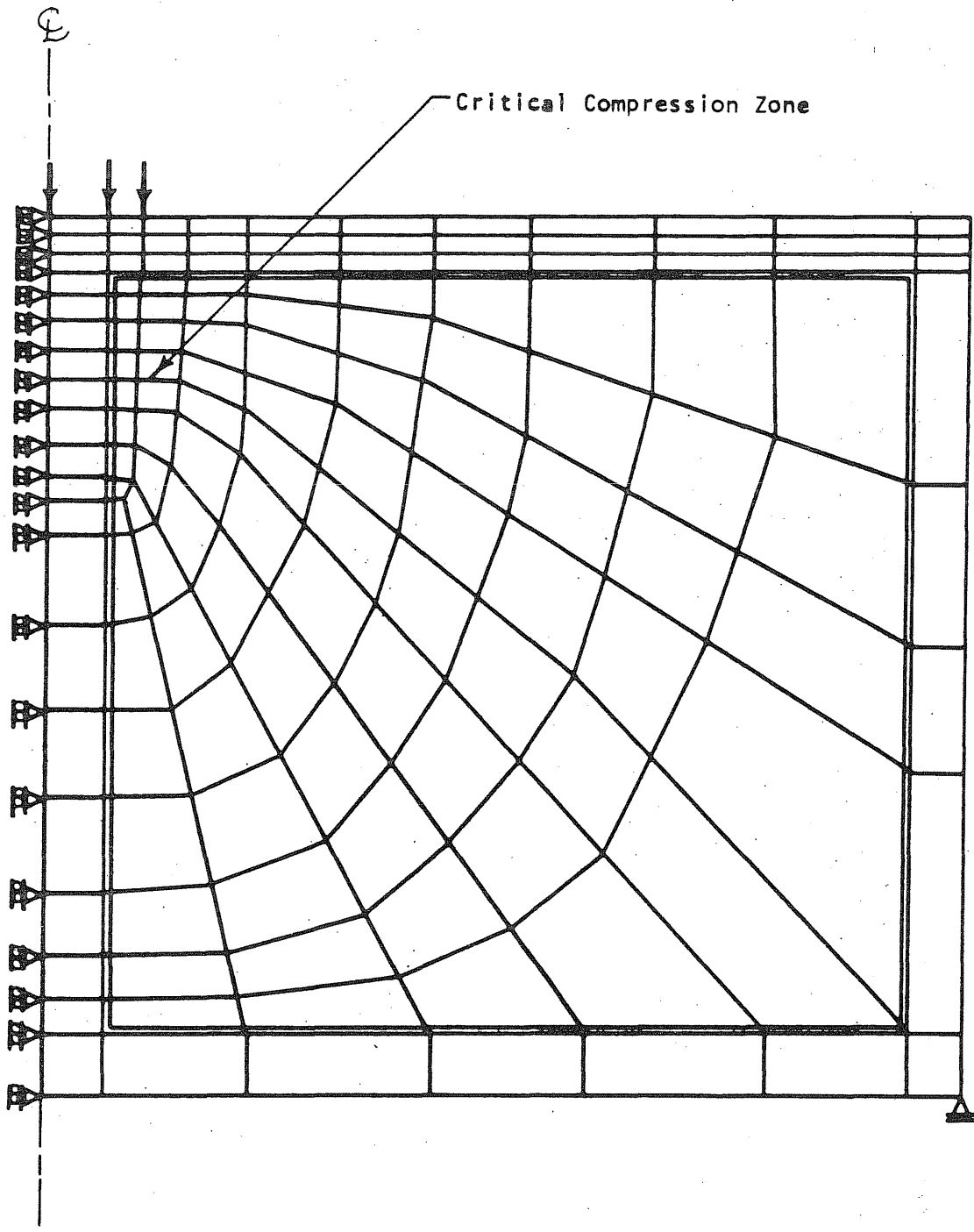


Figure 48, Grading Mesh Suggested

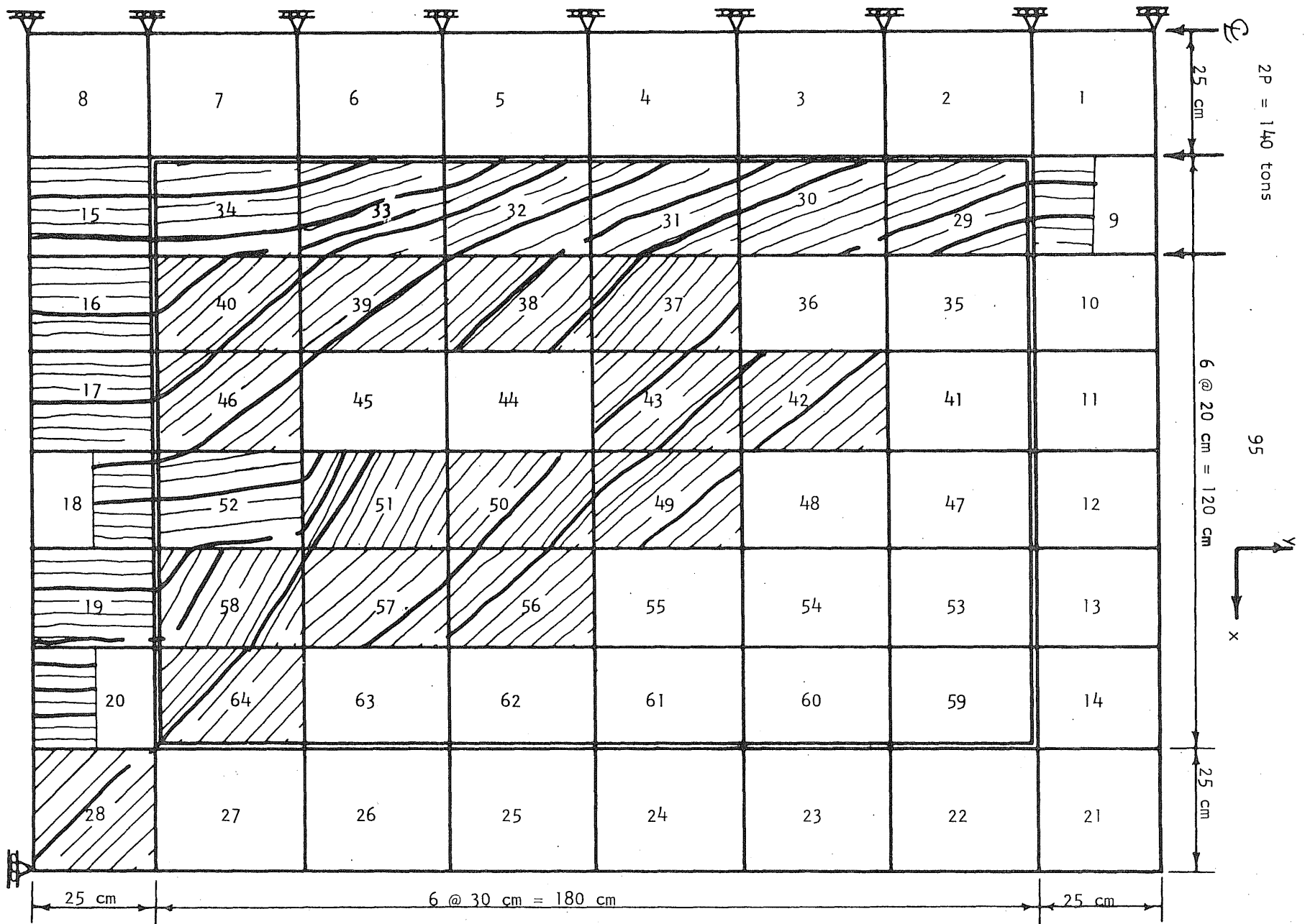


Figure 49, Crack Pattern at 140 tons of Load (Specimen A-1, Solution 2)



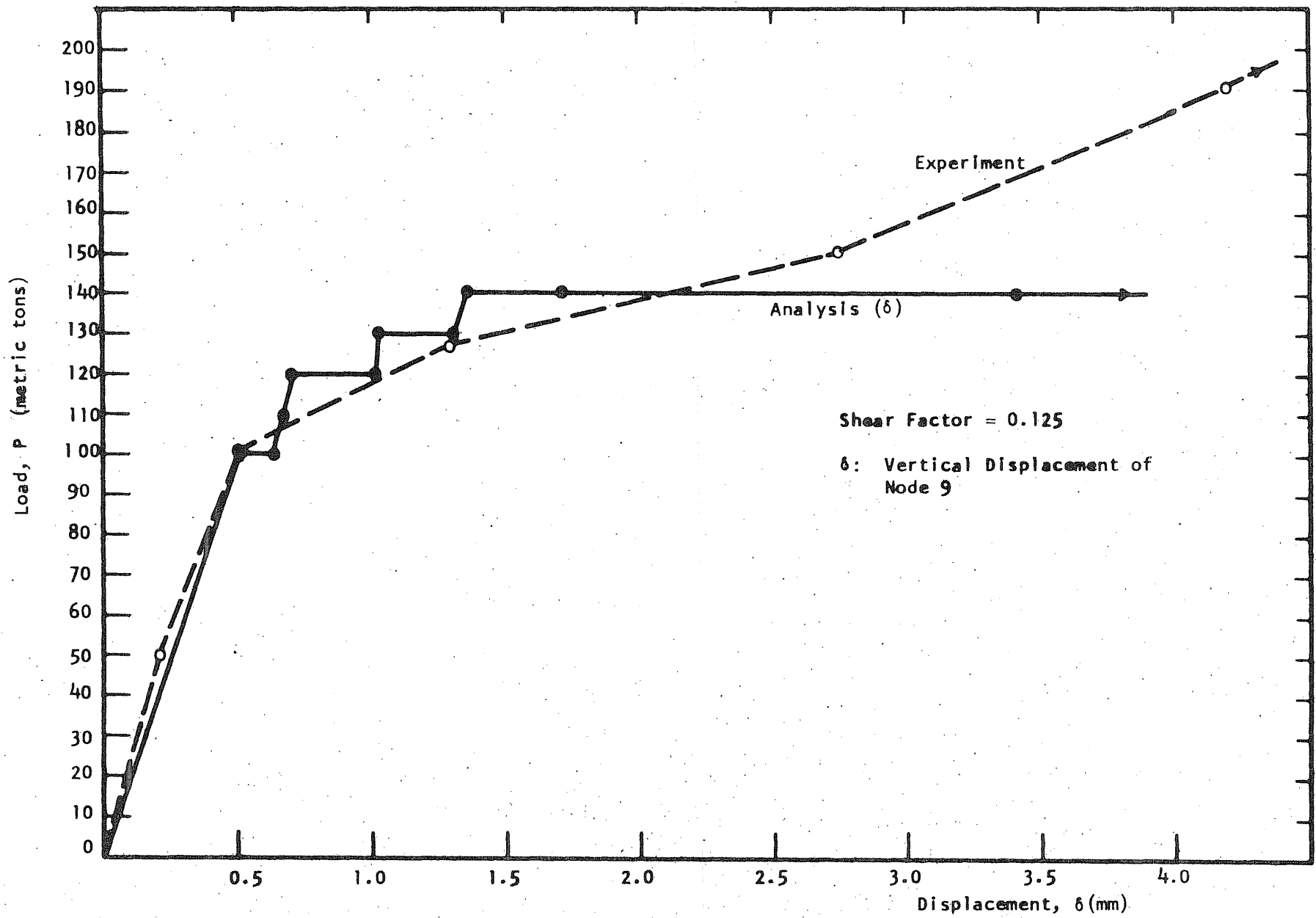


Figure 50, Comparison of the Load-Displacement Curves  
(Specimen A-1, Solution 2)

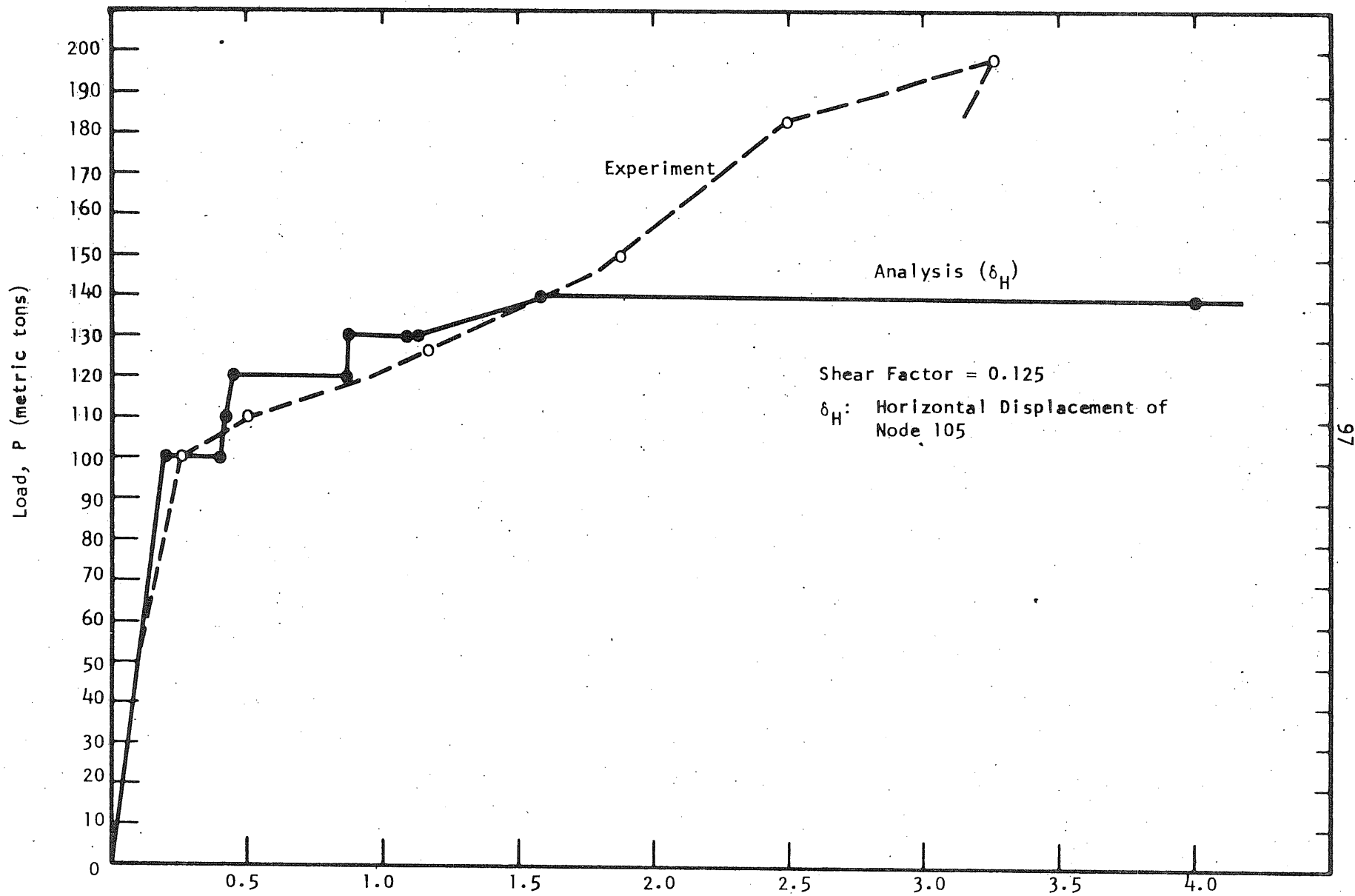


Figure 51, Comparison of the Load-Displacement Curves  
(Specimen A-1, Solution 2)

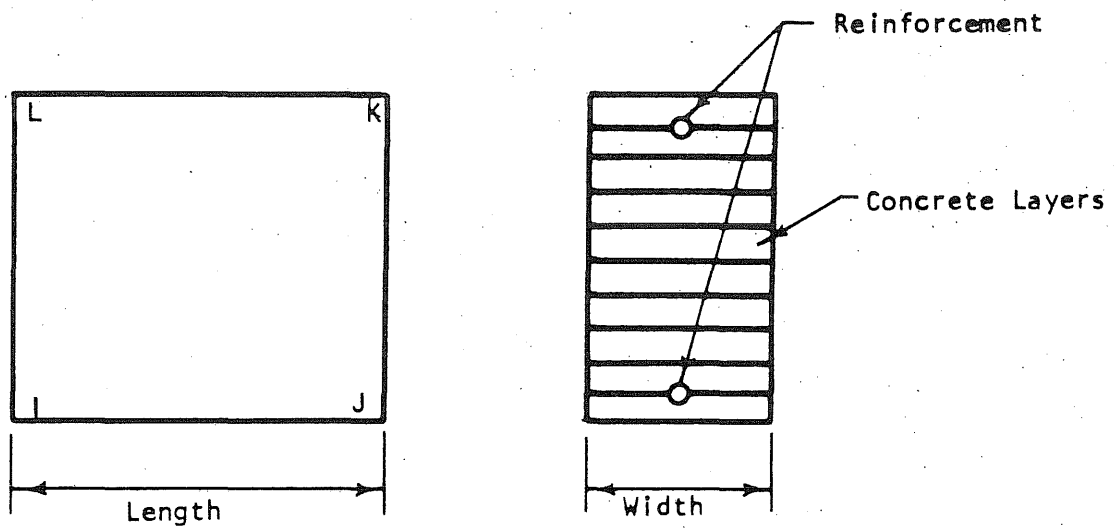
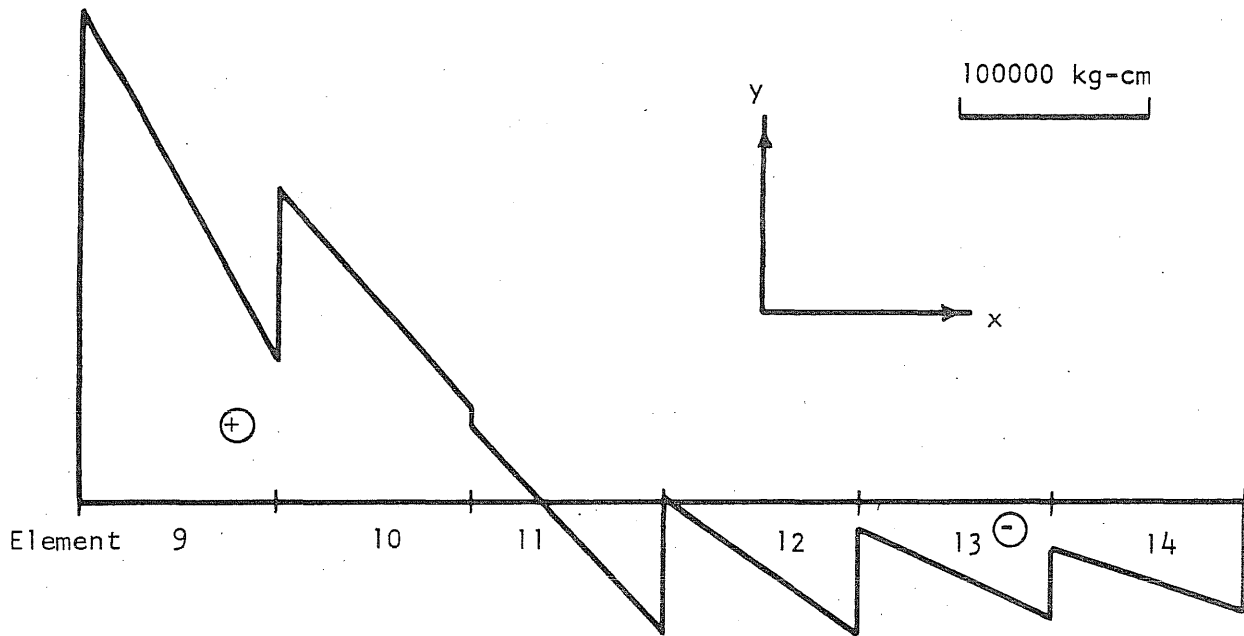
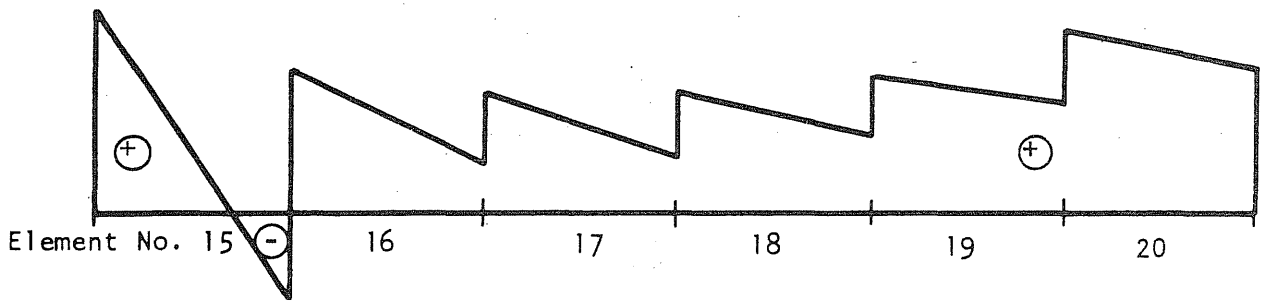


Figure 52, Suggested Layering of a Flexural Element [18]



a) Top Column Moments



b) Bottom Column Moments

Figure 53, Frame Moments at P = 100 Tons (Before Cracking)

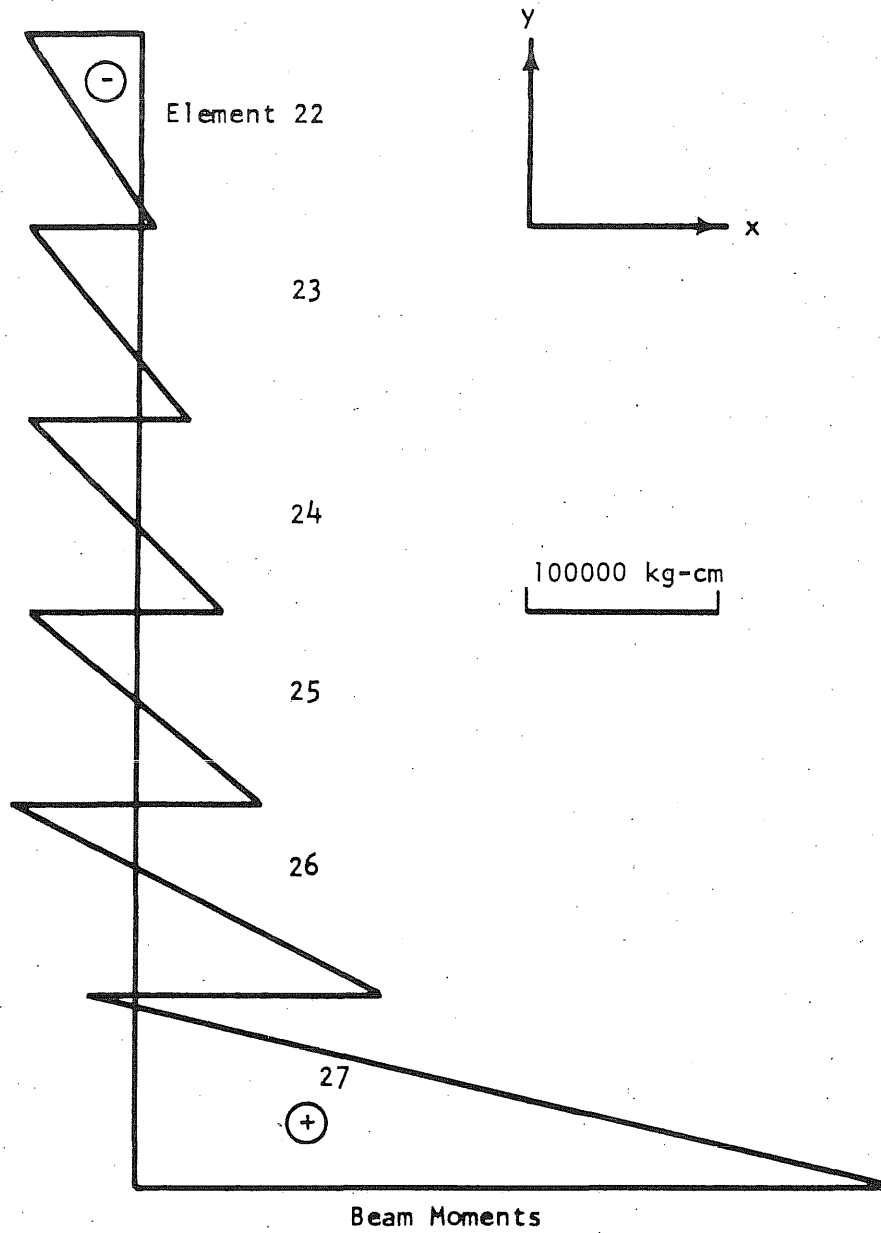


Figure 54, Frame Moments at P = 100 Tons (Before Cracking)

## APPENDIX A

## DEVELOPMENT OF THE ELEMENT STIFFNESS MATRICES AND COMPUTATION OF STRESSES AND STRAINS

## A.1 Quadrilateral Element [30] [31]

Consider the quadrilateral shown in Fig. 1. It is subdivided into four triangles, taking the common or fifth node at the centroid of the quadrilateral. Each triangle is a constant strain triangle, that is, a linear displacement field is assumed over each triangle. The displacements are continuous across the interior boundaries, but the strains are discontinuous.

The equilibrium equations for the element system can be expressed as:

$$\begin{matrix} \underline{F} \\ 10 \times 1 \end{matrix} = \underline{k} \begin{matrix} \underline{u} \\ 10 \times 10 \end{matrix} \quad (\text{A.1})$$

Let us partition Eq. A.1 as follows:

$$\begin{Bmatrix} \underline{F} \\ 8 \times 1 \\ \underline{F}_0 \\ 2 \times 1 \end{Bmatrix} = \begin{bmatrix} \underline{k}_{11} & \underline{k}_{12} \\ \underline{k}_{21} & \underline{k}_{22} \\ 8 \times 8 & 8 \times 2 \\ 2 \times 8 & 2 \times 2 \end{bmatrix} \begin{Bmatrix} \underline{u} \\ 8 \times 1 \\ \underline{u}_0 \\ 2 \times 1 \end{Bmatrix}$$

where  $\underline{F}_0$  and  $\underline{u}_0$  are the load and displacement vectors for the centroidal node of the quadrilateral element. Then:

$$\begin{matrix} \underline{F} \\ 8 \times 1 \end{matrix} = \underline{k}_{11} \begin{matrix} \underline{u} \\ 8 \times 1 \end{matrix} + \underline{k}_{12} \begin{matrix} \underline{u}_0 \\ 2 \times 1 \end{matrix} \quad (\text{A.2})$$

and

$$\begin{matrix} \underline{F}_0 \\ 2 \times 1 \end{matrix} = \underline{k}_{21} \begin{matrix} \underline{u} \\ 8 \times 1 \end{matrix} + \underline{k}_{22} \begin{matrix} \underline{u}_0 \\ 2 \times 1 \end{matrix} \quad (\text{A.3})$$

Solving  $\underline{u}_0$  from Eq. A.3:

$$\underline{u}_0 = \underline{k}_{22}^{-1} \underline{F}_0 - \underline{k}_{22}^{-1} \underline{k}_{21} \underline{u} \quad (\text{A.4})$$

and substituting in Eq. A.2:

$$\underline{F} = \underline{k}_{11} \underline{u} + \underline{k}_{12} (\underline{k}_{22}^{-1} \underline{F}_0 - \underline{k}_{22}^{-1} \underline{k}_{21} \underline{u}) \quad (\text{A.5})$$

so that

$$(\underline{F} - \underline{k}_{12} \underline{k}_{22}^{-1} \underline{F}_0)_{8 \times 1} = (\underline{k}_{11} - \underline{k}_{12} \underline{k}_{22}^{-1} \underline{k}_{21})_{8 \times 8} \underline{u}_{8 \times 1}$$

or

$$\underline{F}^* = \underline{k}^* \underline{u} \quad (\text{A.6})$$

where  $\underline{k}^*$  is the "condensed stiffness matrix" of the quadrilateral element.

If  $\underline{F}_0 \equiv 0$  (i.e., no load applied at the centroidal node) then

$$\underline{F}^* = \underline{F}$$

Once the structure is solved for given loads, the displacements of the four corners of each quadrilateral element are recovered from the displacement vector of the structure. In order to find the strain within each triangle the displacement  $\underline{u}_0$  of the centroidal node should be computed first (Eq. A.4). Next step is to compute the strain of each subtriangle using the strain displacement relationship:

$$\underline{\epsilon}_{3 \times 1} = \underline{B}_{3 \times 6} \underline{u}_{6 \times 1}^e \quad (\text{A.7})$$

where

$$\underline{B} = \frac{1}{2A} \begin{bmatrix} y_{23} & 0 & y_{31} & 0 & y_{12} & 0 \\ 0 & x_{32} & 0 & x_{13} & 0 & x_{21} \\ x_{32} & y_{23} & x_{13} & y_{31} & x_{21} & y_{12} \end{bmatrix}$$

$\underline{u}^e$ : nodal displacement vector for a subtriangle and A is the area of the triangle (Fig. 2), also

$$x_{ij} = x_i - x_j$$

$$y_{ij} = y_i - y_j \quad (i = 1, 2, 3), (j = 1, 2, 3)$$

Average strain of the centroidal node is then:

$$\underline{\epsilon} = \frac{1}{4} \{ \underline{\epsilon}^I + \underline{\epsilon}^{II} + \underline{\epsilon}^{III} + \underline{\epsilon}^{IV} \} \quad (\text{A.8})$$

$3 \times 1 \qquad \qquad \qquad 3 \times 1$

where

$\underline{\epsilon}^I, \underline{\epsilon}^{II}, \underline{\epsilon}^{III}, \underline{\epsilon}^{IV}$  are the strains existing within each subtriangle.

This average strain is used to compute the average stress of concrete:

$$\underline{\sigma}^C = \underline{D}^C \underline{\epsilon} \quad (\text{A.9})$$

$3 \times 1 \quad 3 \times 3 \quad 3 \times 1$

where  $\underline{D}^C$  is the material property matrix of concrete.

The same strain is assumed for the reinforcement too, thus the stress in the reinforcement is:

$$\underline{\sigma}^S = \underline{D}^S \underline{\epsilon} \quad (\text{A.10})$$

$3 \times 1 \quad 3 \times 3 \quad 3 \times 1$

where  $\underline{D}^S$  is the material property matrix of the reinforcement.

## A.2 Frame Elements

The structural frame is divided into segments as shown in Fig. 5a. Two layers of reinforcement are assumed at a distance of  $d'$  from the top and bottom. Let's consider the axial forces, shear forces and moments acting at the reference axis as shown in Fig. 5b. The corresponding displacements are numbered from 1 to 6. This element has the usual 6x6 stiffness matrix:



$$\mathbf{k} = \begin{bmatrix}
 \frac{AE}{L} & & & & & & & & \\
 & \frac{12EI}{L^3} & & & & & & & \\
 & & \frac{6EI}{L^2} & \frac{4EI}{L} & & & & & \\
 & & & & & & & & \\
 \frac{AE}{L} & & & & \frac{AE}{L} & & & & \\
 & & & & & & & & \\
 & & & & & & & & \\
 & & \frac{12EI}{L^3} & \frac{6EI}{L^2} & & 0 & \frac{12EI}{L^3} & & \\
 & & & & & & & & \\
 & & \frac{6EI}{L^2} & \frac{2EI}{L} & & 0 & -\frac{6EI}{L^2} & \frac{4EI}{L} & 
 \end{bmatrix} \quad \text{SYMMETRIC} \quad (A.11)$$

where

A: transformed area of the uncracked section,

I: moment of inertia of the uncracked section with respect to the reference axis,

E: Young's modulus for concrete,

L: length of the element.

Assuming the displacements of the reference axis are related to the displacements of the corners of the element by the following relation:

$$\begin{matrix} \mathbf{u}_r \\ 6 \times 1 \end{matrix} = \begin{matrix} \mathbf{a}_{rq} \\ 6 \times 8 \end{matrix} \begin{matrix} \mathbf{u}_q \\ 8 \times 1 \end{matrix} \quad (A.12)$$

where

$$\mathbf{a}_{rq} = \begin{bmatrix}
 0.5 & 0 & 0 & 0 & 0 & 0 & 0.5 & 0 \\
 0 & 0.5 & 0 & 0 & 0 & 0 & 0 & 0.5 \\
 \frac{1}{D} & 0 & 0 & 0 & 0 & 0 & -\frac{1}{D} & 0 \\
 0 & 0 & 0.5 & 0 & 0.5 & 0 & 0 & 0 \\
 0 & 0 & 0 & 0.5 & 0 & 0.5 & 0 & 0 \\
 0 & 0 & \frac{1}{D} & 0 & -\frac{1}{D} & 0 & 0 & 0
 \end{bmatrix}$$

D: the depth of the element

$\underline{u}_q$ : displacement vector of the corners of the frame element (two at each corner as shown in Fig. 5c).

By the application of principle of virtual work one can arrive at the stiffness matrix of the new frame element which has 8 degrees of freedom:

$$\underline{k}_q = \underline{a}_{rq}^T \underline{k} \underline{a}_{rq} \quad (\text{A.13})$$

The above development of the stiffness matrix was used in Ref. [18]. There, however, 10 slices of concrete were assumed through the depth of the cross-section whereas in this investigation no such slicing is included and to simplify the calculations the properties of the section as a whole are considered.

In the computation of the 8x8 stiffness of the frame element it is implicitly assumed that the displacements 2, 4, 6 and 8 are independent, which implies the possibility of expansion or contraction of the element across its depth. In fact, this type of behavior has been assumed to be negligible in the behavior of the real element. If displacements in the directions 2 and 8, and similarly 4 and 6 can be made equal to each other, then the cross-section will remain unchanged across the depth.

The equilibrium equation of the frame element may then be written in the following form:

$$\underline{S}_{8 \times 1} = \underline{k}_{8 \times 8} \underline{u}_q_{8 \times 1} \quad (\text{A.14})$$

where  $\underline{S}$  is the nodal force vector. Without changing the 8x8 form of the stiffness matrix and also preserving the symmetry (necessary for the equation solver used) it is possible to equate the displacements 2 and 8 by simply adding the second row of the stiffness matrix to the eighth row and then adding the second column to the eighth column and setting all the terms on

the second row and column to zero and adding a (+1) on the positions  $k_{22}$  and  $k_{88}$  and a (-1) on the positions  $k_{28}$  and  $k_{82}$ . Also the load term corresponding to the second row should be set equal to zero. By doing so the second row of the stiffness matrix is replaced by an equation which reads  $v_2 = v_8$ . The same procedure can be repeated for the fourth and sixth directions. This procedure is exact but it has the disadvantage of not being able to apply any external load in the direction where the equilibrium equation is replaced. There is, however, another method in which large stiffness terms are added into the positions  $k_{22}$ ,  $k_{28}$ ,  $k_{82}$  and  $k_{88}$ . Physically this can be visualized as if a fictitious, very rigid bar exists between nodes  $i$  and  $l$  (similarly for  $j$  and  $k$ ). This second procedure is approximate but it is easy to apply and does not have the limitation of the first method. In this research the second approximate method is used.

From the displacement solution of the whole structure the displacements of the corners of each element are recovered. Assuming a linear strain distribution, the strains, thence the stresses at the top and bottom fibers and also at the reinforcement layers, are computed. These strains and stresses are assumed to be constant along the length of the segment.

Referring to Fig. 5c:

$$\text{Concrete strain at the top fiber: } \epsilon^t = \frac{u_5 - u_7}{L}$$

$$\text{Concrete strain at the bottom fiber: } \epsilon^b = \frac{u_3 - u_1}{L}$$

$$\text{Concrete stress at the top fiber: } \sigma^t = E^c \epsilon^t$$

$$\text{Concrete stress at the bottom fiber: } \sigma^b = E^c \epsilon^b$$

Strains at the top and bottom reinforcement layers are interpolated from the concrete strains  $\epsilon^t$  and  $\epsilon^b$ , then these are used to compute the steel stresses at the top and bottom reinforcements:

$$\sigma_{\text{top}}^S = E^S \epsilon_{\text{top}}^S; \quad \sigma_{\text{bottom}}^S = E^S \epsilon_{\text{bottom}}^S$$

The moment, shear and axial forces acting at the reference axis can be computed by using the following relation:

$$\underline{M} = \underline{b}_{\text{rq}} \underline{S} \quad (\text{A.15})$$

where

$\underline{M}$ : vector of forces acting at the reference axis (moment, shear, axial force)

$\underline{S}$ : vector of nodal forces acting at the corners of the element

$\underline{b}_{\text{rq}}$ : inverse of  $\underline{a}_{\text{rq}}$  which is:

$$\underline{b}_{\text{rq}} = \begin{bmatrix} 1 & 0 & D/2 & 0 & 0 & 0 \\ 0 & 1 & 0 & 0 & 0 & 0 \\ 0 & 0 & 0 & 1 & 0 & D/2 \\ 0 & 0 & 0 & 0 & 1 & 0 \\ 0 & 0 & 0 & 1 & 0 & -D/2 \\ 0 & 0 & 0 & 0 & 1 & 0 \\ 1 & 0 & -D/2 & 0 & 0 & 0 \\ 0 & 1 & 0 & 0 & 0 & 0 \end{bmatrix}$$

### A.3 Link Elements

Referring to Fig. 6, the stiffness of the link element in the global coordinates can be written as:

$$\underline{k}_{\text{XY system}} = \underline{R}^T \underline{k}_{\text{UV system}} \underline{R} \quad (\text{A.16})$$

where  $\underline{R}$  is the coordinate transformation matrix and

$$\begin{matrix} \underline{k} \\ \text{XY system} \end{matrix} = \begin{bmatrix} k_{11} & k_{12} & -k_{11} & -k_{12} \\ k_{12} & k_{22} & -k_{12} & -k_{22} \\ -k_{11} & -k_{12} & k_{11} & k_{12} \\ -k_{12} & -k_{22} & k_{12} & k_{22} \end{bmatrix} \quad (\text{A.17})$$

where

$$k_{11} = k_h \cos^2 \theta + k_v \sin^2 \theta$$

$$k_{12} = (k_h - k_v) \cos \theta \sin \theta$$

$$k_{22} = k_h \sin^2 \theta + k_v \cos^2 \theta$$

$\theta$ : angle between XY and UV coordinate systems.

Forces acting between the frame and the wall depend upon the relative displacements of the two ends of a link element connecting a node of the frame to a node of the wall. Those interactive forces can be computed from the following equation:

$$\begin{Bmatrix} S_1 \\ S_2 \end{Bmatrix} = \begin{bmatrix} k_{11} & k_{12} \\ k_{12} & k_{22} \end{bmatrix} \begin{Bmatrix} u_1 - u_3 \\ u_2 - u_4 \end{Bmatrix} \quad (\text{A.18})$$

where  $\underline{S}$  and  $\underline{u}$  are as defined in Fig. 6.

## APPENDIX B

Table B.1, Behavior of the Deep Beam (G24S-11)

| LOAD<br>(kips)         | DISPLACEMENT*<br>(inches) | CRACKED<br>ELEMENTS | STEEL ***<br>PLASTICITY | STEEL **<br>STRAINS % |
|------------------------|---------------------------|---------------------|-------------------------|-----------------------|
| 15                     | -0.00499                  | 5,6,7               | --                      | 0.0206                |
|                        | -0.00607                  | 12,13,14            | --                      | 0.0357                |
|                        | -0.00740                  | 20,21               | --                      | 0.0557                |
|                        | -0.00852                  | --                  | --                      | 0.0742                |
| 20                     | -0.01143                  | 4,27,28             | --                      | 0.1000                |
|                        | -0.01273                  | 11                  | --                      | 0.1150                |
|                        | -0.01318                  | 3                   | --                      | 0.1140                |
|                        | -0.01355                  | 10                  | --                      | 0.1130                |
|                        | -0.01392                  | 18                  | --                      | 0.1130                |
|                        | -0.01439                  | 2,19,25             | --                      | 0.1120                |
|                        | -0.01589                  | 32,9                | --                      | 0.1100                |
|                        | -0.01665                  | --                  | --                      | 0.1100                |
| 25                     | -0.02105                  | 17                  | --                      | 0.1400                |
|                        | -0.02182                  | 33                  | --                      | 0.1400                |
|                        | -0.02232                  | --                  | --                      | 0.1420                |
| 30                     | -0.02703                  | 26                  | --                      | 0.1710                |
|                        | -0.02908                  | 34                  | 6,7                     | 0.2510                |
|                        | -0.07140                  | 35                  | 5                       | 3.0000                |
| Failure - Steel Yields |                           |                     |                         |                       |

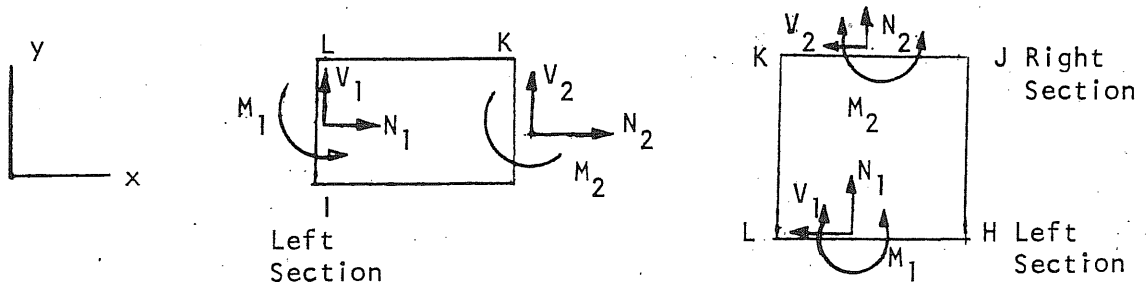
\* Vertical displacement of node 56

\*\* Steel strains of element 7

\*\*\* Yielding of the reinforcement in the elements indicated

Table B.2, Moment, Shear and Axial Forces Acting at the Reference Axis (P = 100 tons, Solution 2)

| Element Number | LEFT SECTION  |               |                  | RIGHT SECTION |               |                  |
|----------------|---------------|---------------|------------------|---------------|---------------|------------------|
|                | $N_1$<br>(kg) | $V_1$<br>(kg) | $M_1$<br>(kg-cm) | $N_2$<br>(kg) | $V_2$<br>(kg) | $M_2$<br>(kg-cm) |
| 2              | 23277         | 1859          | 26577            | -23277        | -1859         | 29197            |
| 3              | 18472         | 2021          | 30840            | -18472        | -2021         | 29787            |
| 4              | 13868         | 1818          | 27756            | -13868        | -1818         | 26781            |
| 5              | 9767          | 1587          | 24467            | -9767         | -1587         | 23139            |
| 6              | 6418          | 1144          | 18713            | -6418         | -1144         | 15628            |
| 7              | 3885          | 1187          | 16009            | -3885         | -1187         | 19627            |
| 9              | 28843         | 9146          | -259469          | -28843        | -9146         | 77177            |
| 10             | 21951         | 10625         | -163299          | -21951        | -10625        | -49209           |
| 11             | 14818         | 5434          | -39953           | -14818        | -5434         | -68732           |
| 12             | 9309          | 3212          | -125             | -9309         | -3212         | -69124           |
| 13             | 5141          | 2369          | 12045            | -5141         | -2369         | -59441           |
| 14             | 2178          | 1629          | 22405            | -2178         | -1629         | -54986           |
| 15             | -30349        | 3120          | -108359          | 30349         | -3120         | 45942            |
| 16             | -28032        | 2278          | -74922           | 28032         | -2278         | 29347            |
| 17             | -25541        | 1551          | -60480           | 25541         | -1551         | 29444            |
| 18             | -23039        | 1061          | -60723           | 23039         | -1061         | 39492            |
| 19             | -20469        | 683           | -71610           | 20469         | -683          | 57948            |
| 20             | -17488        | 832           | -95216           | 17488         | -832          | 78571            |
| 22             | 2471          | 2198          | 59199            | -2471         | -2198         | 6744             |
| 23             | 7427          | 2741          | 55202            | -7427         | -2741         | 27034            |
| 24             | 13951         | 3205          | 54517            | -13951        | -3205         | 41634            |
| 25             | 21886         | 3971          | 57544            | -21886        | -3971         | 61589            |
| 26             | 31936         | 6409          | 64033            | -31936        | -6409         | 128240           |
| 27             | 44151         | 13876         | 24446            | -44151        | -13876        | 391846           |



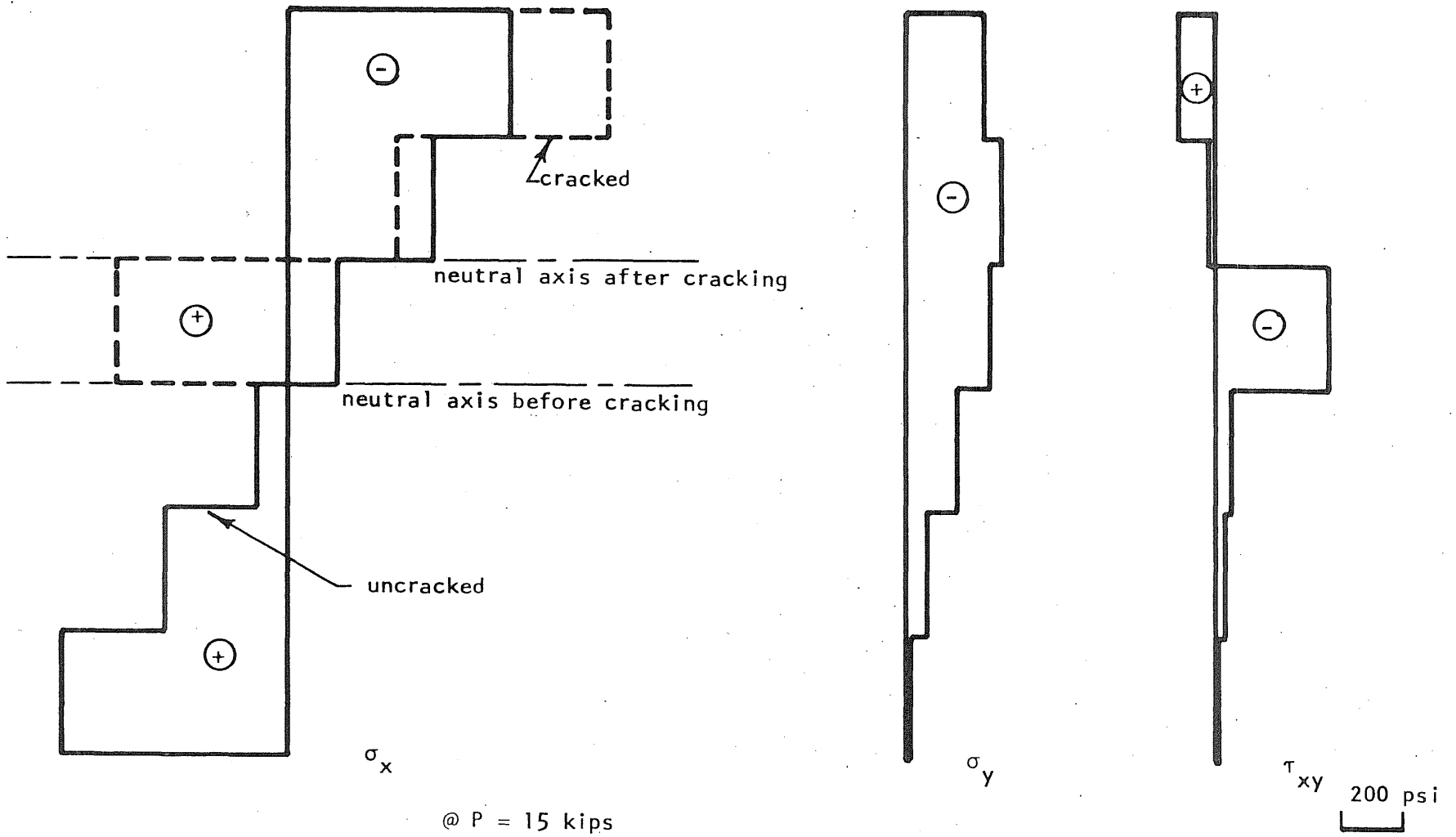


Figure B.1, Stress Distribution at Section A-A (Specimen G24S-11)



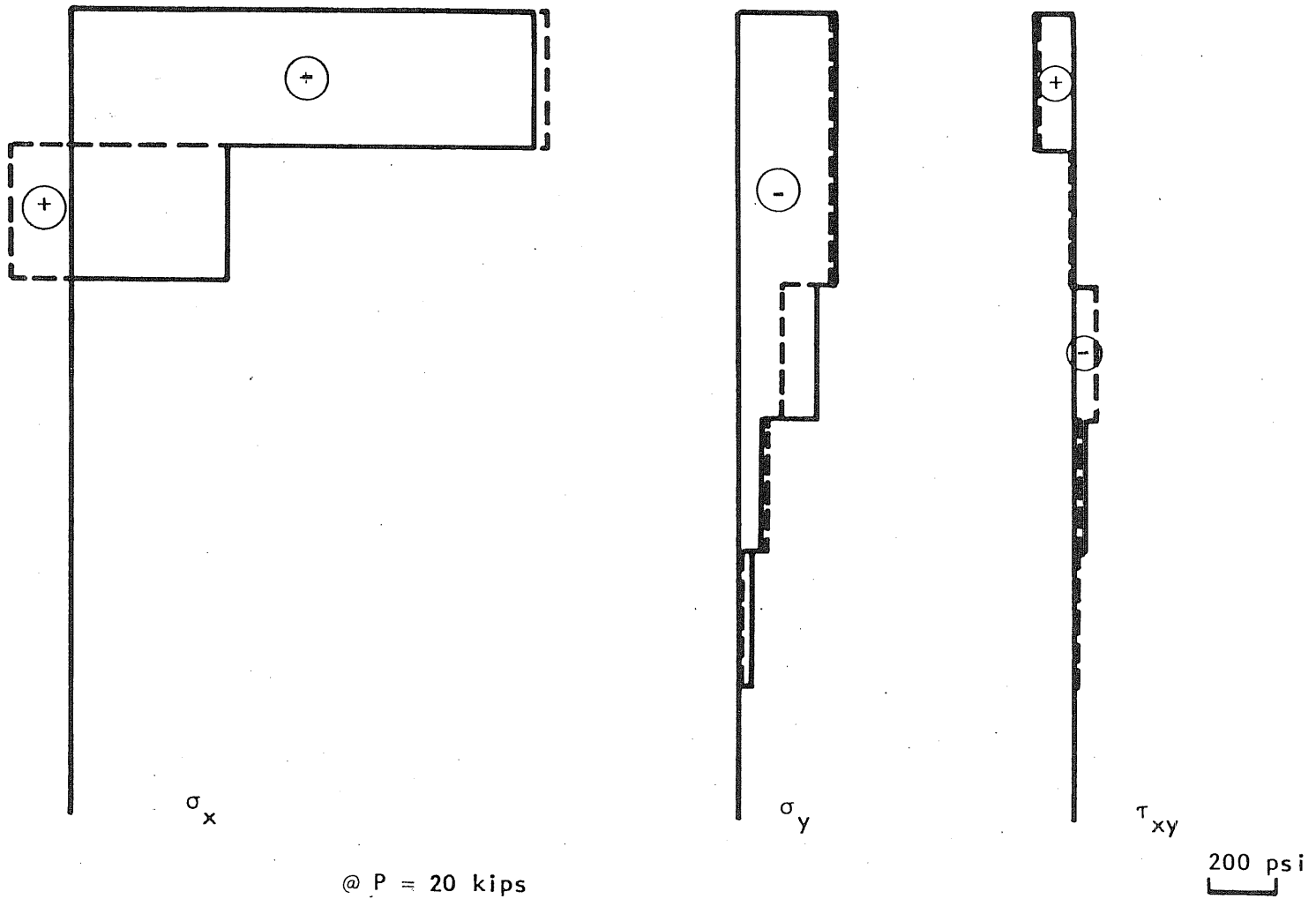


Figure B.2, Stress Distribution at Section A-A (Specimen G24S-11)

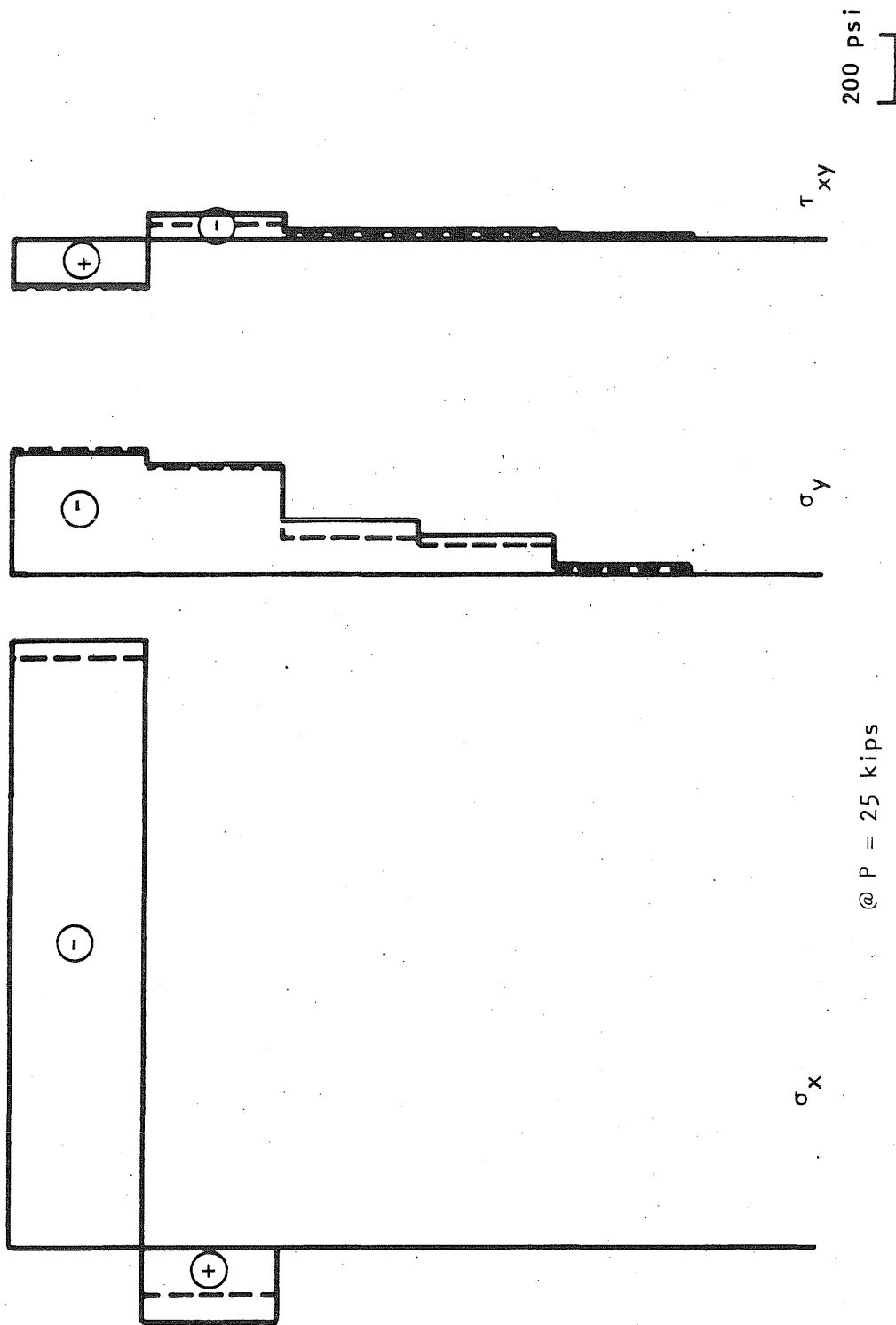


Figure B.3, Stress Distribution at Section A-A (Specimen G24S-11)

Metz Reference Room  
Civil Engineering Department  
B106 C. E. Building  
University of Illinois  
Urbana, Illinois 61801

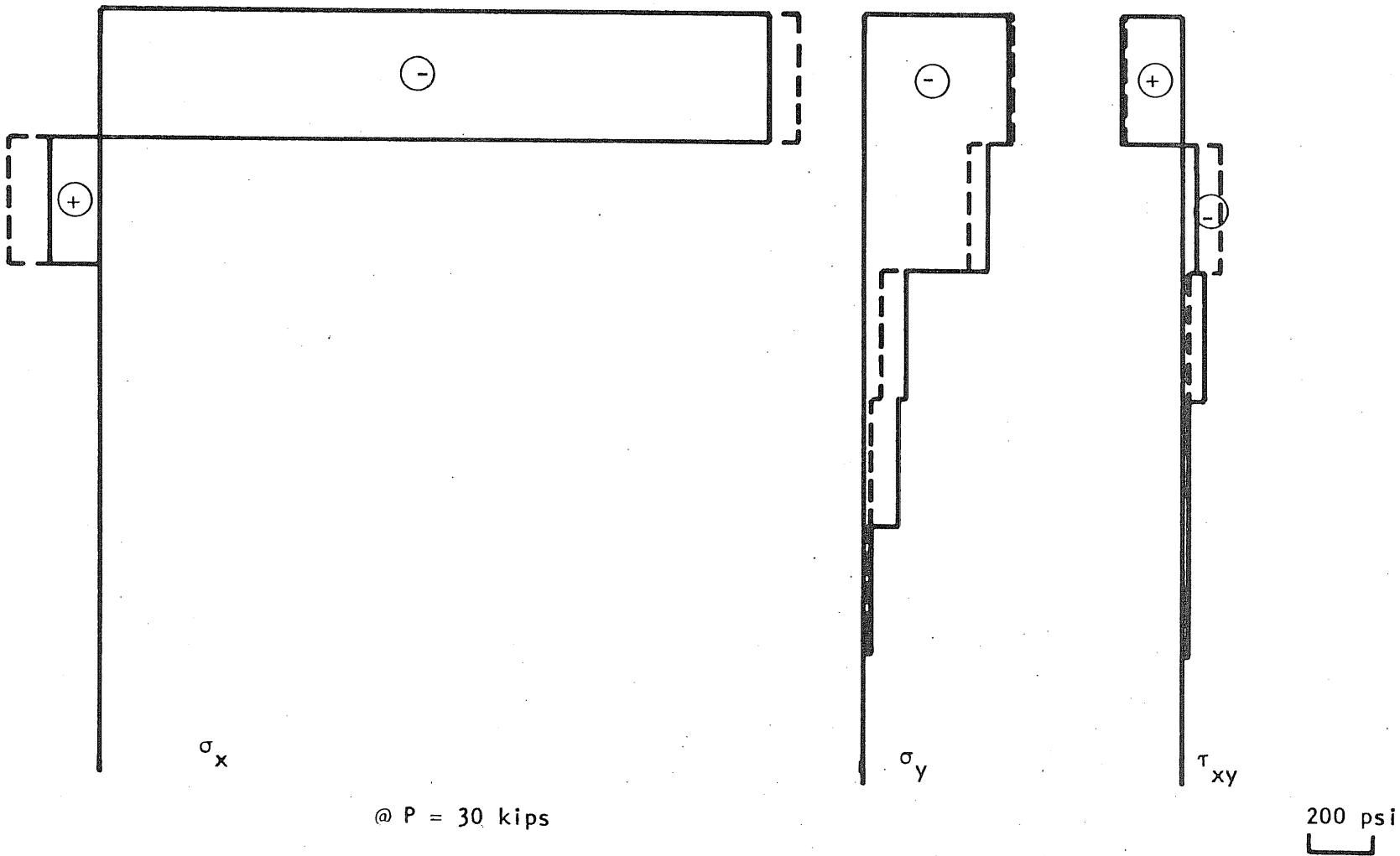


Figure B.4, Stress Distribution at Section A-A (Specimen G24S-11)

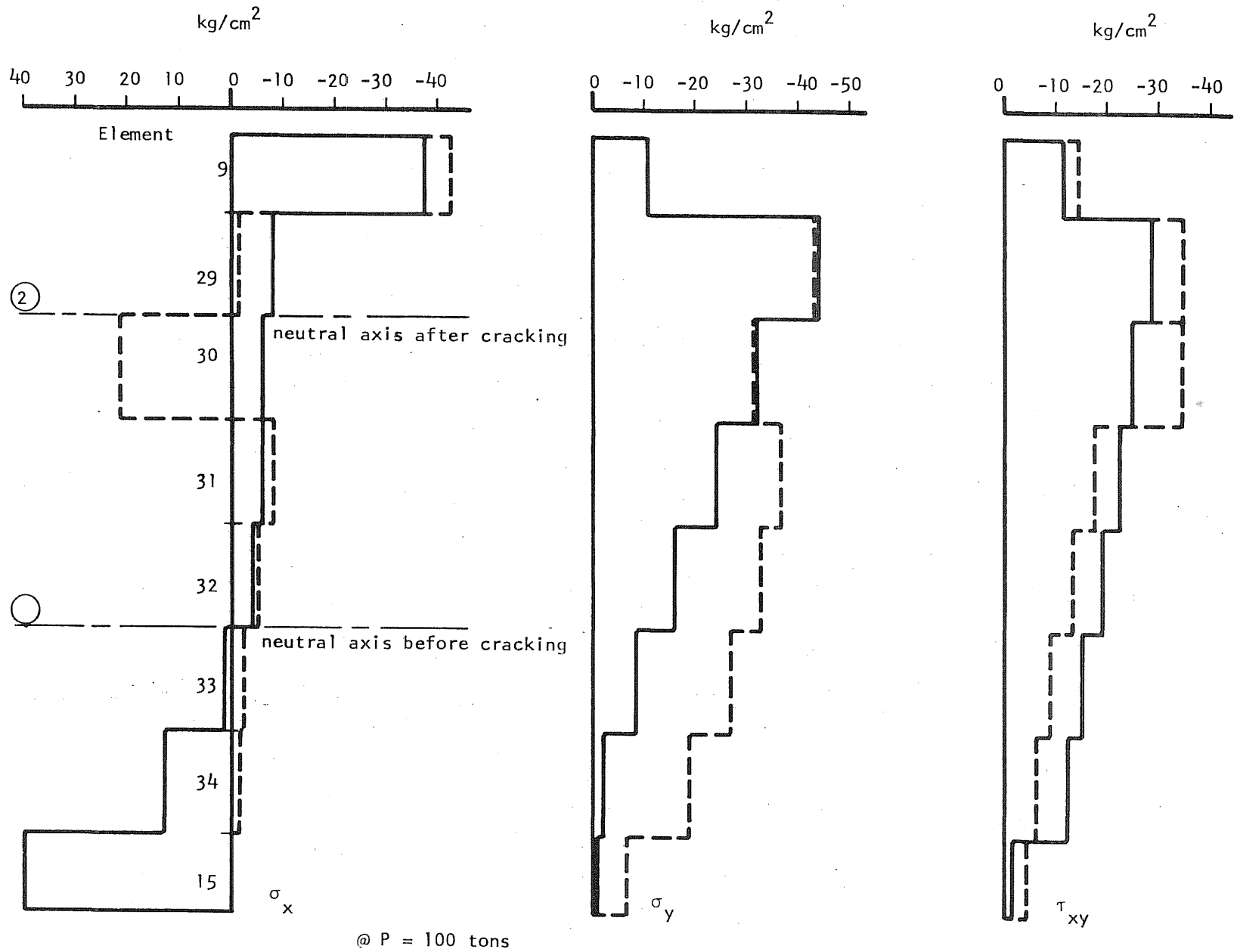
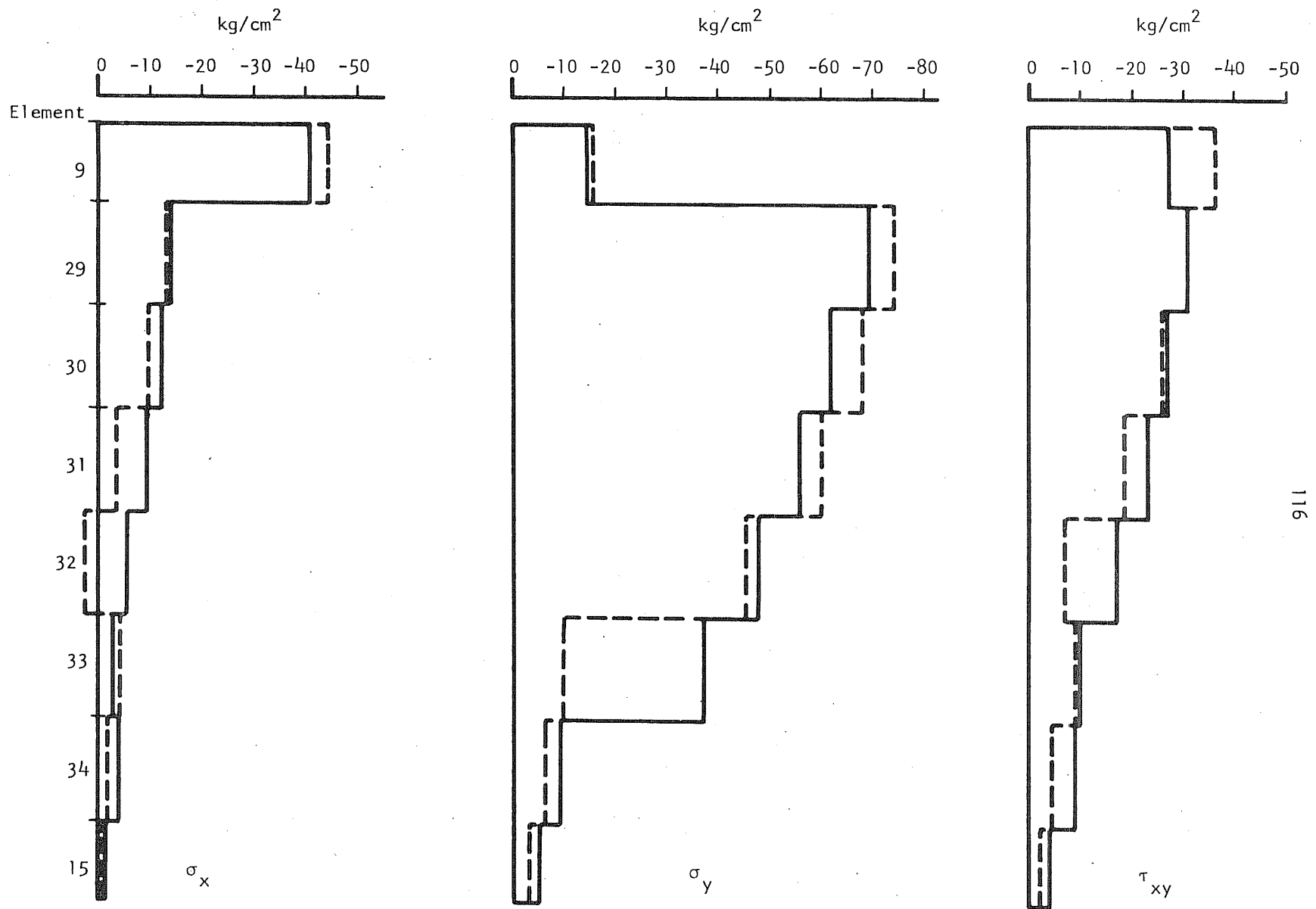
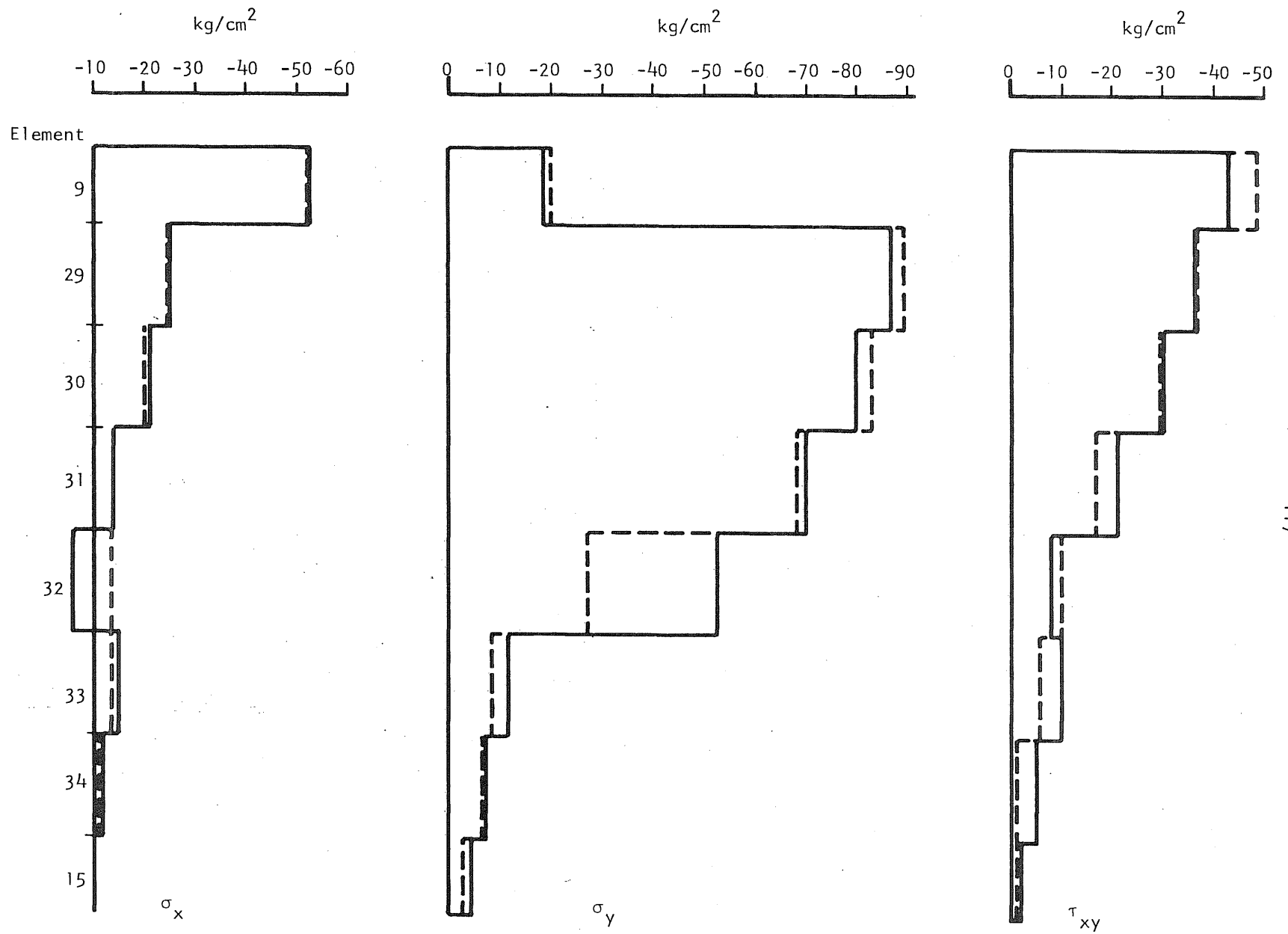


Figure B.5, Stress Distribution at Section A-A (Specimen A-1, Solution 1)



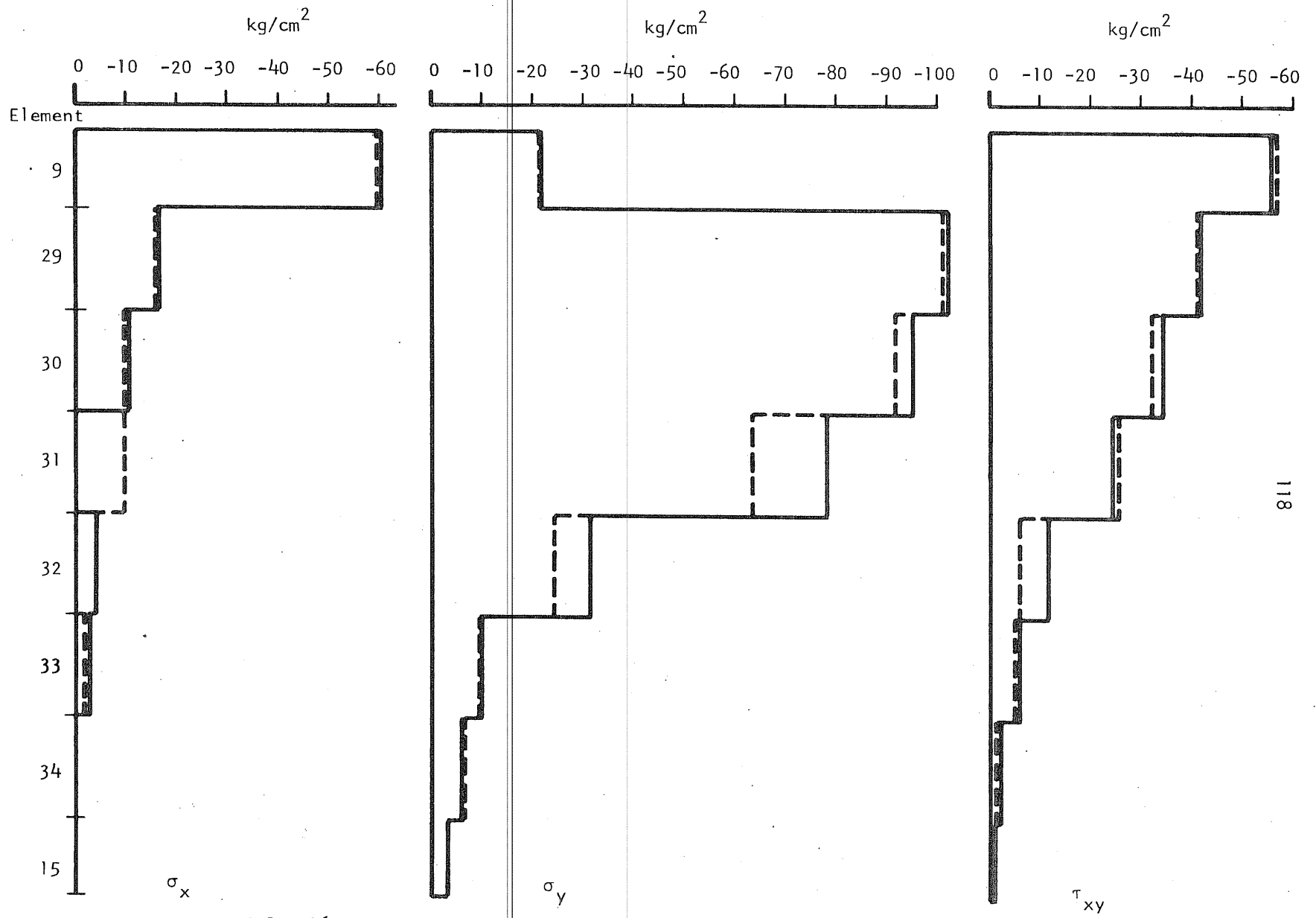
@ P = 120 tons

Figure B.6, Stress Distribution at Section A-A (Specimen A-1, Solution 1)



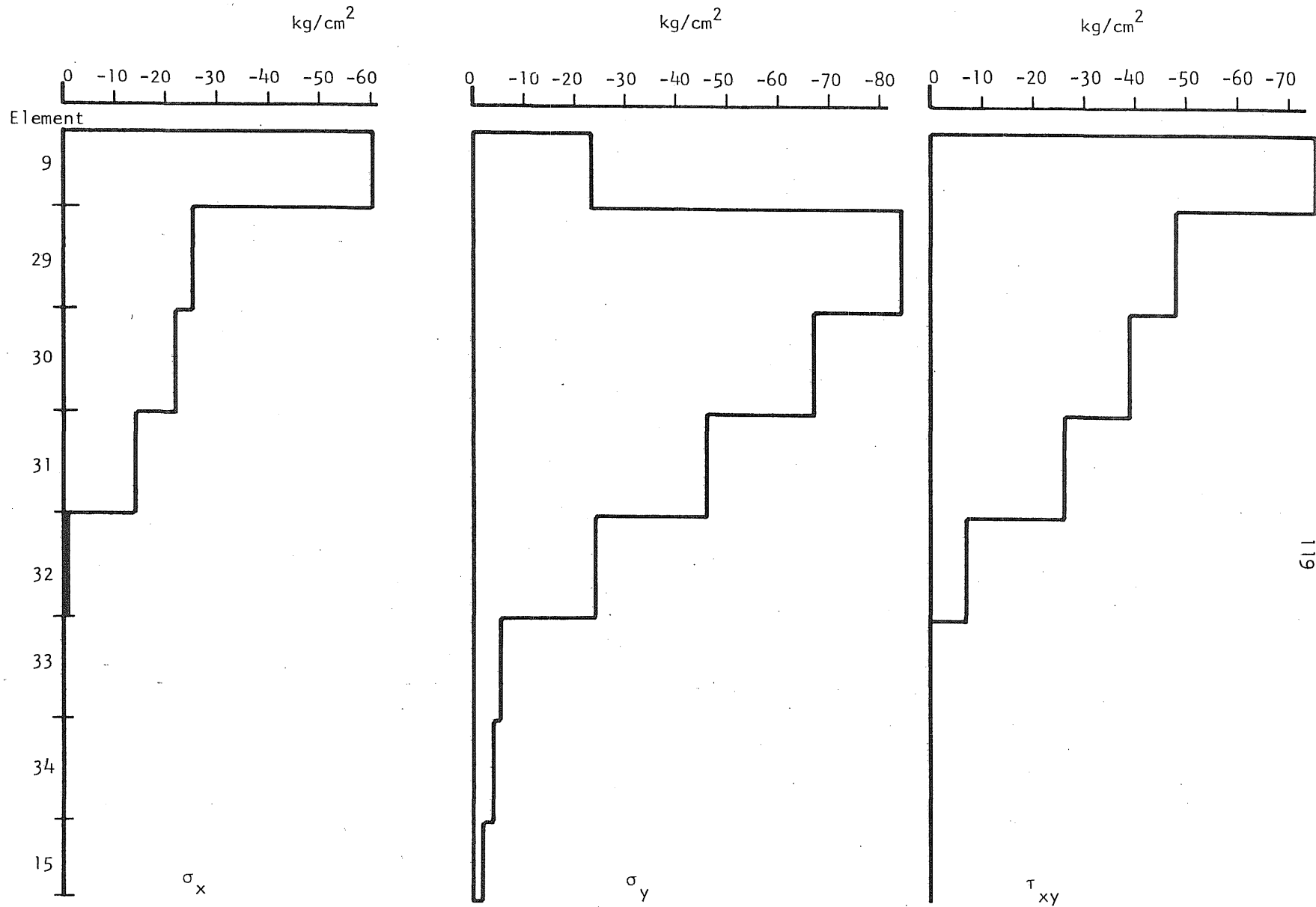
@ P = 140 tons

Figure B.7, Stress Distribution at Section A-A (Specimen A-1, Solution 1)



@ P = 160 tons

Figure B.8, Stress Distribution at Section A-A (Specimen A-1, Solution 1)



@ P = .190 tons

Figure B.9, Stress Distribution at Section A-A (Specimen A-1, Solution 1)



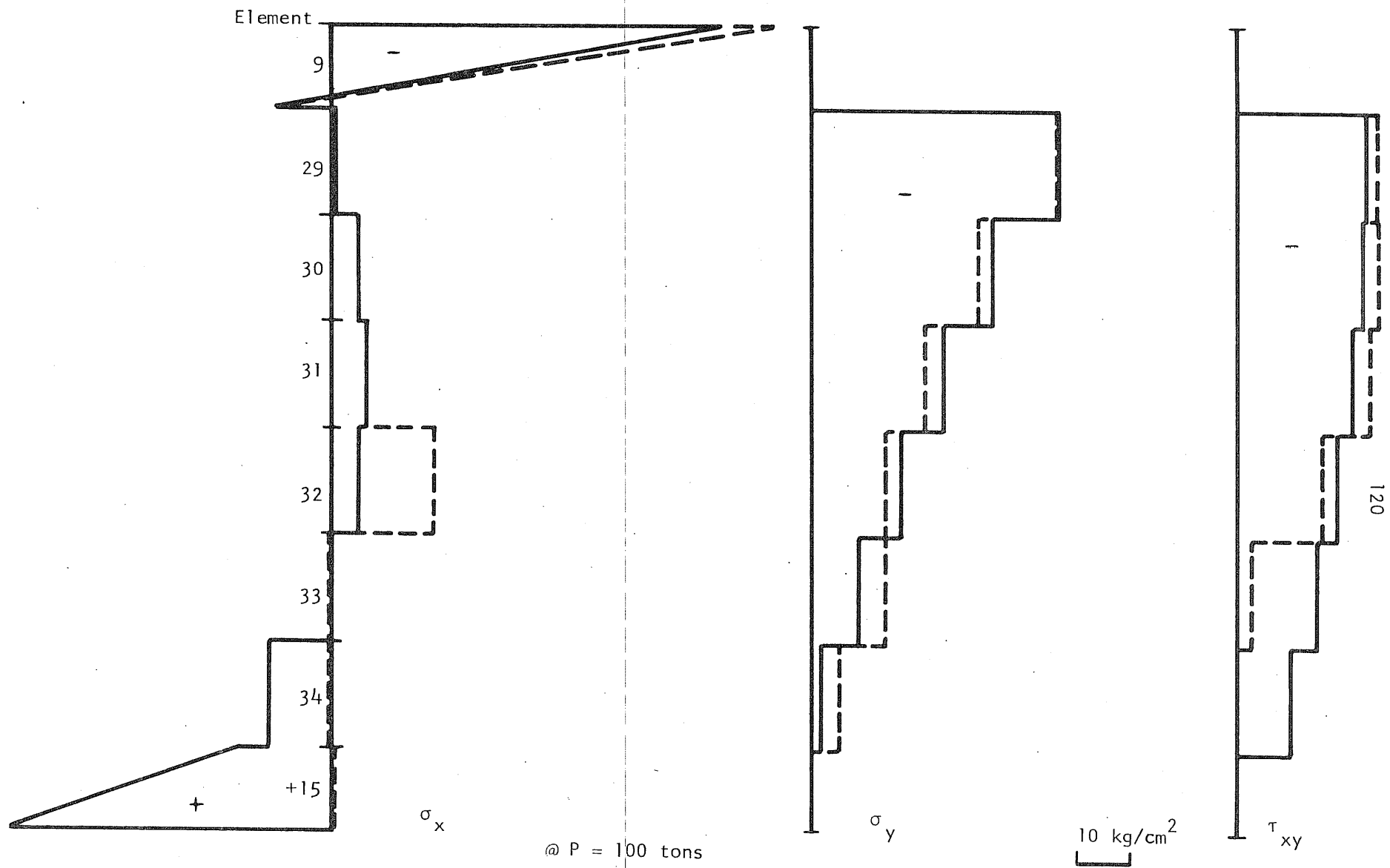


Figure B.10, Stress Distribution at Section A-A (Specimen A-1, Solution 2)

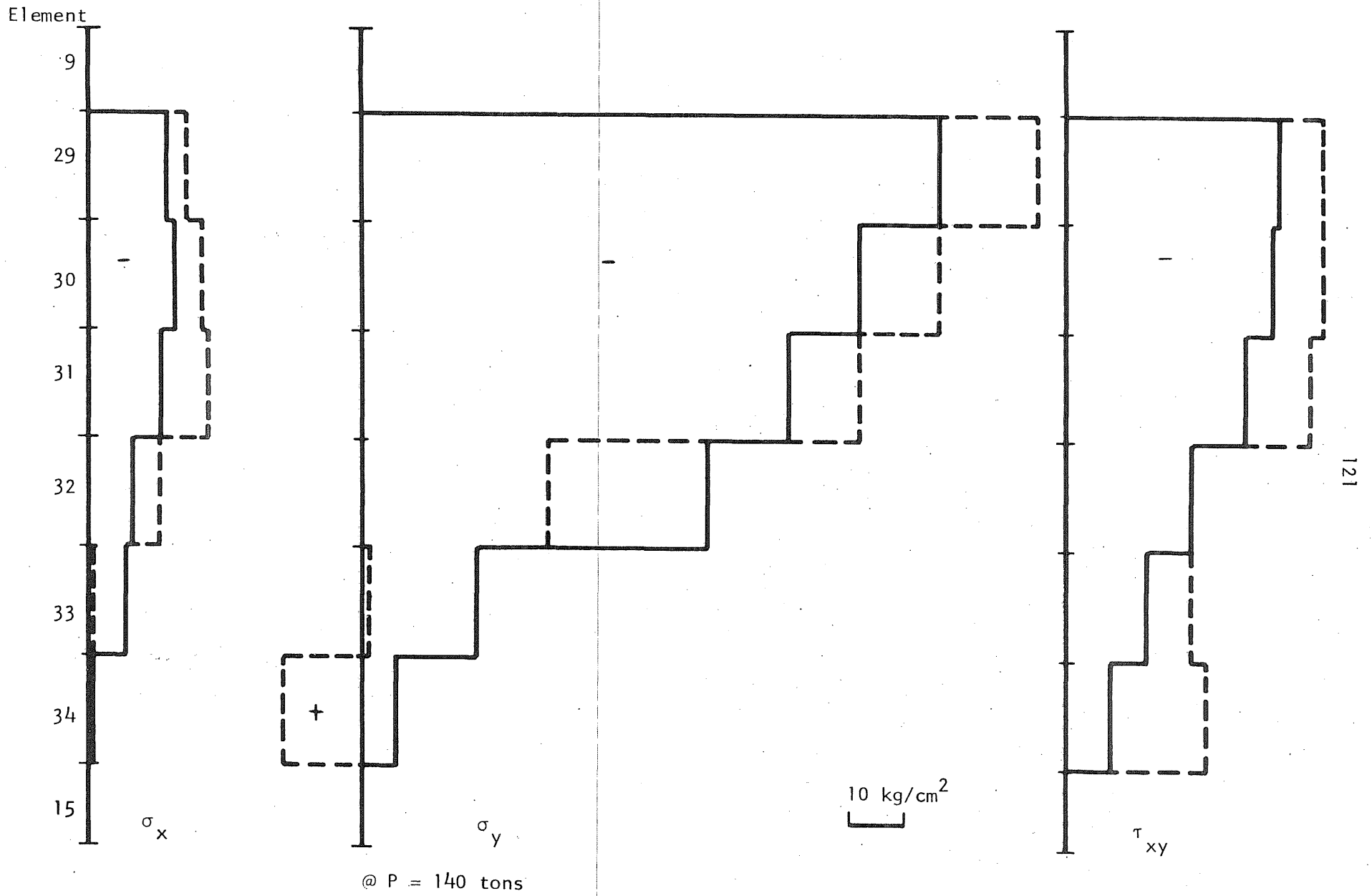
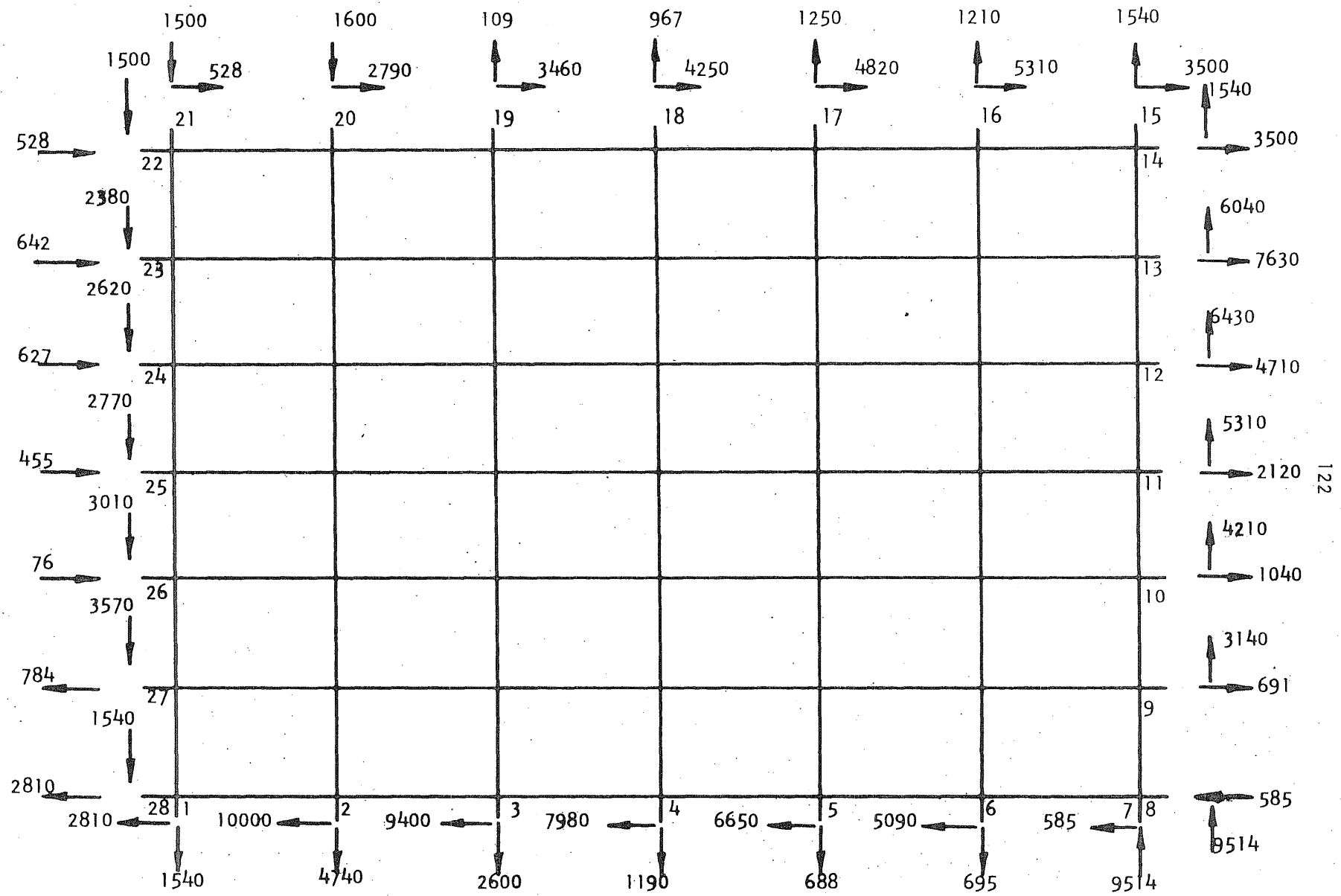


Figure B.11, Stress Distribution at Section A-A (Specimen A-1, Solution 2)



Note: All Forces in (kg).

Figure B.12, Link Forces at P = 100 tons (Before Cracking)

## REFERENCES

1. Rosman, R., "Approximate Analysis of Shear Walls Subject to Lateral Loads," ACI Journal, Proceedings, June 1964, pp. 717-733.
2. Coul, A. and Choudhury, J. R., "Stresses and Deflections in Coupled Shear Walls," ACI Journal, Proceedings, Feb. 1967, pp. 65-72.
3. Coul, A. and Choudhury, J. R., "Analysis of Coupled Shear Walls, ACI Journal, Proceedings, Sept. 1967, pp. 587-593.  
Discussion by Anastasecu, D., Mirsu, O., Munteanu, I., Chandra, R., Shultz, M., and Authors, ACI Journal, Aug. 1967, pp. 515-519.
4. Coul, A. and Irwin, A. W., "Design of Connecting Beams in Coupled Shear Walls," ACI Journal, Proceedings, March 1969, pp. 205-209.
5. Rosenblueth, E., and Holtz, I., "Elastic Analysis of Shear Walls in Tall Buildings," ACI Journal, Proceedings, June 1960, pp. 1209-1222.
6. Cardan, B., "Concrete Shear Walls Combined with Rigid Frames in Multi-story Buildings Subject to Lateral Loads," ACI Journal, Proceedings, Sept. 1961, pp. 299-316.
7. Gould, P., "Interaction of Shear Wall-Frame Systems in Multistory Buildings," ACI Journal, Proceedings, Jan. 1965.
8. Khan, F. R. and Sbarounis, J. A., "Interaction of Shear Walls with Frames in Concrete Structures Under Lateral Loads," Proceedings, ASCE, June 1964, pp. 285-336.
9. Fiorato, A. E., Sozen, M. A., Gamble, W. L., "An Investigation of the Interaction of Reinforced Concrete Frames with Masonry Filler Walls," Ph.D. Dissertation, Nov. 1970, University of Illinois, Urbana, Illinois.
10. Benjamin, J. R. and Williams, H. A., "The Behavior of One-Story Reinforced Concrete Shear Walls," Proceedings of ASCE, May 1957, pp. 1254-1 - 1254-49.
11. Blume, J. A., Newmark, N. M. and Coring, L. H., "Design of Multi-Story Reinforced Concrete Buildings for Earthquake Motions," Portland Cement Association, Chicago, Illinois, 1961.
12. Sozen, M. A., Jennings, P. C., Matthiesen, R. B., Housner, G. W., and Newmark, N. M., "Engineering Report on the Caracas Earthquake of July 29, 1967," National Academy of Sciences, Washington, D. C., 1968.
13. Zienkiewicz, O. C., "The Finite Element Method in Structural Continuum Mechanics," McGraw-Hill, 1967.

14. Clough, W. R., "Analysis of Structural Vibrations and Dynamic Response," Japan-U.S. Seminar on Matrix Methods of Structural Analysis and Design, Aug. 1969, Tokyo, Japan.
15. Ngo, D. and Scordiles, A. C., "Finite Element Analysis of Reinforced Concrete Beams," ACI Journal, Proceedings, March 1967.
16. Nilson, A. H., "Nonlinear Analysis of Reinforced Concrete by Finite Element," ACI Journal, Proceedings, Sept. 1968.
17. Cervenka, V. and Gerstle, K. H., "Inelastic Finite Element Analysis of Reinforced Concrete Panels under In-Plane Loads," Ph.D. Dissertation, University of Colorado, Boulder, Colorado, 1970.
18. Franklin, H. A., "Nonlinear Analysis of Reinforced Concrete Frames and Panels," Ph.D. Dissertation, March 1970, University of California, Berkeley, California.
19. Fedrokiw, J. P., and Sozen, M. A., "A Lumped-Parameter Model to Simulate the Response of Reinforced Concrete Frames with Filler Walls," Ph.D. Dissertation, June 1968, University of Illinois, Urbana, Ill.
20. Paiva, H.A.R. and Siess, C.P., "Strength and Behavior in Shear of Deep Reinforced Concrete Beams Under Static and Dynamic Loading," SRS No. 231, Civil Engineering Dept. University of Illinois, Urbana, Illinois, October 1961.
21. Umemura, H. Aoyama, H., Liao Ming H., "Studies on Reinforced Concrete Shear Wall and Framed Masonry Shear Walls," Research Report, University of Tokyo, Tokyo, Japan, June 1965.
22. Kupfer, H., Hilsdorf, H. K., and Rusch, H., "Behavior of Concrete Under Biaxial Stresses," ACI Journal, Proceedings, Vol. 66, No. 8, August 1969, pp. 656-666.
23. Mikkola, M. J., Schnobrich, W. C., "Material Behavior Characteristics for Reinforced Concrete Shells Stressed Beyond the Elastic Range," Civil Engineering Studies, SRS No. 367, University of Illinois, Urbana, Illinois, August 1970.
24. Cardenas, A., "Strength and Behavior of Isotropically and Nonisotropically Reinforced Concrete Slabs Subjected to Combinations of Flexural and Torsional Moments," Ph.D. Dissertation, May 1968, University of Illinois, Urbana, Illinois.
25. Lenschow, R. J., and Sozen, M. A., "A Yield Criterion for Reinforced Concrete Under Biaxial Moments and Forces," Ph.D. Dissertation, July 1966, University of Illinois, Urbana, Illinois.
26. Zienkiewicz, O. C., Valliappan, S., and King, I. P., "Elasto-Plastic Solutions of Engineering Problems, 'Initial Stress.' Finite Element Approach," International Journal for Numerical Methods in Engineering, Vol. 1, pp. 75-100, 1969.

27. Mast, R. F., "Auxiliary Reinforcement in Concrete Connections," ASCE, Journal of the Structural Division, June 1968, pp. 1485.
28. Mohraz, B., Schnobrich, W. C., and Echeverria, G. A., "Crack Development in a Prestressed Concrete Reactor Vessel as Determined by a Lumped Parameter Method," Nuclear Engineering and Design, Vol. 11, No. 2, 1970.
29. Gupta, A. K., Mohraz, B., and Schnobrich, W. C., "Elasto-Plastic Analysis of Three-Dimensional Structures Using the Isoparametric Element," SRS No. 381, Department of Civil Engineering, University of Illinois, Urbana, Illinois, August 1971.
30. Connor, J. and Will, G., "Computer-Aided Teaching of the Finite Element Displacement Method," Department of Civil Engineering Research Report No. 69-23, School of Engineering, MIT, Cambridge, Mass., February 1969.
31. Turner, M. J., Clough, R. W., Martin, H. C., and Topp, L. J., "Stiffness and Deflection Analysis of Complex Structures," Journal of Aeronautical Science, 23, 1956, pp. 805-823.

